Fabrication and Application of Atomic-scale Silicon Structures

by

Roshan Achal

A thesis submitted in partial fulfillment of the requirements for the degree of

Doctor of Philosophy

Department of Physics

University of Alberta

© Roshan Achal, 2020

Abstract

On a perfect hydrogen-terminated Si(100)-2x1 surface, each surface silicon atom is capped with exactly one atom of hydrogen. When one of the capping hydrogen atoms is removed, the now unsatisfied orbital of the underlying silicon atom is exposed at that site. This site is better known as a dangling bond (DB), and it is an atom-sized building block that has been at the centre of numerous proposals for the next generation of technology over the last two and a half decades. This is because DBs have ideal electronic, chemical, and thermal properties for nanoscale device applications. In one approach, DBs can be used to create ultra-low power electronic circuitry. Atomically defined DB structures for such circuitry can be created with the use of a scanning tunneling microscope (STM). This is achieved by removing hydrogen atoms from the surface one at a time with the STM to make DBs at selected sites. However, due to limitations of the apparatus, it has not yet been possible to build sufficiently error-free structures to realize any of the technological proposals. Without a means to correct errors, this has continued to remain true.

In this work, STM techniques were developed to improve the atomic precision of the automated fabrication of DB structures, hydrogen lithography (HL), on silicon. A scalable method to correct errors and edit DB structures, hydrogen repassivation (HR), was also developed. In this method, single hydrogen atoms on the STM tip are transferred back to the surface, erasing DBs by reforming bonds with them. Using these techniques in conjunction, a perfect sculpture of a maple leaf was fabricated

from just 32 DBs. The techniques were then used to create two rewriteable atomic memory arrays, achieving the highest solid-state storage density (1.1 petabits per in^2). The first array was used to store the alphabet letter-by-letter in 8 bits. The second array was used to store and play back the first 24 notes of the Mario theme in 192 bits. The applicability of these techniques was then explored in different conditions, including at varying temperatures and with deuterium substituted for hydrogen. The nature of the transfer process of hydrogen from the tip to the surface during HR was also examined.

To improve upon HR further, a new, faster and simplified form of error correction was developed, molecular hydrogen repassivation (M-HR), which is able to direct single molecules of hydrogen to erase DB sites (without the use of atoms attached to a scanned probe). This capability was achieved by changing the DBs to be erased into tailored reactive sites for ambient hydrogen molecules. The atomic memory arrays were redesigned to accommodate M-HR as the primary means of rewriting information (0.88 petabits per in^2). It was then used to rewrite information in a 24-bit memory array. In addition to M-HR, two other techniques were developed to bring new functionality to the STM. A charge characterization technique, which reduces the influence of the typically perturbative STM tip field, was created to characterize the charge of structures on the surface. Also, by combining this with the ability to create tailored reactive sites for particular molecules, a technique to electronically detect single molecule binding events was demonstrated.

Now that a full suite of improved fabrication tools is available to manipulate single atoms and molecules of hydrogen, including the ability to easily and reliably correct fabrication errors, the stage is set for DB-based technologies to flourish. The tools and techniques described in this thesis may also help uncover deeper insights into chemical reactivity and dynamics at the atomic scale.

Preface

The results reported in this thesis are from original research that I carried out between September 2015 and September 2019. The work was completed under the supervision of Dr. Robert Wolkow and in collaboration with members of his research group at the University of Alberta.

In this time I contributed to 8 peer reviewed publications and 2 patents (all listed in Appendix A). Some of the work was also picked up by the media. Chapter 2 and Chapter 4 were reproduced from two of the peer reviewed publications. Permissions and contributions are detailed at the beginning of each respective chapter. All other figures and data presented herein are original, unless explicitly indicated otherwise.

The following software and packages were used for data processing and figure creation: Python (with PyROOT, SciPy, NumPy, Matplotlib, Open CV, Pygame) [free], OriginLab, Maple, Nanonis, LabVIEW, Gwyddion [free], Inkscape [free], Paint.NET [free], ImageJ [free], VSDC video editor [free], and Open Broadcaster Software [free]. Mendeley [free] was used for reference management. This document was prepared using the MiKTeX LaTeX distribution [free] and the TeXstudio editor [free].

I wanna be
the very best,
like no one
ever was...

-Pokémon theme (1998)

Acknowledgments

This section of my thesis may have been the most difficult to write. There are so many people to thank for helping me get here and as this is likely the culmination of my formal education, I wanted to do a thorough job. While all the experiments literally happened in a vacuum, the ideas themselves did not form in a vacuum. They were the product of a lot of education and mentoring, collaborative research environments, many (many) trials and errors, and some serendipity.

First and foremost I would like to thank my supervisor, Dr. Wolkow (Bob), who convinced me to continue with silicon through his sheer enthusiasm and passion for the field. There are many things that can be said of Bob, but if I had to choose one word to describe him, I would choose generous. Bob has always been generous with resources, recognition, opportunities, intellectual freedoms, and his time. I enjoyed learning from his intuition of atomic behavior. Bob's vision for the group and the future of technology has led to opportunities for me to pursue cutting-edge science while gaining business and industry experience through his spin-off company QSi, which is something I will always be grateful for. I did not have to travel very far to find one of the most unique hybrid programs in the world. Through your mentorship over my entire grad program I have grown considerably as a scientist, and I feel well equipped for whatever might come next. For everything you have done over the years Bob, thank you.

Many of these results also would not have been possible without the support of the rest of the research group: Marco Taucer, Jeremiah Croshaw, Wyatt Vine, John Wood, Erika Lloyd, Bruno Martins, Jo Onoda, Radovan Urban, Hedieh Hosseinzadeh, Jason Pitters, and Paul Piva. The technical support from Mark Salomons and Martin Cloutier was incredible. I also appreciated the help of Penny Mckelvie

for keeping the group organized. A big thanks to Lucian Livadaru for taking the time to provide helpful comments and hunt down dropped minus signs in this document; I really appreciated the feedback. Mohammad Rashidi, you were always available to lend a hand, plan a new experiment, or even just to kill time. You were a great mentor, and I learned a lot. I am thankful we had the opportunity to work together as much as we did. Taleana Huff, we made a very effective team and you were someone I could continually rely on in the lab. Working with you has been a great blend of heavy metal and science. I would be remiss if I did not acknowledge all of the mentorship and support I received from Ken Gordon as well. Your insight into the business world has been invaluable, and I truly enjoyed discussing topics like business plans and market valuations with you.

I want to thank my supervisory committee, Dr. Frank Marsiglio and Dr. Mark Freeman. You both have always helped me avoid tunnel vision related to my work by asking broad and sometimes difficult questions. Even small discussions during committee meetings helped lead me towards new ideas (some even appeared in Chapter 4). I would also like to thank Dr. Michael Woodside for always being willing to write reference letters and lend his insights into rate equations. The Department administrative staff has also been amazing, and I am thankful to have had such friendly people to help navigate the maze of University forms and procedures. I am extremely grateful for the financial support I received during my degree in the form of scholarships from NSERC, AITF, and the University of Alberta.

I would also like to give a special thanks to Jennifer Pascoe and the rest of the Faculty of Science office. Without your help, this work would have never captured the attention and imaginations of such a wide audience. The opportunities I have had a chance to participate in as a result gave me important perspectives on the intersection between media and science, and have truly enriched my graduate program.

I want to thank all of my fantastic friends, both here and back home. You helped keep me grounded and brought some balance to my academic life. The evening sports were a welcome distraction (although sometimes too distracting...). Along with lunch time frisbee, these activities helped build a great community, which I could count on whenever I needed perspectives from well outside physics.

My parents always provided me with an environment to succeed, from picking me up after late sports practices so I would have time to do my homework, to driving me to early morning tests in snow storms when transit was not running. There is too much to list, but I am forever grateful for everything you have done to help me get here. Thank you to my Aji and Aja for helping motivate me to improve my grades early on; it played a huge role in my pursuit of academics. All of my grandparents sacrificed tremendously to give their future generations better opportunities and I appreciated their endless support to get the best education possible. I unfortunately do not have enough room to individually thank the rest of my family, but I am grateful to all of my uncles, aunts, siblings, cousins, and everyone else for all the love and encouragement along the way.

Last, but certainly not least, I would like to thank my partner Jordan. Your support has been unwavering through this whole process. I appreciate all the little things you have done to make grad school better, like bringing dinner and keeping me company in the lab on days that I ended up working through the night. Your keen editorial skills helped improve any document that I sent your way including many scholarship applications, manuscripts, and reports, catching hilarious typos and frequent, comma splices. It would not have been even remotely as enjoyable of a road without you. I also want to thank your parents for their support of this whole process, and for providing the occasional mountain adventure.

Contents

List of Figures

List of Acronyms

- **AFM** - Atomic force microscope
- **DB** - Dangling bond
- **DNA** - Deoxyribonucleic acid
- **HL** - Hydrogen lithography
- **HR** - Hydrogen repassivation
- **LT** - Low temperature
- **M-HR** - Molecular hydrogen repassivation
- **STM** - Scanning tunneling microscope
- **UHV** - Ultra-high vacuum
- **VB** - Valence band
- **2DFT** - 2D-Fourier transform

Chapter One

Introduction, background, motivation

1.1 Background and motivations

1.1.1 No *Moore* road left

It has been known for some time now that the end of the current semiconductor roadmap is quickly approaching. Silicon-based devices are reaching both performance and size limits as heat generation and quantum effects on leakage currents become more pronounced [1]. The trend of Moore's law, where the number of transistors is expected to double every two years, can only be maintained for several more generations of technology. Even with an increasing transistor density, overall device performance has plateaued (including processing speed) because the amount of heat generated per unit area cannot be efficiently dissipated otherwise. Had these metrics also continued increasing in step with Moore's law, processors would be reaching heat densities near those of a rocket nozzle [2, 3].

Clearly there is a need for lower power technologies, which can reduce the amount of heat generated, in order to increase the speed and performance of future generations of devices. Beyond just the plateau of computational performance, there is also a concern for the global energy demand as the amount of data traffic increases each day [4]. Reducing the power consumption of processing could help slow the increasing growth rate of the total global electricity needed for data centres, devices and networks [4]. Data centres themselves have additional consideration as these buildings can have large land footprints, requiring swaths of dedicated physical space.

One method to minimize the impact of future data centres is to increase the amount of information that can be stored in a given area.

There is an abundance of different proposals to address these issues, as well as to create new technologies (including quantum computers). Many of these proposals rely on the use of atomic-scale fabrication to build devices from the bottom up [5–12]. While such approaches have a lot of potential, there are the ever present questions of scalability and practicality that can make or break any given one. The critical factors that often limit these aspects are the reliability and throughput/yield of atomic-scale fabrication. Advances in these areas can not only support and improve the prospects of candidate technologies, but also spur on new developments as the control over basic units of matter becomes more routine.

1.1.2 The state of atomic manipulation and fabrication

Almost exactly 40 years ago, in 1979, the path towards atomic-scale manipulation began with the filing of a patent application for a "high-resolution surface inspection apparatus" [13]. I find it amazing that the underlying designs and principles of the Scanning Tunneling Microscope (STM) were so thoroughly formed three years prior to the landmark paper by Binnig and Rohrer in the early eighties [14]. Their work truly changed the scientific landscape, earning them the Nobel prize in Physics in 1986, just five short years after they built the apparatus. This work opened the door to a previously elusive world: the atomic scale. One of their first results that fully illustrated the power of this new instrument was the experimental visualization of the Si-7x7 surface reconstruction [15]. While the STM quickly became a ubiquitous tool to image and characterize conductive surfaces, it was not until nearly a decade after its initial inception that it would lead to another disruption of the scientific landscape. In 1989, Don Eigler *et al.* at IBM would demonstrate the controlled manipulation of xenon atoms on the surface of nickel (110) with an STM to fabricate the famous 'IBM' logo [16]. This result inspired the ultimate goal of fabricating devices/structures from the bottom up, atom by atom. Many unique applications have since spawned from chasing the goal of atomic-scale devices and fabrication using an STM [17], including

the construction of "Quantum Corrals" by Crommie *et al.* three years after that [18]. As the instrument and techniques matured further, the power to build magnetic bits became a reality [11], along with single atom transistors [7], and a kilobyte of rewritable atomic memory [9]. However, despite all this progress, many of these applications have been limited to the laboratory by one or more factors such as cryogenic requirements [7, 9, 11], the inhomogeneity of their constituent parts [7, 19], or the lack of atomically precise fabrication [5, 19, 20].

Atomic manipulation *via* STM tip can fall into one of two broad categories: adsorbate manipulation and defect manipulation. Both techniques have useful properties that can be exploited to fabricate atomic structures inside of an STM, depending on the material system in question. Generally, for adsorbate manipulation, sample surfaces held at low temperatures (milliKelvin to tens of Kelvin) are exposed to atoms or molecules, which randomly adsorb throughout. They can then be positioned to form structures with the STM tip [16, 21, 22]. Adsorbate manipulation can be broken down further into lateral manipulation and vertical manipulation. Lateral manipulation involves the formation of a temporary bond with an adsorbed entity and the STM tip [21, 22]. The adsorbate never loses contact with the sample surface, but it can be precisely pushed, pulled, or slid by the tip to a new location [21, 22]. Adsorbates such as iron on copper have been positioned through lateral movements to fabricate the first quantum corral [18], as well as xenon atoms on nickel in the fabrication of the IBM logo [16], and CO molecules on copper to create molecule cascades [23]. With vertical manipulation, on the other hand, the adsorbate is physically removed from the surface, as it becomes attached to the STM tip. It can then be deposited in a new location to build up structures [21]. Xenon and CO have also been used to fabricate structures in this mode [22]. The ability to pick up atoms is an important aspect of tip functionalization which will be discussed in more detail [24, 25].

The remarkable feats accomplished through the manipulation of adsorbates relied on their weak interactions with the supporting substrate, allowing them to be positioned with ease. The flip-side of these weak interactions is that extremely low temperatures are required to build them and prevent thermal disordering [11, 16, 18, 23]. In any widespread practical application, however, these temperatures are unfeasible,

so different approaches were explored within the STM. To relax these cryogenic constraints to some degree, the use of atomic surface defects as opposed to adsorbates presented a potential avenue. The creation of defects on a surface usually involves breaking strong bonds to remove a surface atom [9, 19, 26, 27]. Depending on the substrate, these defects tend to face much higher energy barriers to diffusion and lateral manipulation compared to adsorbates [28, 29]. A good analogy that is often used to describe the two systems is that manipulating adsorbates is like molding clay, whereas manipulating defects is more akin to chiseling in granite. A couple of surfaces where atomic defects have shown promise for fundamental and technological applications are chlorine-terminated copper (100) [9, 30], and hydrogen-terminated silicon [5, 19, 20]. Some work also explores hydrogen-terminated germanium in addition to silicon [31].

By using silicon dangling bonds (DBs) on the surface of an otherwise hydrogen-terminated sample to fabricate devices/structures, several of the limitations that have been described can be immediately overcome. Each DB is identical by their very nature, acting as homogeneous building blocks for next generation devices [5, 6, 19]. Additionally, there are high barriers to diffusion along the surface for DBs, allowing fabricated structures to exist at elevated temperatures without disordering [28, 29]. At minimum, fabricated structures would ideally persist at room temperature, a regime where stable DB structures on the surface of hydrogen-terminated silicon have already been demonstrated [20, 32]. The onset for diffusion of DBs was observed in STM studies to be nearly 500 K [28, 29], giving a wide span of temperatures where devices can operate. This prospect, along with the compatibility of the silicon substrate and current semiconductor fabrication processes, and the electronic properties of the DBs themselves, has made this system both a scientifically and commercially tantalizing platform. Several companies including IBM [33], Zyvex Labs [32, 34], and the local Quantum Silicon Inc. [5, 35] have been actively studying and developing silicon DB-based technologies and fabrication techniques. Within the scientific community, there are a number of researchers focused on fundamental properties of DBs, as well as proposed device properties, and the reliable creation of DBs [33–37]. The area of study is further diversified with a division of experiments on n-type and

p-type silicon samples, where DB behaviours can differ significantly [38, 39].

The creation of DB patterns on the surface of hydrogen-terminated silicon is commonly referred to as hydrogen lithography (HL). It has enabled the development of single atom transistors [7], engineered quantum states on the passivated surface [40], prototype logic structures [5], and small rudimentary memory [41]. The latter few applications especially require the atomically precise removal of hydrogen from the surface to create intricate structures. This is where the field has stalled, as HL techniques have remained largely unchanged from their first reported uses in the 1990s [26, 27, 37, 42]. Alone, these techniques have been unable to provide the necessary yield to form larger structures and really push DB-based technologies further. Very recently, a new discovery made independently by Huff *et al.* [25] and by Pavliček *et al.* [33] provided the framework for a large step forward in lithographic capabilities, that is, the previously absent ability to correct and erase erroneous DBs to create error-free structures. In both reports an atomic force microscope (AFM) was used to transfer an adsorbed hydrogen atom on the tip to a DB on the surface, repassivating it. This work led to the exploration and development of a similar, more scalable, STM-based hydrogen repassivation (HR) technique that is described in Chapter 2. This technique, combined with improved lithography techniques, gave rise to the largest perfect structures ever achieved on this medium (Figure 2.2 and Figure 2.4).

1.1.3 Embarking on a new road

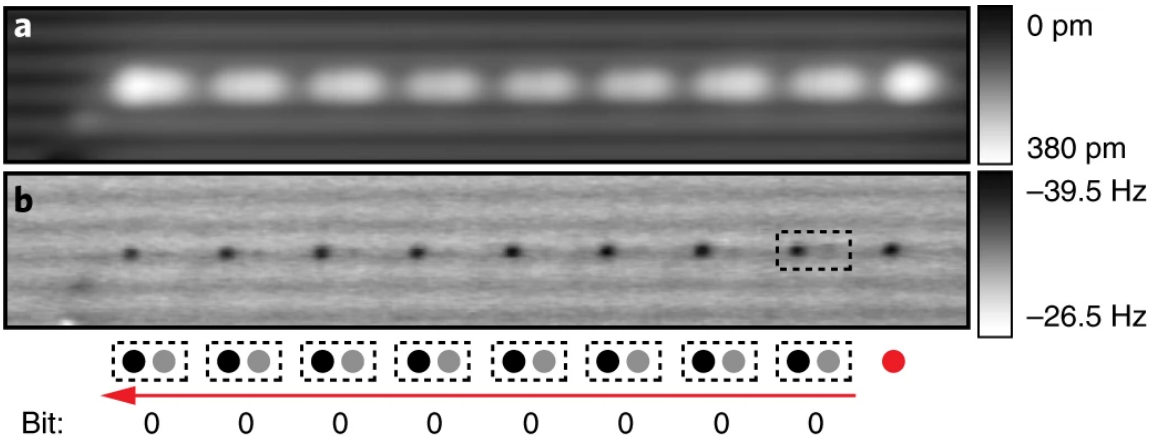

Figure 1.1: A DB binary wire (24 x 3 nm^2).
a) (V = -1.7 V, I = 50 pA) An STM image of eight pairs of coupled DBs, with an isolated DB acting as a negative charge perturbation at the input. **b**) (V = 0 V, Z_{rel} = -330 pm) An AFM image showing that the electron in each pair has localized to the left side in order to minimize interactions due to the perturbation tilting the energy landscape. With the perturbation removed, the electron in each pair would be shared more evenly between the constituent DBs. By observing the leftmost DB, the input state can be determined. This figure was reproduced from [5], where the authors retained copyright for reproduction in a thesis.

A wholly new computing architecture is being developed based on DBs, showing the first illustrations of functional nanoscale computational elements. This field-controlled circuitry holds the promise of ultra-low power operations, which can not only address the thermal restrictions of current semiconductor technologies, but also replicate logic operations with just a handful of atoms [5]. In these designs, pairs of DBs are created such that a shared electron can exist on either side of the pair. By adding a local negative perturbation near one side of the pair, the electron within the pair will move to the other side in order to reduce interactions. Placing these pairs end-to-end in a line forms a type of binary wire, where the repositioning of the electron in one pair causes a cascade of electron repositioning in all of the other pairs, much like dominoes. Figure 1.1 shows an experimental realization of this effect,

where a negative perturbation is added to one end of the wire, causing the electrons within each pair to reposition, thereby transmitting information from one end to the other. This type of information propagation down the wire sees a significant power reduction because there is no conventional flow of thousands of electrons through the wire (which also causes heating). The pairs of DBs can be placed in configurations other than a wire to enable logic operations using the same principles. Figure 1.2 shows an operational "OR-gate" built from DBs. There are already designs in place for other important logic gates, and increasingly sophisticated modeling software is available to mock-up full circuits [5, 43].

To date, the fabrication of large error-free DB structures has been the limiting factor preventing the full testing and realization of DB-based devices [5,6,8,19,20,32]. It is this fact that makes the development of new tools and techniques to enable rapid error-free fabrication, to extend past the proof of principle DB structures described above, of critical importance. To truly embark on a new road, fabrication abilities of any new technologies have to show the potential to eventually meet the throughput requirements of current semiconductor manufacturers.

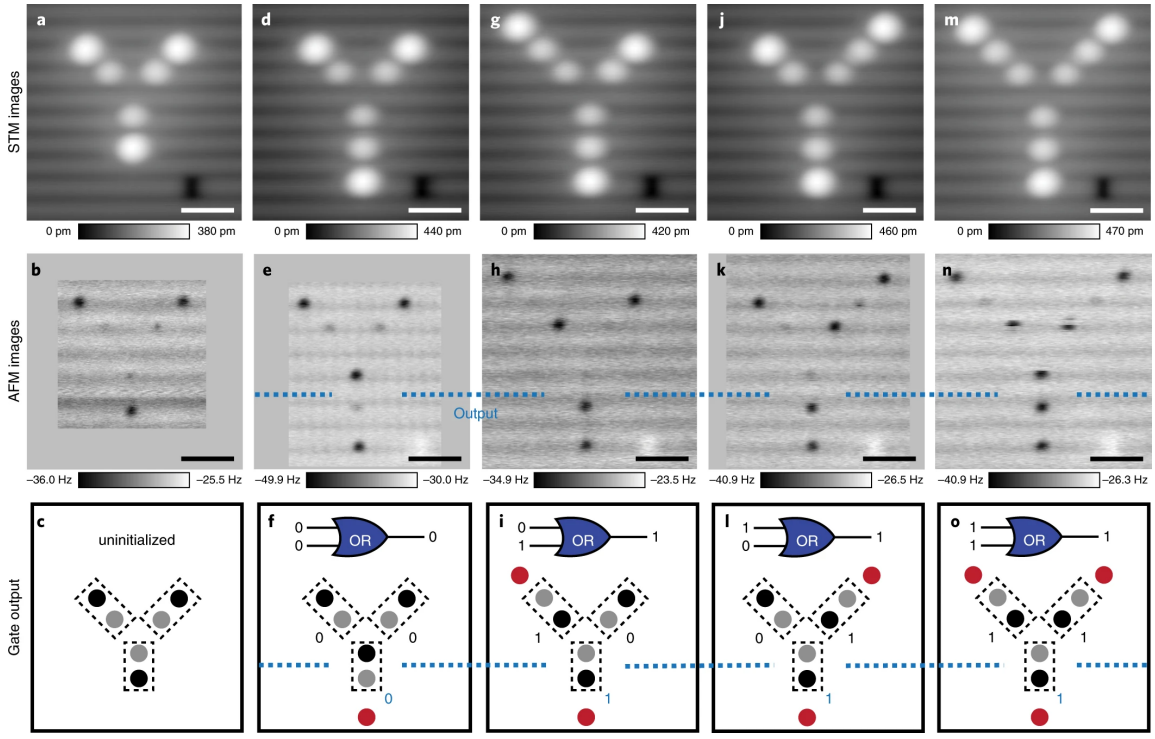

Figure 1.2: An "OR-gate" fabricated from DBs.
a,**d**,**g**,**j**,**m**) (V = -1.8 V, I = 50 pA) STM images of a patterned atomic-scale logic gate made from DBs on the surface of hydrogen-terminated silicon. The STM images show the spatial structure of the gate, but not the location of charge. The two input terminals of the gate are at the top of the images. The main structure of the gate consists of three pairs of coupled DBs shown in **a**, each sharing one net electron between them. **b**,**e**,**h**,**k**,**n**) (V = 0 V, Z_{rel} = -350 pm) AFM frequency shift maps of the same gate structure shown in the row above. The AFM images show the location of where charge accumulates. The darkest depressions in the AFM images are DBs where the net electron in each pair has localized. **d**) By placing an isolated DB near the output terminal to act as a negative charge perturbation, the electron in the closest pair moves into the farther DB to minimize interaction as shown in **e**. This is the full structure of the gate, with the output currently reading logical "zero". By placing an isolated DB at either input terminal (or both) as shown in **g**,**j**,(**m**) the electrons in the gate rearrange to flip the output bit, which now reads logical "one" as shown in **h**,**k**,(**n**). **c**,**f**,**i**,**l**,**o**) A graphical depiction of the full truth table for an OR-gate. Scale bars are 2 nm. This figure was reproduced from [5], where the authors retained copyright for reproduction in a thesis.

On the road to better fabrication tools and techniques for DB-based devices, another complementary application emerged simultaneously. With the ability to now controllably remove and replace single atoms of hydrogen from the hydrogen-passivated silicon surface, the notion of using the presence or absence of hydrogen to represent binary information seemed like a natural extension. By doing so, the highest solid-state data storage densities ever achieved were demonstrated using DBs [10]. At 138 TB per square inch (1.70 bits per nm^2), such memories have the potential to improve today's storage capacities by several orders of magnitude, especially for data archival. However, the serial nature of using the probe of an STM for rewriting operations to erase DBs is an inherent bottleneck in the operating speed of this type of memory. By using hydrogen molecules as molecular erasers, instead of hydrogen atoms to repassivate DBs, it is possible to make rewriting a much faster and more parallel task, which may eventually not necessitate the inclusion of a probe altogether [44].

Beyond the immediate practical applications of DBs, the fabrication of large error-free structures at the atomic scale can also enable the study of fundamental physics through the characterization of interactions between DBs in various arrangements [6, 35, 40]. Better characterization will allow refined theoretical modeling and predictions of these devices [5]. Additionally, the ability to design and pattern structures will provide a unique opportunity to further merge theory and experiment. In two other material systems where atomically precise fabrication is possible, the theoretical Lieb lattice was constructed and characterized experimentally to successfully verify predictions [30, 45]. Artificial molecules have also been created with STM techniques [40, 46, 47]. As DB structures can exist at a range of temperatures [19, 20, 28, 29] and the substrate properties can be altered through doping, there is a vast playground of parameters that can be varied for testing, once fabrication is sufficiently advanced, that are not available in other systems.

1.1.4 DNA storage: complementary not competition

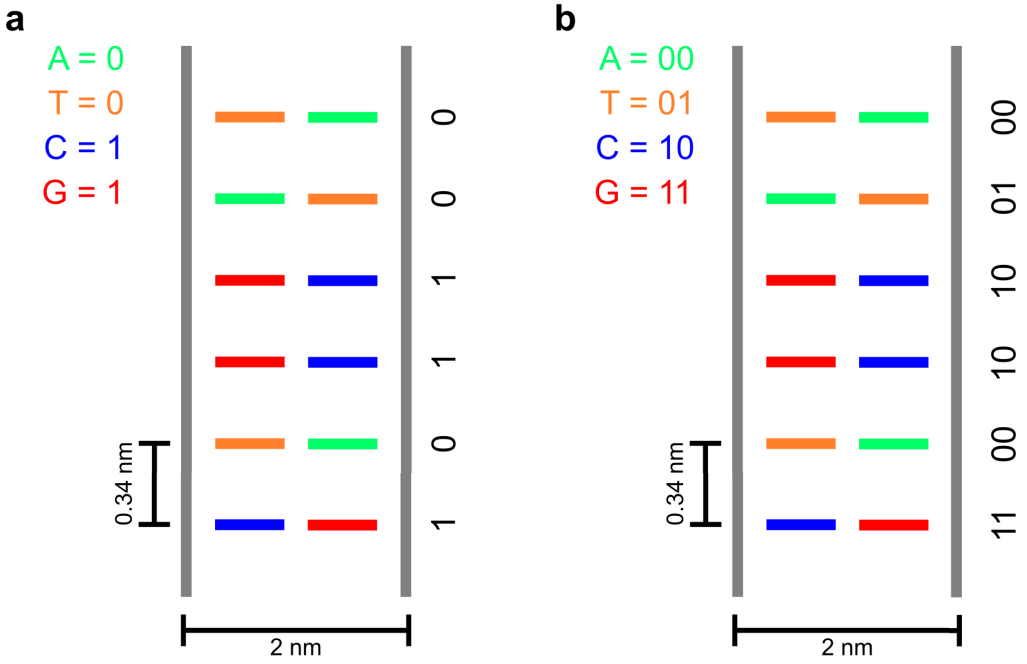

Figure 1.3: Structure of DNA-based memory.
a) The basic structure and encoding of DNA for the storage of binary information. **b**) By utilizing the four unique bases of DNA (A, T, G, C) to represent a string of two bits, the information storage density of DNA can be increased further.

A question that often comes up when ultra-high density data storage is discussed is how it compares to the density of DNA data storage. It is difficult to make a one-to-one comparison because of just how different a planar silicon wafer is compared to the inherently 3D geometry of DNA. However, I decided to go ahead and make a comparison, despite it not being overly meaningful in the context of areal density.

The structure of DNA when laid flat resembles a ladder with each rung containing a base pair [48], as shown in Figure 1.3. These base pairs can only exist in particular combinations, where bases A and T pair, and bases C and G pair. In the most straightforward implementation of storing data in DNA, one half of the ladder represents a string of binary information, where bases A and T represent 0 and

bases G and C represent 1 (Figure 1.3a). In this planar geometry, DNA storage has maximum theoretical areal storage density of 1.47 bits per nm^2. More complex implementations of DNA storage take advantage of the fact that there are four unique bases available, allowing each base to represent a string of two bits [49] (Figure 1.3b). By doing so, each rung can now represent twice the amount of data, bringing the maximum theoretical areal storage density of DNA to 2.94 bits per nm^2. Although, there are biological factors that reduce the theoretical maximum from 2.0 bits per rung to 1.83 bits per rung [49], bringing the density to 2.69 bits per nm^2.

The second implementation of DNA storage exceeds the maximum theoretical storage density of DB-based data storage on hydrogen-passivated silicon (1.7 bits per nm^2) by about 37%. This owes to the fact that DB-based systems have only two available states, whereas DNA has four. Realistically, since DNA does not exist in a planar geometry, as has been assumed for the estimates here, the comparison is not as straightforward. A better comparison would involve the actual volume of DNA in solution and the equivalent volume of a silicon chip (although the minimum thickness of a silicon chip for this type of storage has not been explore or optimized yet).

Instead of competing technologies, I view both DB-based storage and DNA-based storage as complementary systems with different strengths. While both systems are suited towards archival of massive amounts of data, DNA-based memory has more relaxed requirements for shelf-stable storage, lasting over centuries in harsh real-world conditions [50]. A drawback to this form of data storage, though, is that to recall information from DNA the entire strand has to be sequenced in a slow (but well established) process, rather than accessing just the desired bits of data. There have been some advances towards better random access to address this issue [51]. Conversely, DB-based memories have the ability to access only specific regions within a memory array, without disturbing the rest of the stored information. The bits within a DB array can also be rewritten individually, so the memory can be much more dynamic. Both types of storage could be implemented in different roles, as specific applications will require choices between data-density, ease of storage, ease of recall, longevity, and the need for random access and rewritability.

1.2 The scanning tunneling microscope (STM)

The STM used to obtain all of the results in this thesis operates from room temperature down to liquid helium temperature. The scanning chamber outside of the cryo-shielded volume (in which the sample resides) is maintained under ultra-high vacuum at a pressure of approximately $1{\cdot}10^{-11}$ Torr (the pressure inside the shielded area is even lower at cryogenic temperatures). One of the most important components of any STM is the tip itself. In most cases the tip is metallic, commonly tungsten. A tungsten tip was used in all of the proceeding experiments. The tip is first electrochemically etched down to a fine point and is then further processed in vacuum to achieve a single atom at the apex [52].

Independent piezoelectric motors are used to move the tip in the x, y, and z directions inside of the STM respectively. The movement of the tip towards the sample is defined as the negative z direction. An understanding of the apex termination of the tip is crucial to explaining experimental results. Studies detailing changes in imaging resolution when the tip apex is functionalized (through vertical manipulation) with a CO molecule have been reported [24]. The use of functionalized tips with characteristic signatures in resolution helps guarantee a consistent apex character between experiments. Labidi *et al.* also reported changes in resolution when the tip was functionalized with a hydrogen atom through vertical tip movements into the sample surface [53]. The widely used method to condition/change the apex structure of the tip is to bring it into controlled contact with the sample surface. Theoretical models of silicon-terminated tungsten tips, with a hydrogen atom at the apex, have been developed by Jarvis *et al.*, detailing the role of tip structure in the transfer of hydrogen to the surface [54]. The ability to reliably functionalize the tip with hydrogen was a key factor that enabled the correction ability in HL [10, 25].

Once the tip is brought within tunneling distance of the sample surface (on the order of 1 nm), the STM can obtain images of the local sample density of states in one of two modes, either constant height or constant current. In constant height mode, the z position of the tip is fixed as the tip scans above the surface in the x-y plane, recording variations in tunneling current to produce an image. The magnitude

of the tunneling current depends on the overlap of the imaging orbital of the tip and the orbitals of features on the surface. Conversely, in constant current mode, feedback control circuitry is used to actively adjust the z position of the tip as it scans to maintain a set current value. The z heights are recorded to produce an image of the surface topography. The magnitude of the tunneling current in an STM is exponentially sensitive to the tip-sample distance, resulting in the ability to resolve atomic scale corrugations in the local sample density of states [14, 55–58]. The bias applied between the tip and sample to induce a sustained tunneling current can have two polarities. When the sample bias is positive, the tip is injecting electrons into the empty states of the sample near the surface. Alternatively, when the sample bias is negative, the tip is drawing electrons from the filled sample states near the surface.

1.3 Hydrogen-terminated Si(100)-2x1

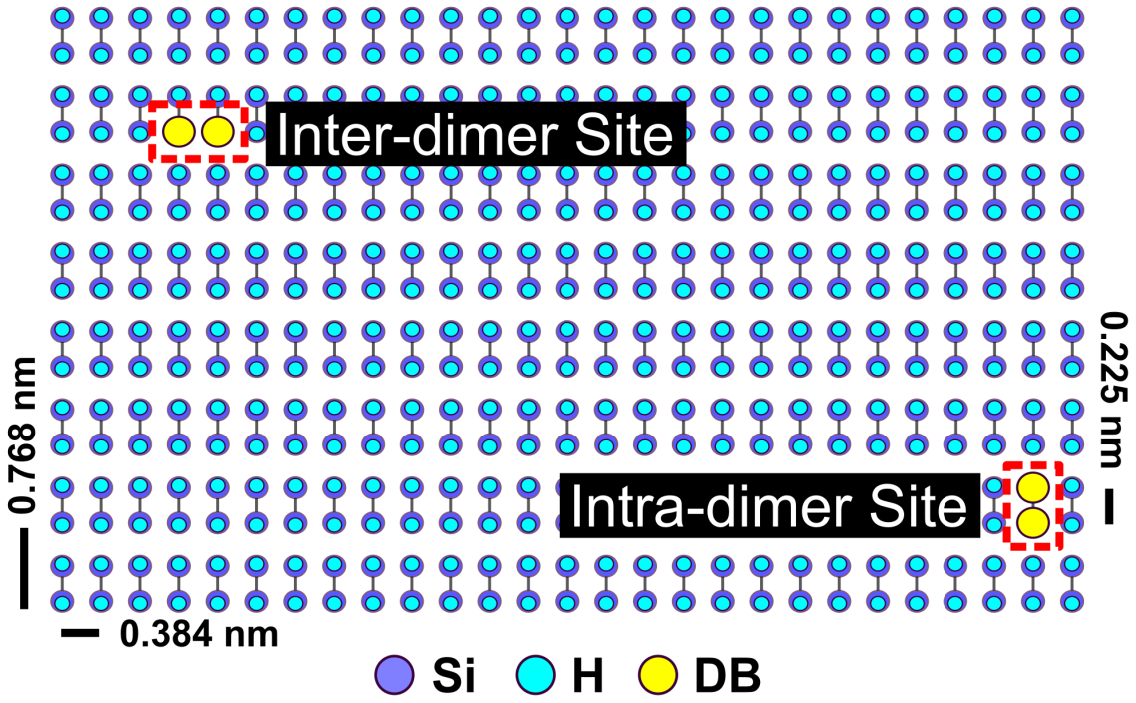

Figure 1.4: Schematic of the hydrogen-terminated Si(100)-2x1 surface. A schematic representation of the hydrogen-terminated Si(100)-2x1 surface viewed from above. The geometry of the inter-dimer and intra-dimer sites are indicated respectively.

The modern semiconductor industry is built upon silicon, and as such it is one of the most studied materials available. In the bulk, each silicon atom is bonded to four neighbouring atoms *via* sp^3 hybridization, forming a diamond structure. The distance between monolayers of atoms is 0.136 nm, which is given by a/4, where a = 0.543 nm is the lattice constant of the diamond cubic unit cell for silicon. By cutting the crystal along the appropriate plane, the (100) surface can be exposed. Here, the surface atoms can no longer form four bonds as in the bulk, leaving two exposed DBs per silicon atom. In order to reduce the number of unpaired bonds, the surface reconstructs into a 2x1 structure, where two adjacent atoms on the surface bond with

each other (forming a dimer), reducing the number of surface DBs by half [55, 59]. These remaining DBs on the surface can be passivated with hydrogen atoms to produce the hydrogen-terminated silicon(100)-2x1 surface (Figure 1.4) [59–61]. The hydrogen termination procedure is described in more detail in Sections 2.5.2 and 4.5.2.

Silicon is an indirect bandgap semiconductor with a bandgap energy of 1.12 eV at room temperature. At lower temperatures, this value increases slightly to a value of 1.17 eV near 0 K [62]. One of the reasons that semiconductors such as silicon are so versatile is that they can be doped to alter bulk and local electronic properties. With the appropriate selection of dopant type and doping concentration, the majority charge carrier can be varied between electrons for n-type and holes for p-type. Typical n-type dopants include arsenic and phosphorous, and typical p-type dopants include boron and gallium. During the preparation of the highly arsenic doped (approximately 10^{19} As atoms per cubic cm) hydrogen-terminated Si(100)-2x1 surface used in this thesis, the repeated heating to 1250 °C can cause the doping concentration near the surface to drop by over an order of magnitude [63]. The dopants in this region are isolated from the higher density of dopants deeper into the bulk (Figure 1.5), and remain un-ionized until perturbed by the STM tip field [64]. It is possible to reduce the level of dopant depletion by preparing the surface at lower temperatures. Another common preparation temperature is 1050 °C, which results in demonstrably different properties of DBs on the surface [39]. All samples in this work were prepared with a 1250 °C treatment.

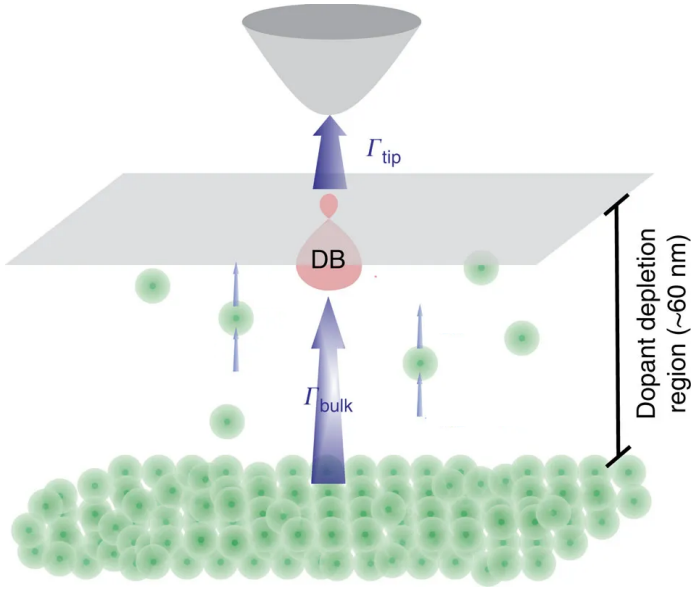

Figure 1.5: Dopant depleted region.
A side-view schematic of the dopant depleted region. During imaging, the filling and emptying rates of electrons from the bulk through the DB state into the tip, Γ, vary depending on the ionization state of nearby dopant atoms. The ionization state of the dopants depends on a competition between separate rates of electron filling from the bulk and the emptying into the tip. This figure was adapted from [64] with permission under the Creative Commons Attribution 4.0 International License.

1.4 Making a dangling bond (DB) in an STM

The removal of hydrogen from hydrogen-terminated Si(100)-2x1 surfaces with an STM tip has been studied in detail since the first demonstration of lithographic capabilities in the early 1990s [26, 27, 37, 42, 65–67]. There are two mechanisms available for hydrogen desorption with an STM tip, giving rise to two modes of operation: coarse lithography (with feature sizes larger than 1 nm) and atomically precise lithography (the type employed for HL). In coarse lithography mode the STM is operating in a field emission regime (bias greater than sample work function), and the Si-H bond can then be broken with direct excitations of electrons from the bonding to the anti-bonding state when the sample bias exceeds approximately

6 V [26, 68]. This type of lithography does not have the atomic resolution necessary to precisely remove individual atoms from the surface, but is ideal for creating larger patterns quickly [46, 65, 69]. Figure 5.5 shows an example of a desorption area created with coarse lithography.

To achieve atomically precise lithography, the STM tip can be used to break single Si-H bonds through multiple vibrational excitations of the Si-H stretch mode with low energy inelastic tunneling electrons (less than 3.5 eV) [26, 65, 70]. The excited lifetime for a Si-H stretch mode is relatively long (approximately 10 ns), requiring four phonons to relax [26, 71]. This allows for the possibility of acquiring enough energy from the small fraction (on the order of 10^{-3}) of inelastically tunneling electrons available from the large STM tunneling current to break the Si-H bond [26]. The lifetime of the excited stretch mode can change with temperature, altering the efficiency of hydrogen atom extraction (Si-H bond breaking). The highest efficiencies occur at temperatures below 10 K [26]. At higher temperatures the competition between excitations and dissipative pathways increases, reducing the likelihood of bond breaking and lowering desorption yields by as much as 300x at room temperature [26].

The lithography procedure implemented for all the work presented in this thesis to create single DBs at 4.5 K is as follows: First, the tip is positioned directly over top of the hydrogen atom to be removed at a bias voltage of $V = 1.4$ V and a current setpoint of $I = 50$ pA (the current can be increased to improve removal probability at the risk of uncontrolled tip changes). A 20 to 40 ms voltage pulse of 1.8 to 3.0 V is then applied, while locking the z position of the tip (feedback control disabled). Several automation routines have been created that greatly enhance the speed and ease with which DBs can be made. If the voltage pulse is unsuccessful at creating a DB, then the voltage is incremented by a fixed value (0.1 V) and another pulse is initiated. This procedure repeats until the successful creation of a DB is detected (Section 2.5.3). Voltage pulses near 1.8 V are preferred as higher voltages have an increased tendency to alter/damage the tip structure. These parameters would need to be adjusted for different temperatures, different doping levels [26, 27], and different surface passivations [26, 27, 72].

In spite of the atomically precise nature of HL, some sources of error lead to

imperfect lithography. One source of error that arises during fabrication is alignment of the STM tip with the hydrogen atom. As the tip is moved from site to site, thermal drift and piezo creep can cause uncertainty in its position. At 4.5 K thermal drift is minimal and the creep can be controlled to some extent by allowing sufficient settling time between large tip movements between hydrogen removal sites. Multi-apex tips, which can have more than one roughly equivalent "apex", can also introduce error during fabrication. Tunneling electrons from these additional apices may induce hydrogen desorption in an undesired location, rather than at the intended site. Because of this, it is imperative to work with atomically sharp single atom tips for reliable fabrication. However, the tip may become multi during the course of fabricating many DBs. A solution to this problem has been implemented by Rashidi *et al.*, where machine learning was used to train the software to recognize when the tip is not optimal for fabrication and initiate tip conditioning procedures until a suitably sharp single apex is achieved [73].

Aside from the creation of single isolated DBs, two DB structures that are commonly fabricated and referred to in this work are the inter-dimer site and the intra-dimer site. The inter-dimer site consists of two adjacent DBs along a dimer row. The intra-dimer site, also known as a bare dimer, consists of two adjacent DBs across a dimer row. Both sites are shown schematically in Figure 1.4.

1.5 General DB properties

Many fundamental explorations of DB properties have been undertaken to date, including systematic studies on the creation of single DBs *via* STM tip [26,27,37,65], and DB diffusion dynamics on the surface with temperature [28, 29]. Taucer *et al.* reported the first measurements of the single electronic dynamics of an isolated DB interacting with an STM tip [35], observing exponentially dependent electron filling rates into the DB with radial tip distance, and nearly constant emptying rates into the bulk silicon that were independent of tip distance. These results agreed well with the theory of non-equilibrium charging dynamics put forward by Livadaru *et al.* [74]. Controlled charge trapping in DBs has been observed on p-type samples [38],

although there is some debate surrounding these results.

A DB on the surface of hydrogen-terminated silicon is an unsatisfied sp^3 orbital of the underlying silicon atom, which extends into both the bulk and vacuum [74]. The DB can be thought of as an atomic quantum dot, introducing a single surface state within the silicon band gap that is capable of localizing a maximum of two electrons to achieve a positive, neutral, and negative charge state [35]. As with any electronic level, the occupation of the DB level depends on its relative position to the sample Fermi-level, which can be altered by the local potential landscape [75] and interaction with the STM tip through tip-induced band bending and charge injection [35]. Alternatively, the position of the Fermi-level can be altered through variation of doping type and concentrations to set the unperturbed charge character of surface DBs in absence of the STM tip.

The location of the DB level in the gap is of particular importance in device applications, as it is largely electronically decoupled from the bulk semiconductor. The energy above the silicon valence band (VB) at which the DB transitions between charge states is not known exactly, and the energy of the DB level depends on its charge [74]. Estimates of the energy of the DB level when it is negative and neutral have been made [20, 35, 74, 76, 77]. It was found that the DB level is approximately 0.85 eV above the silicon VB when the DB is negative (containing two electrons), and approximately 0.35 eV above the VB when it is neutral (containing one electron) [35, 74].

When the tip is over a DB at a negative sample bias (filled states), the current through the DB into the STM tip depends on the competition between how fast electrons from the bulk conduction band can replenish the DB level and how fast they are being withdrawn by the tip (Figure 1.5). The filling rate of electrons into the DB level depends on the local electrostatic environment of the DB, which can be altered by the ionization of nearby dopant atoms. When a dopant atom is ionized due to the STM tip field, the induced change in electrostatic landscape increases the filling rate of electrons into the DB level, which in turn increases the current into the STM tip [64]. This is discussed in more detail in Section 4.3.1. Such an ionization event can be observed as a sharp turn-on of current in the $I(V)$ spectrum taken over

a DB. The $I(V)$ measurement is performed by holding the tip at a fixed z position above the DB and sweeping the voltage.

In regard to the thermal stability of DB structures, experiments have measured DB surface diffusion at elevated temperatures with STM techniques. It was determined that there is a minimum energy barrier of 1.4 eV for diffusion in any direction along the surface [28, 29].

1.6 Layout of thesis

Following this introductory chapter the thesis consists of two published chapters (Chapter 2 and Chapter 4) that are each respectively followed by chapters that extend their discussions and details (Chapter 3 and Chapter 5). Final thoughts, extensions, and conclusions are then given in Chapter 6.

Chapter 2 reports on the improved automation of HL, the realization of STM-based HR, and the implementation of both to create ultra-high density rewritable memory. The fabrication results of Chapter 2 builds upon a tremendous body of foundational work on hydrogen-passivated Si(100)-2x1. This includes the early work, as described in Section 1.4 and Section 2.2, in addition to the local knowledge, expertise, and innovations of the entire research group including: Dr. Robert Wolkow, Taleana Huff, Mohammad Rashidi, and Marco Taucer. Marco Taucer began the automation of atomic-scale fabrication, working to develop the backbone of the current software (Figure B.1). Mohammad Rashidi and I then continued the development together to refine the process even further towards perfect fabrication (Figure B.2). This was an ambitious goal as there were several sources of error that needed to be addressed (Section 1.4). The discovery of error correction using an AFM by Huff *et al.* [25] really relaxed this constraint and spurred on the development of the same functionality for STMs, which had been lacking for decades, leading to the ability to make perfect structures (Figure B.3).

Chapter 4 reports on the development of new tools for the STM on hydrogen-terminated Si(100)-2x1. The previously reported HR technique was improved by using hydrogen molecules instead of atoms, and then was applied to improve prac-

tical aspects of ultra-high density data storage as well. The ability to characterize charge within DB structures was demonstrated, along with the ability to detect single molecule binding events. The charge characterization and molecular detection results of Chapter 4 also builds upon previous work of the group. The insights and understanding that Rashidi *et al.* developed related to the STM tip-field ionization of dopant atoms [64] were integral in the development of both schemes. The characterization of the charge occupations of DB structures with AFM by Huff *et al.* [5] was also important in verifying the reliability of STM-based charge characterization.

Chapter Two

Lithography for robust and editable atomic-scale silicon devices and memories

Authors: Roshan Achal[1,2], Mohammad Rashidi[1,2], Jeremiah Croshaw[1,2], David Churchill[3], Marco Taucer[1,2], Taleana Huff[1,2], Martin Cloutier[4], Jason Pitters[2,4], Robert A. Wolkow[1,2,4]

[1]Department of Physics, University of Alberta, Edmonton, Alberta, T6G 2E1, Canada
[2]Quantum Silicon, Inc., Edmonton, Alberta, T6G 2M9, Canada
[3]Memorial University, St. John's, Newfoundland, A1B 3X5, Canada
[4]Nanotechnology Research Centre, National Research Council of Canada, Edmonton, Alberta, T6G 2M9, Canada

Author contributions: R.A. conceived the memory design and hydrogen repassivation procedure. R.A., M.R. and J.C. performed the experiments to test the procedure and collect hydrogen repassivation curves. R.A., T.H. and M.R. discussed methods of repassivation. R.A. fabricated all structures presented in the manuscript. M.R., R.A. and J.C. developed automated hydrogen repassivation. J.P., M.C., M.T., M.R., R.A. and T.H. developed automated hydrogen lithography software. D.C. and R.A. developed memory readout. R.W. supervised the project. R.A. and M.R. prepared the manuscript. All authors participated in review of the manuscript.

This chapter has been reproduced from the original manuscript published by Nature Communications under the Creative Commons Attribution 4.0 International License. The full manuscript is available at: https://www.nature.com/articles/s41467-018-05171-y [Open Access] [10]. The article was placed in Nature Communications' top 50 physics collection of 2018, ranking 18th. I was not sure where else to put this image they gave me, so here it is!

2.1 Abstract

At the atomic scale there has always been a trade-off between the ease of fabrication of structures and their thermal stability. Complex structures that are created effortlessly often disorder above cryogenic conditions. Conversely, systems with high thermal stability do not generally permit the same degree of complex manipulations. Here, we report Scanning Tunneling Microscope (STM) techniques to substantially improve automated hydrogen lithography (HL) on silicon, and to transform state-of-the-art hydrogen repassivation into an efficient, accessible error correction/editing tool relative to existing chemical and mechanical methods. These techniques are readily adapted to many STMs, together enabling fabrication of error-free, room-temperature stable structures of unprecedented size. We created two rewriteable atomic memories (1.1 petabits per in^2), storing the alphabet letter-by-letter in 8 bits and a piece of music in 192 bits. With HL no longer faced with this trade-off, practical silicon-based atomic-scale devices are poised to make rapid advances towards their full potential.

2.2 Introduction

The first demonstration of controlled atomic manipulation [16] fostered a vision of practical atomic-scale devices. Today, with recent innovations exhibiting control over approximately 8000 atomic sites [9] this vision is slowly materializing. Yet realization of functional atomic-scale devices outside of the laboratory has been limited by their instability at room-temperature [9, 16] and their poor electronic isolation from supporting substrates [19, 78]. Hydrogen lithography (HL), the removal of hydrogen atoms (depassivation), on hydrogen-passivated silicon surfaces is becoming an important technique in next-generation device designs [6–8, 25, 33, 79, 80]. These designs have potential to surmount both limitations [5, 28, 29] without introducing materials incompatible with current semiconductor fabrication processes [32, 36, 37]. Many disruptive applications have been proposed based on HL such as single atom transistors [7], quantum computing platforms [6, 8, 79, 80], and atomic-scale logic devices [19, 25], drawing both scientific and commercial interest alike. Several companies have even formed upon this and related techniques [5, 32, 79]. Overall device development has been delayed, however, by the inability of HL to fabricate large error-free atomic-scale structures [32–34, 37, 40, 66, 81], increasing the need for reliable error correction techniques.

The atomically precise removal of hydrogen from hydrogen-passivated silicon surfaces *via* a Scanning Tunneling Microscope (STM) tip has been studied extensively for HL [32, 37, 65, 68, 81]. A select Si-H bond is broken using low energy inelastic electron scattering, exposing a dangling bond (DB) of the underlying silicon atom [37, 65, 68]. The DB can be thought of as an atomic quantum dot, capable of localizing two electrons, with its electronic states isolated within the silicon band gap [35, 40]. DBs present an ideal platform for new technological applications [6–8, 25, 40, 64, 79, 80] because of this electronic isolation and their stability at temperatures near 500 K [28, 29], overcoming two major hurdles for practical implementation of atomic-scale devices [19]. Beyond that, the placement of DBs with atomic precision and their ability to couple to one another enables delicate control over their properties and electronic occupation [20, 25], permitting engineering

of quantum states [6, 40] and artificial molecules [19, 40]. Precise HL also offers a route to other atomic-scale and molecular devices through atomically site-selective chemical templating [7, 8, 19, 79, 80].

Although HL has been incrementally improving over time, the path towards perfect large-scale structures and the full realization of silicon DB-based devices has been unclear [32, 36, 37, 40, 65, 66]. Increasing atomic precision during HL was the main focus of efforts [66], since any hydrogen removed in error could render structures inoperable. Non-site-specific chemical repassivation of DBs has been observed [82], but without the means to deterministically repair mistakes, this strict requirement of 0% error has hindered the development and prototyping of novel device designs [7, 19, 25, 41]. A means to controllably correct errors was recently shown using a cryogenic atomic force microscope (AFM), where individual DBs were repassivated with a hydrogen-functionalized tip [5, 33]. While a striking demonstration of atomic control, the utility of this technique is limited as the reported repassivation procedure is slow (approximately 10 s per DB) [5], reducing its practicality for larger structures. The frequency shift signal utilized in AFMs requires two independent feedback loops, restricting the maximum speed of the overall process. This procedure is further slowed by the need to re-functionalize the tip with hydrogen in between each event [5, 33]. Existing methods of hydrogen deposition onto a silicon surface with an STM tip [83, 84] are unsuitable to edit or correct DB-based devices. They involve harsh parameters capable of damaging fabricated structures or the tip itself [66].

Here, working at 4.5 K we demonstrate straightforward STM methods for automated HL and hydrogen repassivation (HR), which do not significantly alter tip structure. Controlled application of voltage pulses are used for lithography, while repassivation uses linear tip movement towards the sample surface under small applied bias voltages. In both techniques the STM feedback controls are suspended, employing changes in tunneling current as the only signal. We discovered two unique signatures in the STM tunneling current associated with successful HR events. When implemented as control signals, they will increase the viability of rapid fully automated error correction. In conjunction, HL and HR techniques substantially advance

our fabrication abilities towards functional atomic-scale devices. To illustrate their precision and practicality we created functional 8-bit and 192-bit rewritable atomic memory blocks from DBs with the highest reported storage density to date [9, 41].

Interest in atomic memory has been reignited with foundational work on chlorine-passivated Cu(100), establishing a sophisticated scanned probe architecture to create a kilobyte of memory from surface vacancies, without the need to vertically manipulate atoms [9]. The memory operates near 77 K, where it remains stable for at least 44 hours [9]. There are several key features of DB-based memories that allow us to push atomic-scale storage even further than this already substantial progress. Patterned DB structures exhibit improved thermal stability, remaining stable for an additional 400 K above liquid nitrogen temperature [28, 29]. The maximum storage density of memory blocks can be increased by 32%, as DBs can be placed in close proximity to one another. In addition to density, the number of available bits is not predetermined at the time of sample preparation [9]. DBs can now be created or removed as needed using HL and HR (assuming a sufficient supply of hydrogen atoms), theoretically allowing the entire hydrogen-terminated surface to be written to. Creating additional vacancies/bits in the Cu(100) system is currently not possible without damaging the STM tip [9]. Furthermore, a semiconducting substrate as opposed to a metallic one opens the possibility of interfacing with integrated electronics, whether at the atomic-scale or using more conventional nanofabrication.

2.3 Results

2.3.1 Hydrogen lithography

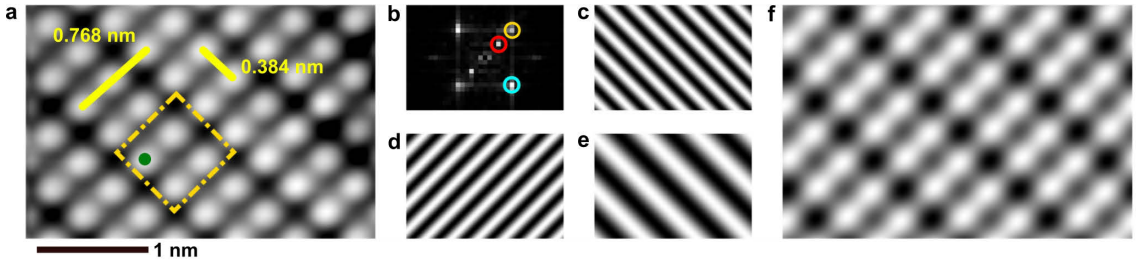

Figure 2.1: Surface geometry of hydrogen-passivated Si(100)-2x1. **a**) (V = 1.4 V, I = 50 pA, T = 4.5 K, 2 x 3 nm^2) Scanning Tunneling Microscope (STM) image of hydrogen atoms bonded to the Si(100)-2x1 surface. The distance between identical sites along and across a dimer row are shown in yellow (solid). The surface geometry allows for the creation of single atom bits at ultra-high densities. The area of one bit (including spaces between atoms), 0.590 nm^2, is outlined in yellow (dashed), and is defined as a binary zero. The hydrogen atom denoted with a dot (green) is removed with an STM tip to create a dangling bond, changing the bit to a binary one. **b**) 2D Fourier transform (power spectrum) of **a**, where the three dominant spatial frequencies have been isolated. **c**-**e**) Filtered STM images of **a**, for each dominant frequency (peak) shown in **b**, (**c** bottom peak (blue), **d** top peak (yellow), **e** middle peak (red)). **f**) The resulting image from the sum of frequencies shown in **c**-**e**, reconstructing the essential features of the STM image shown in **a**, allowing for the position of each surface hydrogen atom to be determined.

To begin automated HL, the location of every hydrogen atom in a select area needs to be determined for accurate STM tip registration during fabrication. Slight errors in the tip position can result in incorrect atoms being removed. Fast, fully autonomous lithography also requires the location of each atom to be known, such that the surface doesn't need to be reimaged after each removal event to determine the next site. The periodicity of the hydrogen-passivated Si(100)-2x1 surface (Figure 2.1a) permits the location of every hydrogen atom to be determined from a single STM image (while accounting for nonlinearities in the scanner) through the use of

Fourier analysis [85] (Figure 2.1b-f). Such an analysis is relatively immune to the presence of small surface defects and DBs due to their spatially localized nature in the images compared to the extended periodicity of the surface itself. Figure 2.1 illustrates the basic features of this process. In practice, we use images between 10 $\times$ 10 nm^2 and 40 $\times$ 40 nm^2 to determine the location of the hydrogen atoms on a given sample terrace. Once the surface has been characterized, the desired pattern is mapped onto the lattice. Next, the tip is brought over each lattice site of the pattern and 20 ms voltage pulses between 1.8 and 3.0 V are repeatedly applied at a fixed tip-height ($V = 1.4$ V, $I = 50$ pA) until the successful removal of hydrogen has been detected. Figures 2.2a,b,d show the process of building DB structures (Figure 2.2e) with HL while using HR to correct errors (Figure 2.2c). Unlike conventional HL [37, 86], the STM feedback control is disabled during the voltage pulses. This allows jumps in the tunneling current to be used as an indicator of success [36], which can be detected faster and more accurately than jumps in tip-height through the feedback circuitry (see Methods).

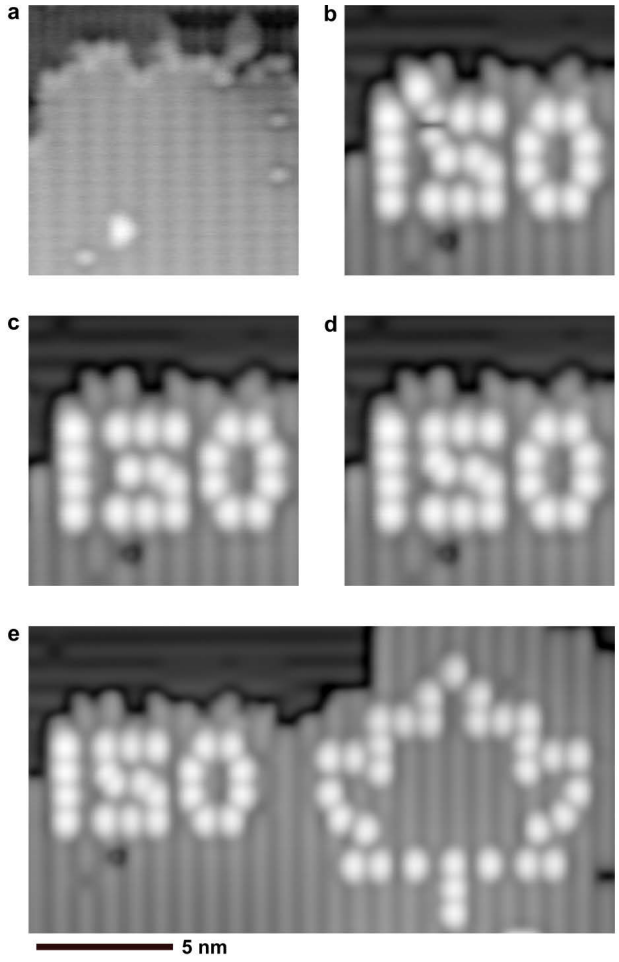

Figure 2.2: Fabrication and correction on hydrogen-terminated Si(100)-2x1 *via* hydrogen lithography and hydrogen repassivation.
a) (V = 1.4 V, I = 50 pA, T = 4.5 K, 10 x 10 nm^2) Scanning Tunneling Microscope image of the fabrication area used to determine the location of each hydrogen atom through Fourier image analysis. **b**) (V = -1.7 V, I = 50 pA, T = 4.5 K, 10 x 10 nm^2) Fabrication of the characters "150" using hydrogen lithography (HL), one atom has been removed in error above the characters and one atom is incorrectly placed inside the "5". The created dangling bonds (DBs) appear as bright protrusions. **c-d**) Using the hydrogen repassivation technique, the errors were subsequently erased, then the correct hydrogen atoms were removed with HL to create an error-free structure. **e**) (V = -1.7 V, I = 50 pA, T = 4.5 K, 11 x 21 nm^2) The completed structure of 54 DBs, depicting the characters "150" and a maple leaf.

Using this procedure, the probability of detrimental uncontrolled apex changes is low. By beginning removal attempts at 1.8 V (see Methods), higher voltages, which are more likely to change or damage the tip, are only reached when necessary. Conservatively, on the order of 10 DBs can be created consecutively without some type of minor modification to the tip. However, we have found that HL efficiency is not particularly sensitive to minor changes of the tip, so the actual number of DBs that can be created without altering removal efficiency during fabrication is often larger. Should the tip change so much that it is no longer suitable for HL purposes, an automated tip forming routine can be called to recondition the tip through controlled contact with the surface [73]. This routine takes advantage of a machine learning algorithm, and STM image data for training sets, to automatically identify the quality of the probe by imaging a DB, initiating reconditioning when necessary [73].

An important consideration inherent in all scanned probe lithography is the existence of thermal drift and creep, both of which can also cause uncertainty in the position of the tip, leading to errors. At 4.5 K these factors can be well controlled by allowing the STM to stabilize over a period of several hours. However, at warmer temperatures or in situations where allowing the STM to stabilize is not an option, a more active solution is required. To address these factors, we implemented periodic image realignments into the HL workflow. Before initiating the HL procedure, an area near the lithography location (around 10×10 nm^2) is imaged as a reference. After a set time, lithography is paused, and this area is reimaged to determine how much the tip has been offset from its intended position due to creep and drift. The remaining sites in the pattern are shifted appropriately to compensate and lithography resumes. The effectiveness of this realignment can be increased by reducing the interval between reference checks, permitting an optimization between speed and accuracy depending on a given application. We found that without realignment the lithographic accuracy during HL using a non-stabilized STM was near 35% for a particular structure. Under the same conditions using moderate active realignment it was over 85%, which is within a suitable range to then correct the remaining errors using HR.

2.3.2 Hydrogen repassivation

To correct errors, we use the STM tip to address individual lattice sites with atomic precision to repassivate select DBs (Supplementary Figure 2.5). *Ab initio* calculations have revealed that certain silicon terminated tips with a hydrogen atom bonded to the apex (functionalized) are capable of repassivating DBs [54]. Through controlled contact of the STM tip with the surface during tip-conditioning, silicon atoms may become affixed to the tip to form the necessary structure for HR [5,33,54]. When the tip becomes functionalized with a hydrogen atom there is a change in STM imaging resolution [5,33]. With a functionalized tip, the first step of HR is to position it over a DB at a sample voltage of 1.4 V and current of 50 pA. The feedback control is then disabled, and the sample voltage is changed to a value between 100 mV and 1.0 V. While recording the tunneling current, the STM tip is brought 500 to 800 pm towards the sample, then is retracted to its original position. The voltage is reset to the original value of 1.4 V and the feedback control is restored. This entire process, once a user has selected a site, has been automated, taking approximately 1 s. It can be initiated at the press of a button and repeated until a successful repassivation signature is observed. Work is underway to integrate this new HR process within the HL workflow to enable fully autonomous fabrication and correction. Errors will be automatically detected *via* image recognition, and subsequently corrected using the HR technique (see Methods).

A necessary element for the implementation of fully automated HR is the existence of a reproducible, easily distinguished, signature indicative of successful repassivation, much like the jump in tunneling current used during HL. We usually observe a sudden increase in the tunneling current while approaching the surface when a DB is successfully repassivated that is not present as the tip retracts (Figure 2.3a). The measured current is related to the overlap of the imaging orbital of the tip, and orbitals of features on the surface [24,37]. We associate this signature (type-I) with the removal of a hydrogen at the tip apex and a return to pre-hydrogen-functionalized imaging resolution. The increase in current is possibly due to the new apex orbital having a larger spatial extent, creating a greater overlap between the tip and sample

surface compared to that between a DB and a hydrogen-functionalized tip (held at the same tip-sample separation).

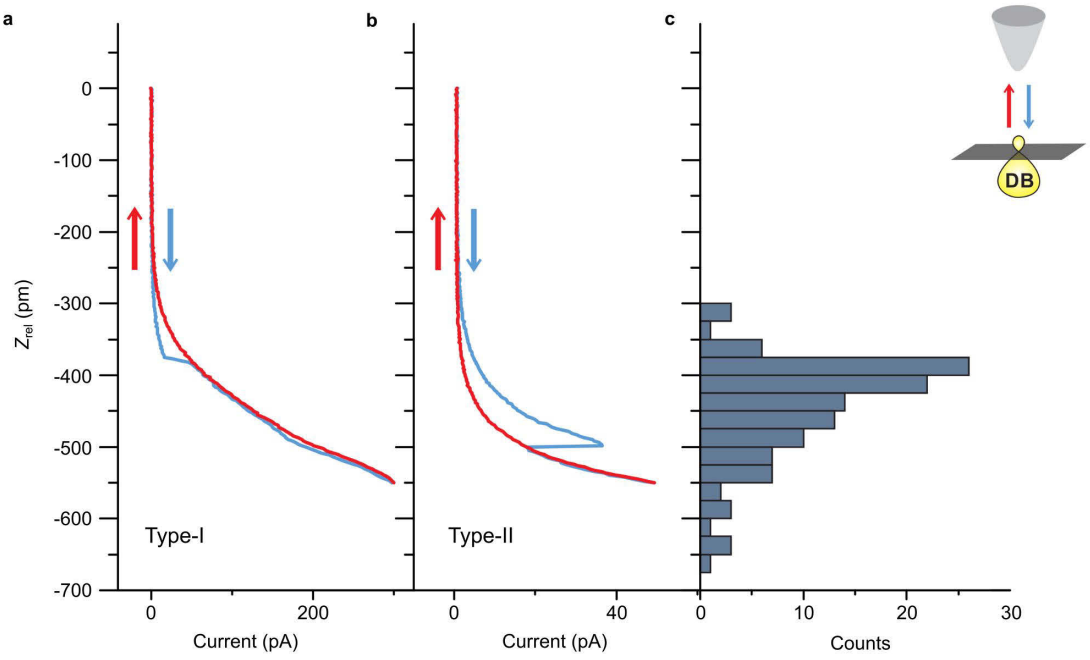

Figure 2.3: Tunneling current signatures of hydrogen repassivation and the number of successful events with tip approach distance.
a) ($V = 0.4$ V, $T = 4.5$ K) The recorded tunneling current as the Scanning Tunneling Microscope (STM) tip (set over a dangling bond (DB) at 1.4 V and 50 pA) is brought towards the surface (blue) and as the STM tip is retracted (red) during hydrogen repassivation (HR). A sudden increase as the tip approaches the surface can be observed in the tunneling current (blue), indicating a successful HR event. This signature (type-I) is typically associated with a change in STM imaging resolution, and a removal of hydrogen from the tip apex. **b**) ($V = 0.2$ V) A second distinct signature (type-II) has also been observed during HR, with a sudden decrease in tunneling current during the approach towards the surface (blue). This type-II signature is not typically associated with a change in STM imaging resolution. **c**) The tip approach distance where either signature occurred was recorded for 119 unique HR events. Nearly 90% of events occur before 550 pm. The inset depicts the STM tip approaching a DB on the surface.

Following the same HR procedure with a tip that is not functionalized, we have found it is also possible to repassivate DBs with no associated change in imaging resolution. Since STM imaging resolution is particularly sensitive to changes in the tip apex orbital [5, 24, 37], we assume the imaging orbital is unchanged and that the hydrogen atom comes from the off-apex region. In addition to functionalization there are several mechanisms through which atomic hydrogen may be available on the (off-apex) surface of a tip for HR. The surface of silicon terminated tips can become passivated with hydrogen [54], allowing atomic hydrogen to physisorb on top [5] (see Supplementary note 2.6.1, Supplementary Figure 2.6). If the tip is not silicon terminated, it has been shown that hydrogen is also capable of physisorbing on the surface of some metallic tips [83, 84, 87]. Since the precise structure of the tip is unknown, the available hydrogen on the tip is likely due to a combination of these mechanisms. We have found that the STM tip can be loaded with hydrogen atoms through the creation of several DBs (far from the current structure) using HL [5]. We observed that an average of three DBs (to a maximum of five) can be repassivated successively, without the need to load the tip with additional hydrogen (Figure 2.4a). During HR, when the DB is repassivated with an off-apex hydrogen we see a second signature in the tunneling current (type-II), a sudden decrease (Figure 2.3b) (also observed during HR at 77 K, Supplementary Figure 2.7). The sudden drop in current is due to a reduction in overlap between the tip and sample. DBs appear as bright protrusions on the sample surface (Supplementary Figure 2.5b) compared to the surrounding hydrogen (orbital more spatially extended towards tip). There is a decrease in the size of the surface orbital after the DB has been repassivated, which reduces overlap/current, as the tip orbital remains unaltered.

Unlike the type-I process, which theoretically relies on a particular tip state to enable the transfer of hydrogen [54], the type-II process appears to be much less restrictive. We have been able to observe type-II HR events even after impressing the tip approximately 1 nm into the sample surface. Both processes have been observed and reproduced on a number of physically different tungsten tips, during the fabrication of numerous different structures. The structures in Figure 2.2 and Figure 2.4 were created using different tips for example. We recorded the location of type-I

and type-II signatures in the tunneling current for 119 successful HR events collected using seven different tips (see Supplementary Figure 2.8 for additional recordings). Figure 2.3c shows the distribution of distances the tip traveled towards the surface for HR to occur. The majority of events (around 90%) occur before moving 550 pm. Closer tip approaches have an increased tendency to change the tip structure. This value provides an ideal parameter for fully automated HR, optimizing the probability of repassivation while mitigating that of harmful apex changes.

During our observations we noted that when a tip is hydrogen-functionalized, as indicated by a change in STM imaging resolution, it is still possible to transfer an off-apex hydrogen to the surface (type-II signature) without altering the apex itself (leaving the tip functionalized). That is, with a hydrogen-functionalized tip, it is not guaranteed to first remove the apex atom and observe a type-I HR signature, as an off-apex hydrogen may be more mobile and easily transferred to the surface first, causing a type-II HR signature. We have also never observed sequential type-I signatures without deliberately re-functionalizing the tip in between HR attempts, suggesting the tip is unable to functionalize spontaneously with off-apex hydrogen. This observation is consistent with experimental imaging data, where spontaneous changes in image resolution with a tip suitable for HL/HR are rare.

With the ability to know when a tip is hydrogen-functionalized, and when the apex atom has been removed, it may now be possible to correlate $\mathrm{d}I/\mathrm{d}V$ spectroscopy curves over hydrogen-terminated silicon with the specific tip states necessary for hydrogen transfer to occur [54] (type-I). If such a correlation is found, $\mathrm{d}I/\mathrm{d}V$ spectroscopy would provide a new, more rapidly acquirable metric to determine if the tip is suitable for HR. These curves could then be used as training data in the automated tip forming routine to always ensure the tip is in the required state, without the need to take an entire STM image [73].

2.3.3 Atomic-scale memories

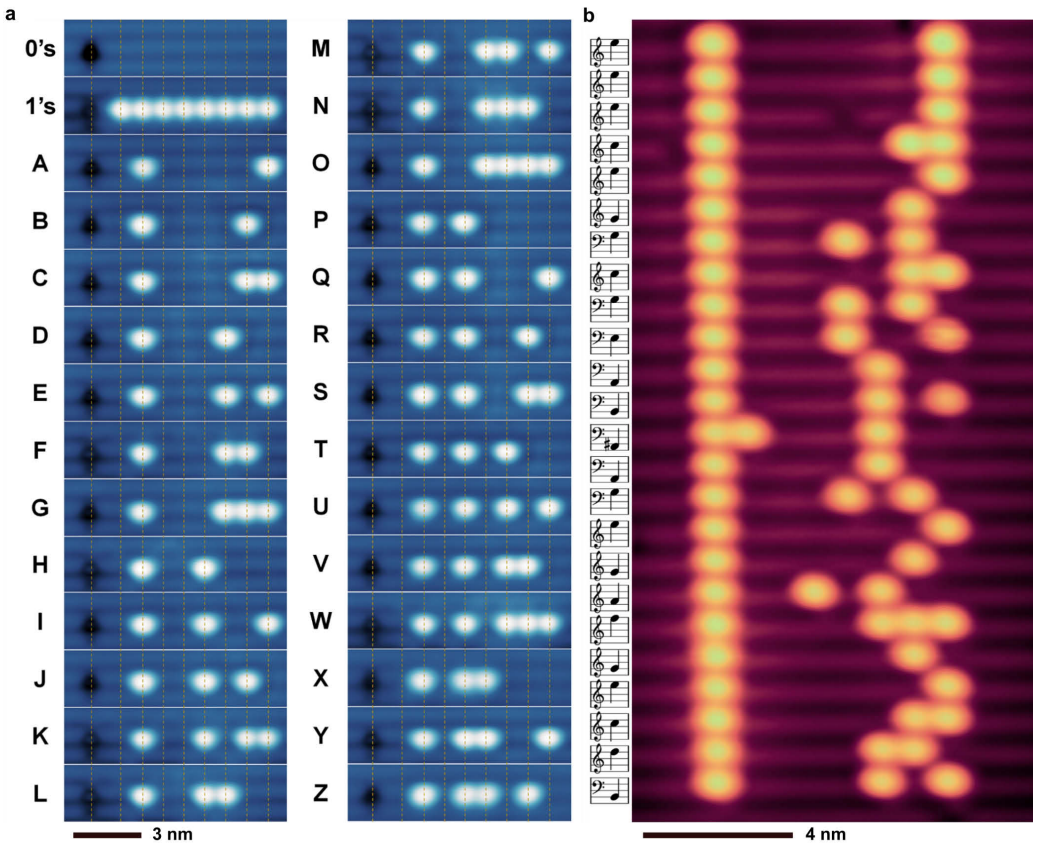

Figure 2.4: 8-bit and 192-bit atomic rewritable memories.
a) (V = -1.75 V, I = 50 pA, T = 4.5 K, 2.4 x 10 nm^2) Scanning Tunneling Microscope (STM) images of a rewritable 8-bit memory constructed from dangling bonds (DBs). The DBs appear as bright protrusions in the images, the black defect is an area of missing silicon. The letters of the English alphabet were converted to their ASCII binary forms (e.g. A=01000001) and written to the same area using hydrogen lithography and hydrogen repassivation techniques. An average of three bits could be repassivated sequentially between the letters shown. **b**) (V = -1.8 V, I = 50 pA, T = 4.5 K, 21.5 x 10.7 nm^2) An STM image of an expanded 192-bit memory, storing 24 simplified notes (converted into binary) of the popular Mario videogame theme song. The notes consist of 62 DBs, forming the largest error-free DB structure to date. Both memories have a bit density of 1.70 bits per nm^2 and can be read directly from the STM or from a stored image.

We used HL combined with HR to create two different working atomic-scale memories (Figure 2.4). We defined a bit with four lattice sites, giving a one atom buffer between neighbouring DBs (Figure 2.1a). Due to the ideal geometry of the hydrogen-passivated Si(100)-2x1 surface, this arrangement yields an extremely high bit density of 1.70 bits per nm^2. Conservatively estimating a 20% reduction in storage density to integrate practical control architecture, this system still provides the highest density solid-state storage medium available. We used the 8-bit memory to sequentially encode the ASCII binary representation of each letter of the English alphabet, overwriting the previous letter each time (Figure 2.4a). Writing each letter took between 10 and 120 seconds, depending on how many DBs needed to be created and repassivated. Random changes in the tip apex occurred infrequently, altering HL and HR efficiencies, remedied through controlled contact of the STM tip with the surface to condition the apex structure. The HR stage is currently the slowest step, limited by the number of available hydrogen atoms on the surface of the tip. Moving away from the structure to reload the tip after repassivating several DBs introduced a significant delay. This may only be a factor for structures with a small number of DBs, like those we have presented. With structures requiring more DBs there will be a continued source of hydrogen to the tip as each new DB is created (equivalent to the reloading procedure). With enhanced automation to incorporate periodic intervals for HR/error correction during HL the need to travel away from the structure to reload the tip can be reduced or altogether eliminated. Further improvements to HR speeds may be possible through tip materials like platinum, which is able to hold at least 1000 atoms of hydrogen on its surface [84].

We created a larger 192-bit memory with the same bit density, encoding the iconic notes (simplified) of the Mario videogame theme song (Figure 2.4b). This 62 DB arrangement took 250 s to create, and represents a leap forward in HL capability. We can read the 192-bit memory directly from the STM as the tip scans over the structure, or later from recorded images (see Supplementary Movie 2.6.2). The room-temperature stability of DB structures has already been well established in prior works [19, 20, 32, 41, 81]. DBs on the surface of silicon are known to face barriers to diffusion in excess of 1.4 eV in either direction [28, 29]. Taking an exponential

prefactor of A = $2{\cdot}10^{14}$ s^{-1} and the lowest energy barrier of 1.46 eV [29] (intra-dimer diffusion), a DB is expected to experience only one hop in over 500 years due to thermally activated processes at 300 K. Such stability and density make DB-based memories a unique candidate for data archival and long-term storage.

Held at 4.5 K we detected no unintentional changes in the memory at the end of 72 hours of observation (Supplementary Figure 2.9). In this environment, we have worked with samples that have shown no significant surface degradation after half a year. The ultra-high vacuum requirements may also eventually be relaxed as isolated DBs can be protected against spontaneous reactions through the appropriate choice of doping level of the silicon substrate. Highly doped n-type silicon results in negatively charged DBs, which have a barrier to reaction with closed shell species [88]. There is also only a subset of entities that are known to readily react with DBs [82,88–90]. Molecular hydrogen, which is commonly present in vacuum environments, requires two directly adjacent DBs along a dimer row for adsorption [91], reducing the likelihood of spontaneous repassivation of isolated DBs at greater separations (as in the memory) due to ambient gas. The inability to eliminate all naturally occurring DBs during sample preparation in an environment of $1{\cdot}10^{-6}$ Torr of hydrogen gas, or with intentional chemical dosing further supports this notion [82].

2.4 Discussion

While these new HL and HR techniques are in their infancy, we demonstrated their immediate utility and applications by creating and editing large error-free DB structures through accessible STM-based means. Both these techniques can be implemented on many STMs with no modifications, operating over a range of temperatures. Though the exact parameters reported here are specific to hydrogen-terminated silicon, they can be adapted to other chemically similar systems such as hydrogen-terminated germanium [31,92], hydrogen-terminated diamond [92,93], and chlorine-terminated silicon [94]. There is also the potential to eventually extend these protocols to room temperature, as forms of HL have already been successfully demonstrated there [20,37,65,66], and the uncontrolled transfer of hydrogen from an STM

tip to a DB has been observed for HR [89]. However, fabricating structures/devices at cryogenic temperatures (where creep and thermal drift are not as pronounced) for use at room-temperature may already be sufficient for many applications. Further, the high-temperature stability of DBs removes one of the logistical issues surrounding the transportation of fabricated nano-devices to an end user, regardless of the temperature required for their operation.

Together, HL and HR unlock an array of new possibilities including the creation of hundreds of precisely placed identical qubits for quantum computation [6], the realization of room-temperature stable atomic-scale memory, and the long sought-ability to controllably create regions with no DBs [82]. HR can also augment the yield of existing commercial fabrication methods for multi-atom-wide DB structures, where patterned edges are prone to errors [32, 34, 66]. As these HL/HR techniques mature they will play an integral role in accelerating the progress of many of the proposed disruptive technologies [7, 8, 25, 33, 79, 80]. Supported with methods of preserving the surface outside of vacuum [36, 95], along with efforts in parallelizing scanned probe fabrication [96], these techniques bring the vision of practical atomic-scale devices one step closer to reality.

2.5 Methods

2.5.1 Experimental setup

We took all measurements with a commercial low-temperature Omicron LT-STM operating at either 4.5 K or 77 K. The base pressure inside the STM ranged from $3{\cdot}10^{-11}$ to $7{\cdot}10^{-11}$ Torr. The STM tips consisted of a polycrystalline tungsten wire (50 μm diameter), electrochemically etched in a solution of 2 M NaOH. The tips were then processed under ultra-high vacuum (UHV) conditions to further clean and sharpen them [52].

2.5.2 Sample preparation

We first degassed a highly arsenic-doped Si(100) (0.003-0.004 ohm-cm) sample at 600 °C in UHV for 24 h to remove any adsorbed water. We then resistively heated the sample *via* rapid flashes to 1250 °C several times to remove all native oxide. Following that, we exposed the sample to $1{\cdot}10^{-6}$ Torr of hydrogen gas. A nearby tungsten filament held at 1900 °C was used to crack the gas into atomic hydrogen. We exposed the sample to the gas for 120 s with no heating, then rapidly flashed it to 1250 °C, after which we quickly brought the temperature down to 330 °C for 150 s to achieve the desired hydrogen-terminated 2x1 surface reconstruction. The sample remains in the preparation chamber for up to 15 minutes as the pressure slowly returns towards the initial base pressure.

2.5.3 Automated hydrogen lithography

The HL program was designed in-house, including a graphical user interface for atomic pattern input. An artifact-free positive sample voltage STM image of the working area is first analyzed to determine the position of each atom through a 2D-Fourier Transformation (2DFT), extracting the dominant spatial frequencies of the surface from the power spectrum. This method accounts for nonlinearities in the STM motors as each directional motor (x and y) may have slightly different responses to an applied voltage, which can be recovered in the spatial frequencies. Additionally, the angle of each sample may differ slightly, and this information is also present within these 2DFT data. After the surface is characterized, a desired device design or pattern may be input *via* the graphical user interface to be mapped onto the surface. Once a pattern has been mapped onto each hydrogen atom the HL procedure initiates. With the STM feedback controls on (I = 50 pA, V = 1.4 V) the tip is brought over the first site in the pattern. The feedback controls are then suspended, fixing the tip-height over the site. The tunneling current is recorded for reference, and approximately 20 ms voltage pulses are applied in the range of 1.8 to 3.0 V. The number of attempts (N) at each voltage, and the voltage increment can be set beforehand. Typical values are N=10 with a 0.01 V increment. During the

voltage pulse phase, the tunneling current is sampled immediately after each applied pulse and compared to the reference value. If the measured current is 60% larger than the reference value, it is deemed a successful hydrogen removal event. With this technique false detections have been brought well below 0.5%, with most fabrication runs producing no false detections. After a successful hydrogen removal, or after the maximum number of pulses has been reached (unsuccessful removal) the feedback controls are restored, and the tip is brought to the next site in the pattern (following a raster path) where the process repeats.

In an effort to better control drift and creep, after a set number of HL events a routine can be called to check tip alignment with a reference STM image. If any misalignment is detected [97], the remaining pattern is shifted appropriately so the next locations for atom removal are again centred over their corresponding atom. The patterning-realignment cycle can continue until the pattern is complete. The image realignment can detect sub-nanometer shifts between images.

2.5.4 Automated hydrogen repassivation

The tip is set directly over the lattice site where a DB is present (I = 50 pA, V = 1.4 V). The feedback controls are switched off, locking the tip height. The sample voltage is changed to a value between 100 mV and 1.0 V, and then the tip is moved linearly towards the sample surface while recording the tunneling current. After the tip has traveled a distance of 550 pm towards the surface it is retracted to its original position. The original parameters are re-established, and the feedback control is restored. To date, no significant correlation between voltage and HR efficiency has been observed. The choice of voltage serves to limit the tunneling current to within ranges that prevent significant tip apex changes, while still providing adequate feedback signals. Typically, we perform HR at a bias of 200 mV and only adjust this value in the program when the signal falls outside of the desired range (3 pA to 300 pA). The strength of the signatures depends on the exact structure of the apex, as they can vary by an order of magnitude at the same applied bias (Supplementary Figure 2.7, 2.8). Even though the strength of the signatures vary,

their shape remains characteristic, making them ideal for the detection of successful events (Supplementary Figure 2.7, 2.8). If the initial HR attempt is unsuccessful, the process can be repeated until a type-I or type-II signature is detected. Work is in progress to include automatic error detection after HL using image recognition to define arbitrary groups of sites for HR in an image. This will eventually enable fully automated HR, without any user intervention to select individual sites to initiate the HR process.

2.5.5 Memory readout/image recognition

The memory readout was accomplished with the use of Python and Open CV. The periodicity of the hydrogen-terminated Si(100)-2x1 surface allows for a grid to be defined over the surface, where each bit is contained within one cell. The image contrast of when a DB is present or not lends to threshold detection to determine if the bit is one or zero. Memories can be read directly from recorded STM images, or as the image is built up while the STM scans over the surface, populating each cell element. Readout speed is limited by the maximum STM scan speed. The musical playback was created with the use of the Pygame package, where detected bit patterns can be mapped into notes for playback.

2.6 Supplementary information

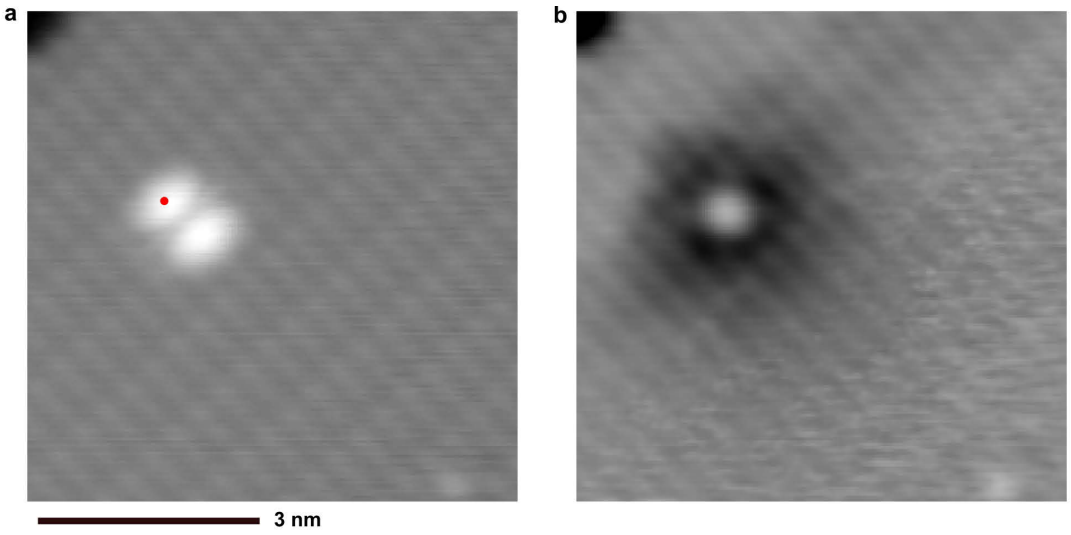

Figure 2.5: Atomically precise hydrogen repassivation of one dangling bond in a pair.
a) A Scanning Tunneling Microscope (STM) image (V = 1.4 V, I = 50 pA, T = 4.5 K, 6.5 x 6.5 nm^2) of two dangling bonds (DBs) on the hydrogen-passivated Si(100)-2x1 surface at the closest possible spacing, commonly known as a bare dimer structure. An STM tip, with adsorbed hydrogen on its surface, is positioned above the site denoted with a red dot for repassivation. **b**) The STM image immediately following the hydrogen repassivation of the site in **a**. Only the desired DB has been repassivated, leaving the other unaltered, illustrating the precise nature of this technique.

2.6.1 Supplementary note 1: Atomic hydrogen

On rare occasions during hydrogen lithography we observe atomic hydrogen physisorbing onto the sample surface after the creation of a dangling bond (DB), instead of the assumed action of traveling into vacuum [25, 34]. It has been found that instead of sticking to the sample surface there is a probability it may absorb to the tip surface instead [25]. The atomic hydrogen can be dragged by the Scanning Tunneling Microscope (STM) tip, where in Supplementary Figure 2.6c it has been moved

away from the DB towards the middle of the structure. The STM tip can be reliably functionalized with this atom for the purpose of repassivation [25], or to remove it from the area where a structure is being built.

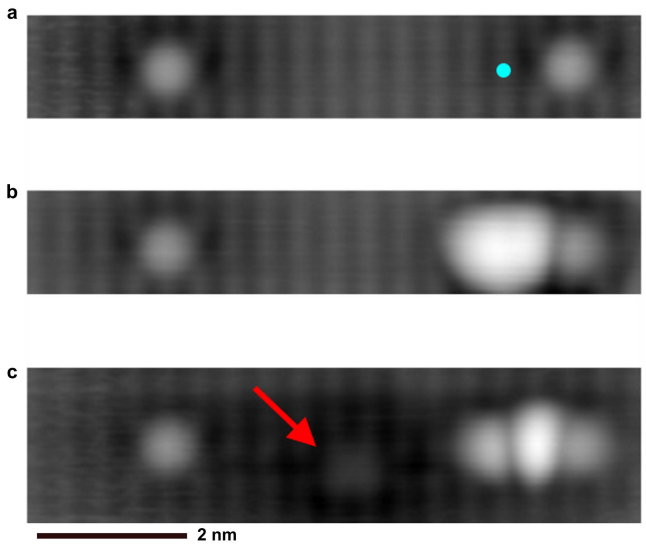

Figure 2.6: Atomic hydrogen physisorption on hydrogen-passivated silicon.
a) (V = 1.4 V, I = 50 pA, T = 4.5 K, 1.7 x 8 nm^2) A two dangling bond (DB) structure with the location of the next site for hydrogen lithography denoted with a blue circle. **b**) The DB structure after an attempted hydrogen removal, it appears an error has been made as the site in **a**, does not resemble a single DB, instead appearing brighter, as if multiple hydrogens have been removed from the surface. **c**) After repeated scans over the structure the error was no longer present and a faint object (red arrow) was now visible. The object is atomic hydrogen that physisorbed to the sample surface after extraction instead of traveling into vacuum [25]. The hydrogen atom was altering the appearance of the newly created DB in **b**, causing it to look like an error had occurred. The hydrogen atom is able to sit in close proximity to the DB in **b**, without rebonding. A description of the feature in between the two DBs on the right-hand side in **c**, has been proposed elsewhere [40].

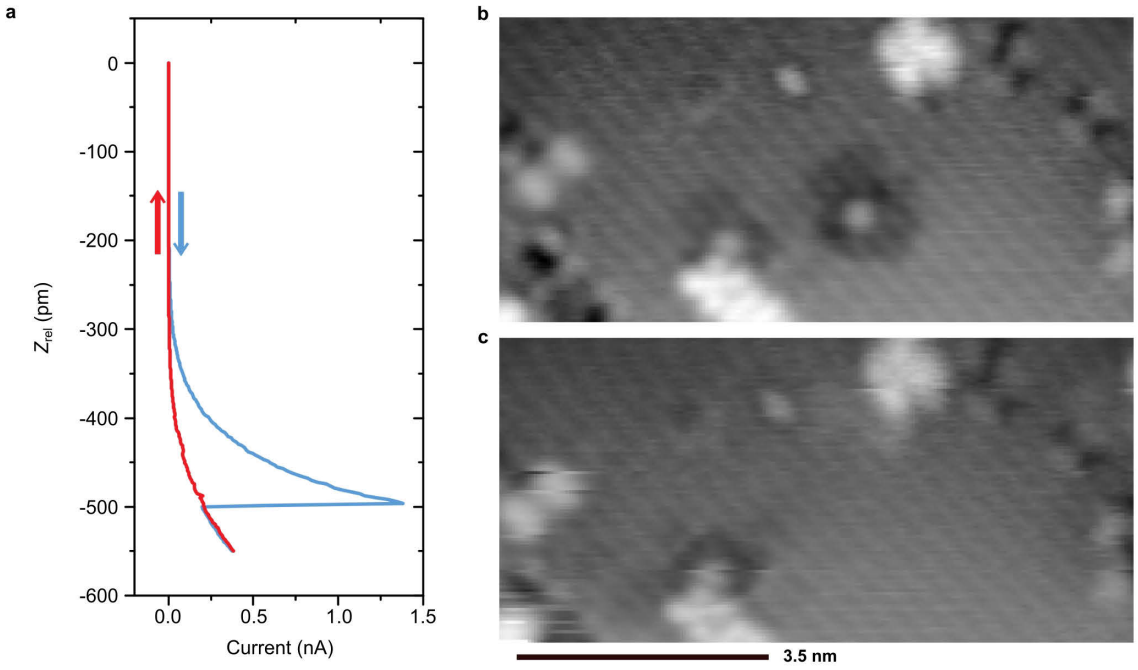

Figure 2.7: Hydrogen repassivation with type-II signature at 77 K. **a**) (V = 0.2 V) Type-II signature in the Scanning Tunneling Microscope (STM) tunneling current recorded during hydrogen repassivation (HR) at 77 K. **b-c**) (V = 1.4 V, I = 50 pA, T = 77 K, 4.5 x 9.3 nm^2) STM images before and after successful HR.

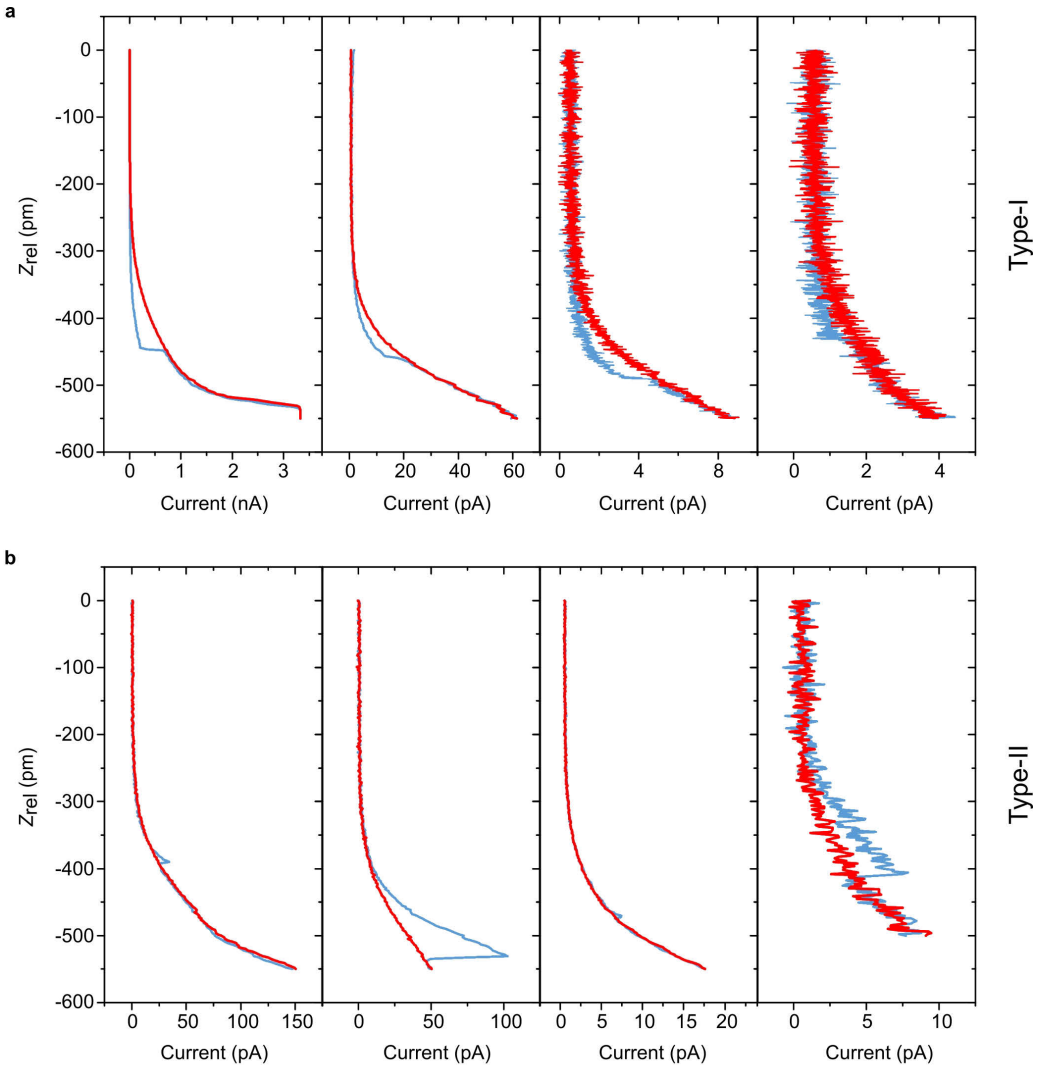

Figure 2.8: Taxonomy of type-I and type-II hydrogen repassivation signatures.

a-**b**) A representative sample of different type-I and type-II signatures recorded during hydrogen repassivation (HR) events ($T = 4.5$ K), with the tip set over a dangling bond at 1.4 V and 50 pA. Applied bias voltages in **a**, from left to right, are 0.5 V, 0.3 V, 0.2 V, 0.2 V respectively. Applied bias voltages in **b**, from left to right, are 0.2 V, 0.4 V, 0.2 V, 0.2 V respectively. While the magnitude of both signatures can vary depending on the apex orbital and the choice of applied voltage to limit the tunneling current during HR, their overall shapes remain very characteristic. The reliability and reproducibility of these features makes them excellent indicators of successful repassivation for automation routines.

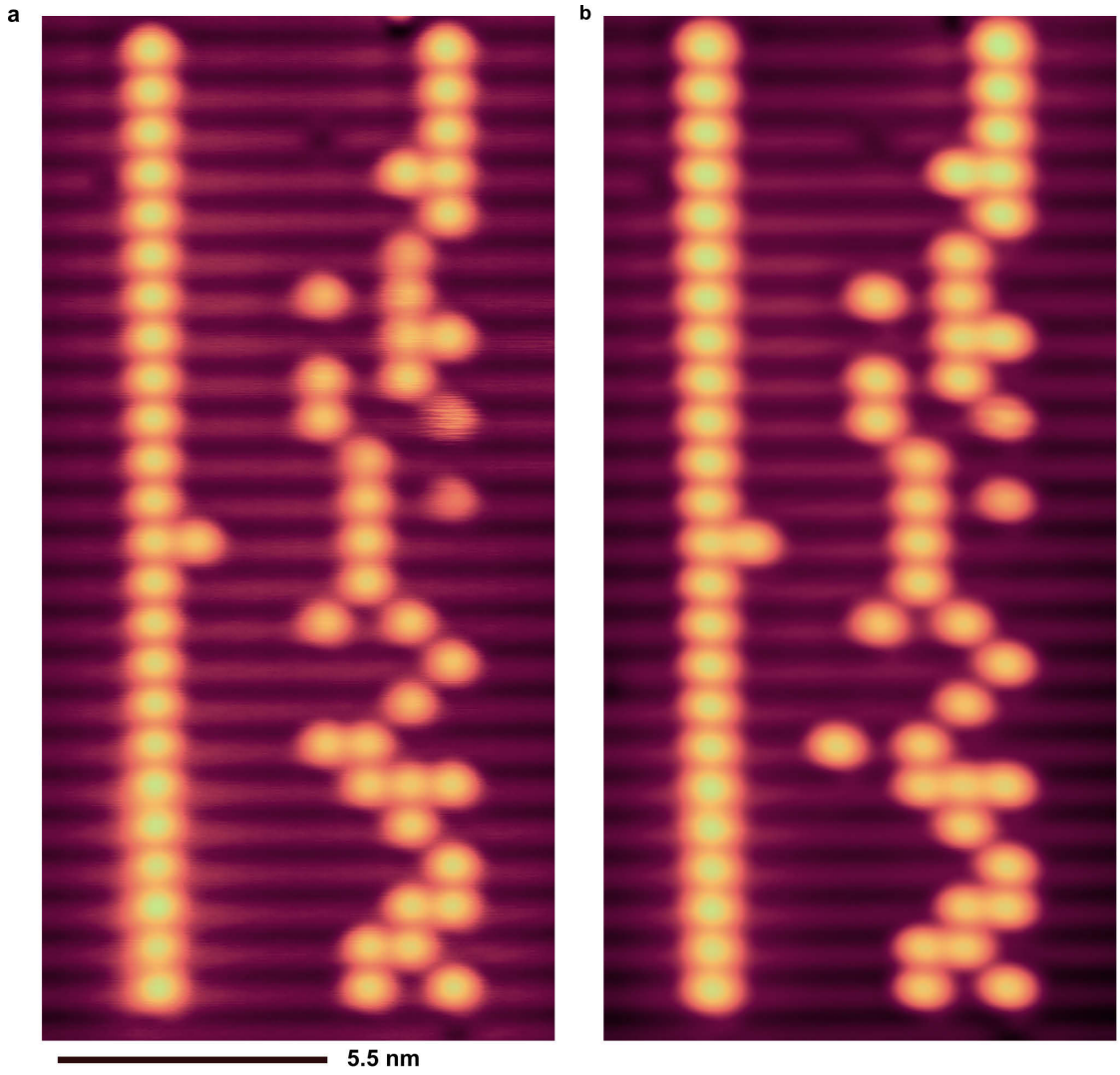

Figure 2.9: Stability and rewriting of the 192-bit memory.
a) (V = -1.75 V, I = 50 pA, T = 4.5 K, 21.5 x 10.7 nm^2) The original memory structure created through hydrogen lithography (HL) and hydrogen repassivation (HR). The pattern was initially entered into the HL program incorrectly through human error. As a result, one of the lines was incorrectly written. **b**) The same memory 72 hours later with the incorrect line rewritten using HR, no additional changes were made to the structure. The cryo-fluid in the Scanning Tunneling Microscope had to be replenished during this time, so the memory was subjected to temperature spikes up to 12 K and pressure spikes on the order of 10^{-8} Torr.

2.6.2 Supplementary movies

The playback of musical information stored in the 192-bit memory from a Scanning Tunneling Microscope image can be found in the supplementary material with the published manuscript at: https://www.nature.com/articles/s41467-018-05171-y. Additionally it can be found on YouTube at: https://www.youtube.com/watch?v=CIUxkceinXk.

2.7 Acknowledgments

The authors thank M. Salomons for his technical assistance, K. Gordon for helpful discussions, and J. Phillips for editing and proofreading the manuscript. We would like to also thank NSERC, AITF, NRC, and QSi for their financial support.

2.8 Competing interest

Patent applications are in process related to the subject presented in the manuscript. Some of the authors (R.A., M.R., M.T., T.H., J.P., R.A.W.) are affiliated with Quantum Silicon Inc (QSi). QSi is seeking to commercialize atomic silicon quantum dot-based technologies. All other authors declare no competing interests.

Chapter Three

Extended details - Lithography for robust and editable atomic-scale silicon devices and memories

3.1 Updated hydrogen repassivation stats

The histogram in Figure 2.3c contained the Z_{rel} of the tip where 119 unique HR events occurred. These data were collected over several months, with microscopically different tips. In each HR attempt the tip height was set over a DB at a bias of 1.4 V and a tunneling current of 50 pA before the feedback control was disabled to fix the starting tip position. During the following few months, an additional 49 HR events were recorded using other microscopically different tips, during the fabrication of various other structures. Figure 3.1 contains the full distribution of all the recorded events.

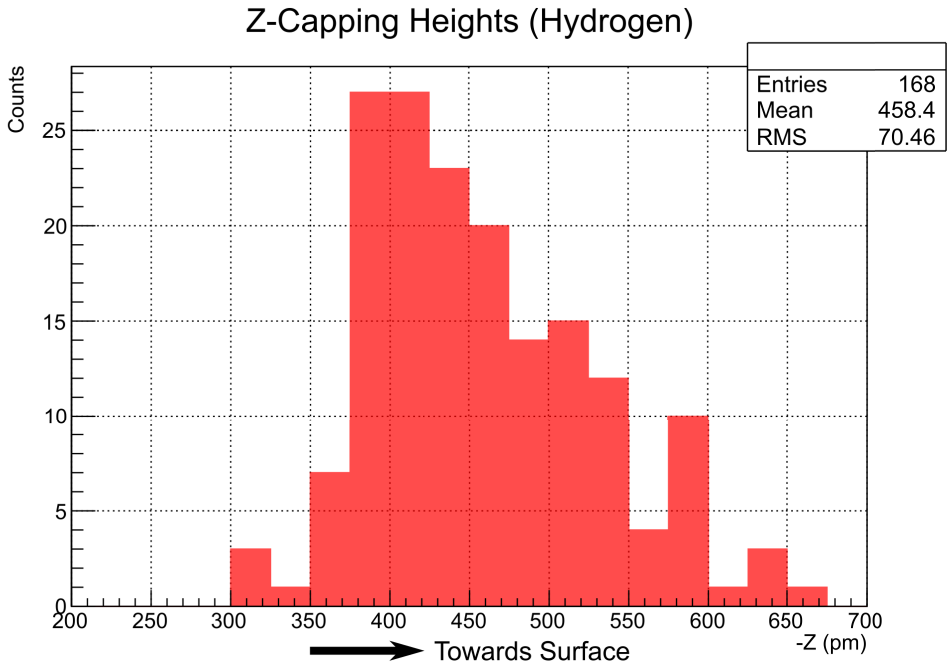

Figure 3.1: Full distribution of HR events.
The tip approach distance where either a type-I or type-II signature occurred for a total of 168 unique HR events.

3.2 Transfer mechanism and deuterium repassivation

When the ability to repassivate surface DBs with hydrogen atoms on the tip was first reported [25, 33], it was proposed that the mechanism of hydrogen transfer was mechanically induced bond formation (*i.e.* bringing the tip towards the sample surface), causing a competition between the reactive site on the tip (apex) and on the surface [54]. Due to the small size of hydrogen atoms, along with the relatively small distances between the tip and sample (less than 1 nm), I was intrigued by another possible explanation for the occurrence of the transfer: quantum tunneling. It is possible that the hydrogen atoms on the tip tunnel through the vacuum barrier to reach the DB on the sample surface.

Studies of hydrogen and deuterium diffusion on metal surfaces have shown that at low temperatures hydrogen diffusion displays a transition to a quantum tunneling regime, whereas deuterium diffusion does not [98]. This difference is due to the kinetic isotope effect, where the heavier deuterium atoms have low tunneling probabilities [98, 99]. The kinetic isotope effect is often used to uncover reaction mechanisms, where if tunneling is an important aspect the observed rates are dramatically slowed when deuterium is substituted for hydrogen [99, 100]. It is important to note that the substitution does not change the potential energy landscape of the reaction, only the rate at which it occurs, due to the lower zero-point energy of a deuterium bond.

To better elucidate whether or not tunneling was the mechanism behind the transfer of hydrogen in this particular case, I attempted DB repassivation on a deuterium-terminated surface utilizing the same techniques described in Section 2.3. If tunneling was involved with the transfer, it would be expected that for deuterium either no repassivation would be observed at all, or a significantly closer tip-sample approach would be required to achieve repassivation.

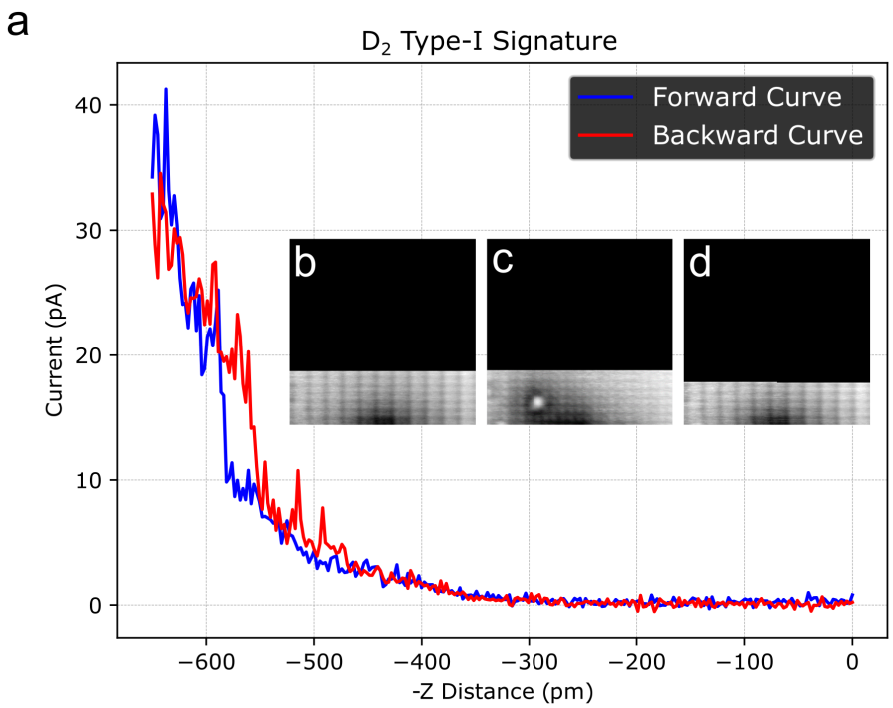

Figure 3.2: Type-I repassivation signature using deuterium ($V = 1.4$ V, $I = 50$ pA).
a) A type-I signature recorded in the tunneling current during a deuterium repassivation event. **b**) A partial STM image of a deuterium terminated Si(100)-2x1 surface prior to creating a DB by removing a deuterium atom from the surface. **c**) After the creation of the DB, the tip resolution changed, indicating the tip is now functionalized with a D atom. **d**) After undergoing the repassivation procedure, the tip resolution returned to its pre-functionalized state.

The deuterium-terminated surface was prepared using 99.7% pure D_2 gas in an identical way to the standard hydrogen-terminated surface. A freshly etched tungsten tip was utilized to ensure no hydrogen atoms were present from earlier experiments. The tip was formed using controlled contact with the deuterated surface to condition it into a repassivation-capable geometry. After several conditioning attempts, I was able to produce a tip that was capable of repassivating surface DBs with deuterium. Figures 3.2 and 3.3 show before and after images of DBs repassivated with deuterium.

Figure 3.5 shows the distribution of recorded deuterium repassivation events. During the creation of a DB, it was even possible to image a deuterium atom that physisorbed on the surface (Figure 3.4), which is analogous to Figure 2.6 and the observations in [25] of a physisorbed hydrogen atom.

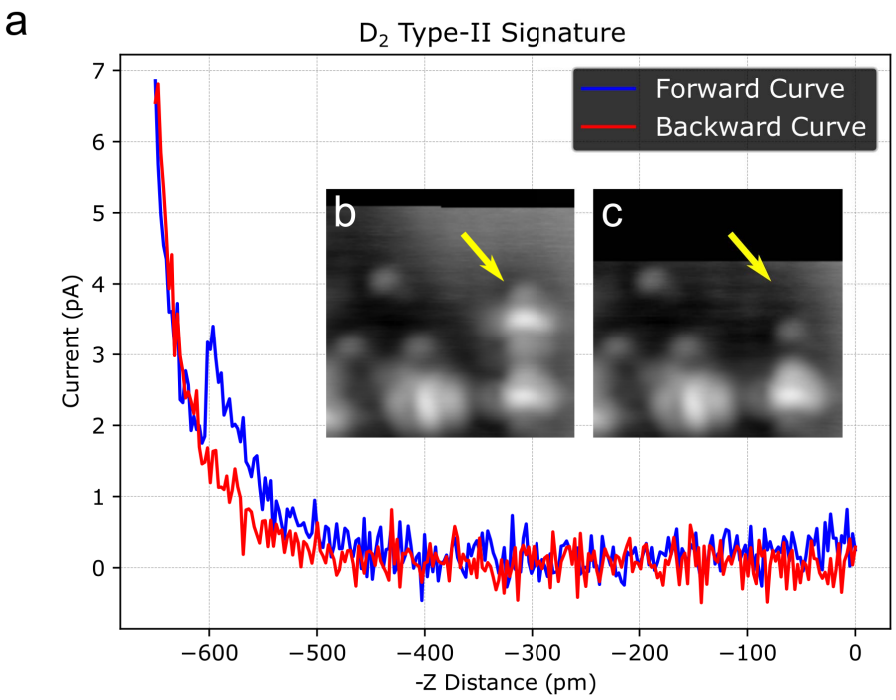

Figure 3.3: Type-II repassivation signature using deuterium ($V = 1.4$ V, $I = 50$ pA).
a) A type-II signature recorded in the tunneling current during a deuterium repassivation event. **b**) A partial STM image of a deuterium terminated Si(100)-2x1 surface prior to undergoing a repassivation procedure. **c**) After undergoing the repassivation procedure, the tip resolution remained unaltered.

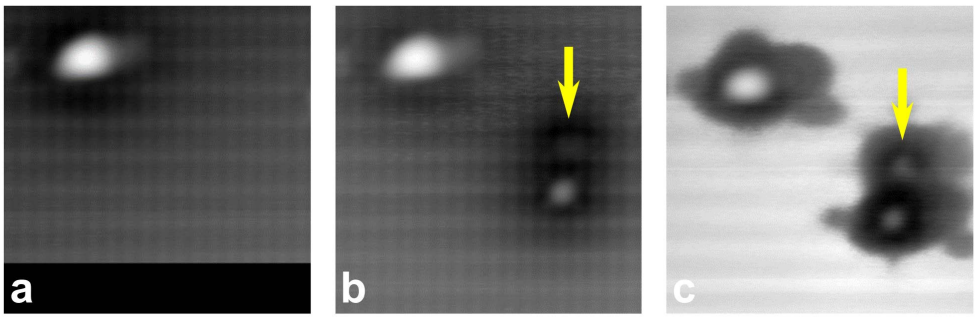

Figure 3.4: Deuterium physisorbed on D-Si(100)-2x1.
a) (V = 1.4 V, I = 50 pA) The D-Si(100)-2x1 surface prior to the creation of a DB. **b**) After the creation of a DB, the deuterium atom did not adsorb to the tip or leave into vacuum. It is physisorbed on the surface at the location of the yellow arrow. **c**) (V = 2.0 V, I = 50 pA) Higher bias image of the absorbed D.

A total of 16 repassivation events were recorded using deuterium, which also exhibited the same repassivation signatures as hydrogen (Figures 3.2a and 3.3a). The resulting distribution (Figure 3.5) appears to be similar to that of hydrogen transfer events (Figure 3.1). Figure 3.6 shows the overlay of both distributions to facilitate comparisons. To better estimate the mean and standard error of both distributions, bootstrap sampling was used to generate ten thousand new distributions (each with unique means) by sampling each respective data set with replacement. The resulting means were then placed into their own distributions for each isotope, and the mean (of means) and standard error were then calculated from the results respectively. For the hydrogen distribution, a mean repassivation distance of -458.4 +/- 5.5 pm was determined, while for deuterium a mean repassivation distance of -450.7 +/- 20.4 pm was determined. Given the values for standard error, it appears that there is no significant statistical difference between the mean repassivation distance of hydrogen and deuterium.

These results indicate that the transfer of atoms from the tip to the surface is very unlikely to be caused by tunneling of atoms through the vacuum barrier. Recording a greater number of deuterium repassivation events would help reduce the standard error of the mean, allowing for a more equivalent comparison to the

hydrogen values. It is still possible that the mean of the deuterium events will be larger than that of hydrogen due to the mass difference between the isotopes. If the mean is indeed the same for the two, then that is indicative of them experiencing the same physisorbed potential, which is mostly due to the electronic structure of the surface and adsorbed atom. Experiments studying the van der Waals interaction of hydrogen and deuterium physisorption on copper for instance have shown that they do experience the same potentials on that surface [101].

While the potential might be the same, it may be possible to experimentally test if there is a difference in rates between hydrogen transfer and deuterium transfer. Once a tip is loaded with hydrogen, the tip can be brought towards a DB until just before the measured mean transfer distance (no transfer should occur). At this fixed distance, the fluctuations of the tunneling current can be recorded over time until a transfer occurs (it will manifest as a large jump in current). From many of these observations, an average transfer rate can then be deduced. This process should then be repeated for deuterium to obtain its average transfer rate for comparison.

One difference noted during the repassivation attempts with deuterium was that it was often more difficult to achieve a repassivation event when compared to hydrogen. It appeared as if deuterium did not become physisorbed as readily on the tip. However, due to the limited sample size, this observation could have been due to the tip not possessing an ideal repassivation geometry, rather than any inherent property of deuterium itself. More trials, using different tips, are required to explore this observation further.

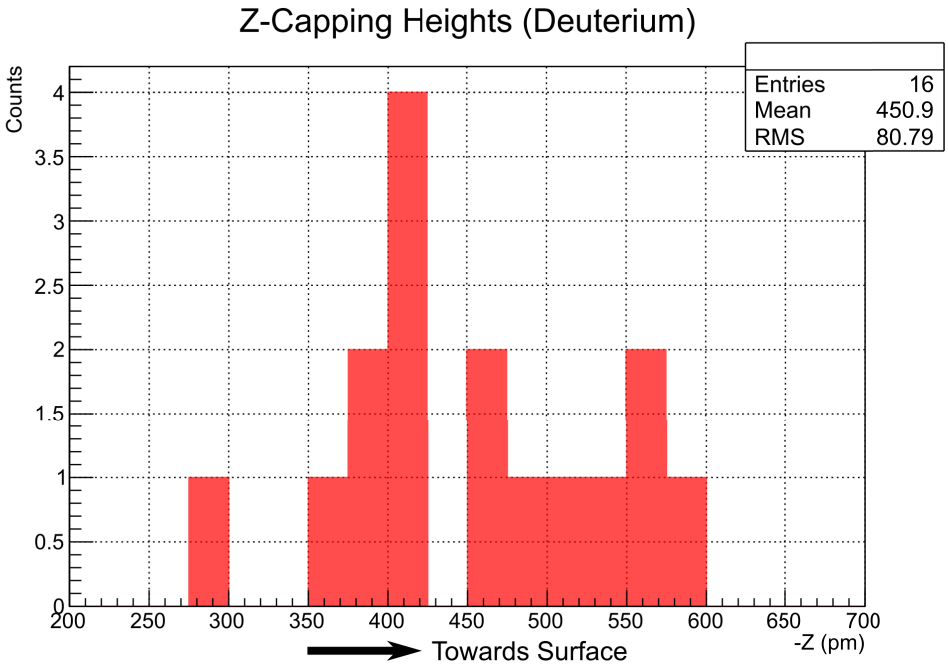

Figure 3.5: Full distribution of deuterium repassivation events.
The tip approach distance where either a type-I or type-II signature occurred for a total of 16 unique deuterium repassivation events.

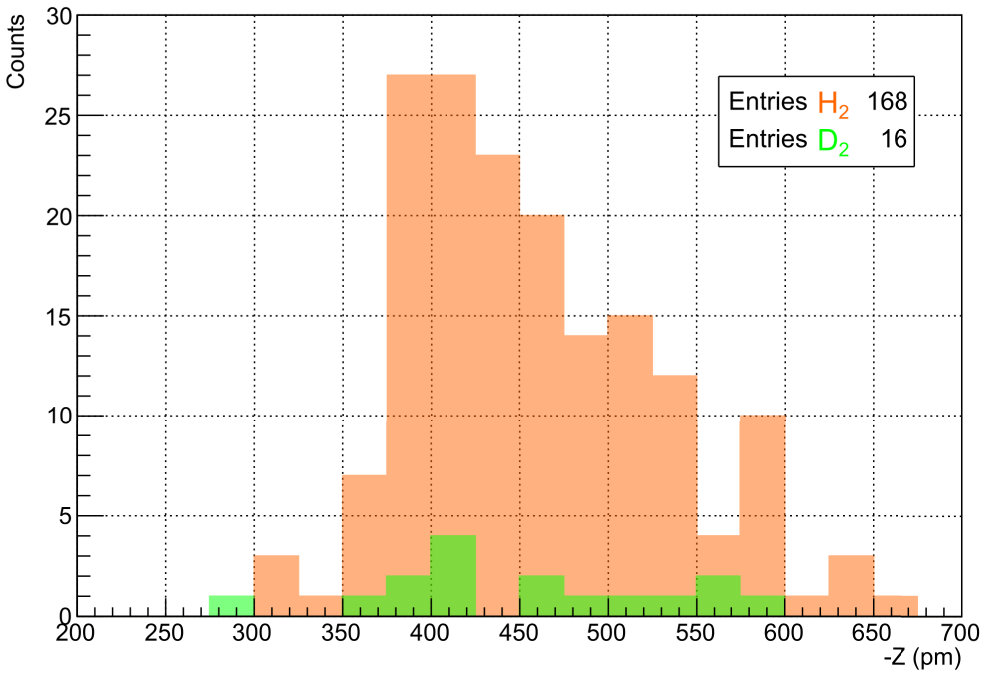

Figure 3.6: Histogram overlay of hydrogen and deuterium repassivation events.
The tip approach distance where either a type-I or type-II signature occurred for both hydrogen repassivation events and deuterium repassivation events.

3.3 Toy model of hydrogen transfer

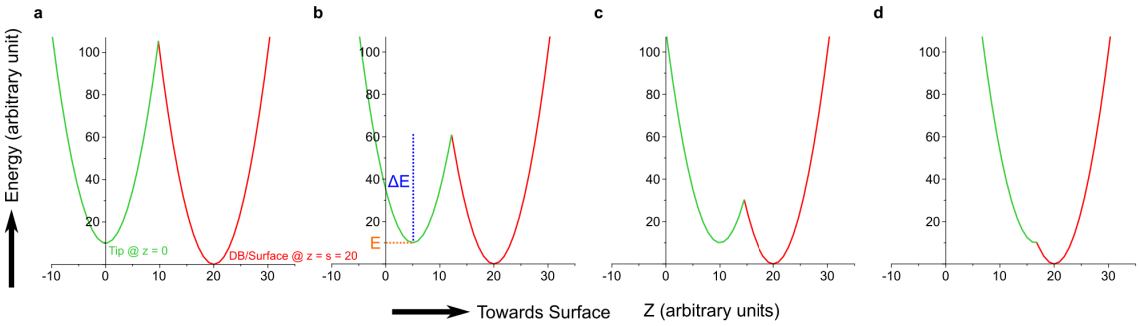

Figure 3.7: Toy potential curves.
The simulated potential curves from Equations 3.1 (green) and 3.2 (red). **a-d**) Energy barrier ΔE with decreasing separation between the tip and sample (20, 15, 10, 3.2 units respectively).

Now with tunneling ruled as an unlikely mechanism, it seemed like a good opportunity to test whether or not, with some very basic assumptions, the essential features of Figure 3.1 could be reproduced in a simulation. In this case, simple potential energy curves of the form of Equation 3.1 and Equation 3.2 were chosen to represent the hydrogen atom physisorbed on the tip and bonded to the sample at a DB respectively. To further simplify the problem, both wells were assumed to have an identical shape (Equation 3.3).

$$V_{tip+H} = K_1 \cdot (Z - z)^2 + E, \tag{3.1}$$

$$V_{DB+H} = K_2 \cdot (Z - s)^2, \tag{3.2}$$

$$K_1 = K_2 = 1, \tag{3.3}$$

where Z is the unit distance, z is the position of the tip apex, s is the position of the surface, and E is the energy offset between the minima of the potential wells corresponding to hydrogen physisorbed on the tip and bonded on the surface. Due to the toy nature of the model, all quantities are dimensionless, that is, expressed

in units that are natural to the system, but not specifically set here. Figure 3.7 shows the system with the choice of $s = 20$, $E = 10$. As z is increased and the tip is brought closer to the surface, the barrier between the wells (measured from the bottom of the tip-hydrogen potential curve) ΔE becomes smaller and smaller. ΔE as a function of z can be found by solving for the position where the two potentials curves intersect (Z_{inter}), less the value of E (Equation 3.6).

$$V_{tip+H} = V_{DB+H}, \tag{3.4}$$

$$\Rightarrow Z_{inter} = \frac{-z^2 - E + s^2}{2 \cdot (s - z)}. \tag{3.5}$$

$$\Delta E = V_{tip+H}(Z_{inter}) - E, \tag{3.6}$$

$$\Rightarrow \Delta E = (\frac{-z^2 - E + s^2}{2 \cdot (s - z)} - z)^2. \tag{3.7}$$

Assuming the transfer process is due to thermal activation, then it should be governed by the Arrhenius equation. Since the temperature, T, is constant in the experiment, the probability of a transfer occurring is then proportional to:

$$p = e^{-\frac{\Delta E}{k_b T}}, \tag{3.8}$$

$$\Rightarrow p(z) \ \propto \ e^{-\Delta E} = e^{-(\frac{-z^2 - E + s^2}{2 \cdot (s - z)} - z)^2}. \tag{3.9}$$

Equation 3.9 can now be used in a basic Monte Carlo-type simulation, with the premise of mimicking the overall experiment. In each trial z is incremented in finite steps (0.1 units) to act as the tip moving towards the sample until a transfer event occurs. At each position Equation 3.9 is used to calculate the probability of overcoming the barrier for a single attempt. A finite number of attempts (1000) are then undertaken to determine if a transfer has occurred before incrementing z

to the next position and repeating this process. To determine if a transfer occurs, the calculated probability is used in a roulette wheel selection process. That is, a random number is drawn from a flat distribution between zero and one; if the random number is less than $p(z)$, then a transfer has occurred. This entire process can then be repeated for a set number of trials (500) to generate a simulated distribution of transfer events. Figure 3.8a shows the experimental distribution obtained for hydrogen transfer events, and Figure 3.8b,c show the simulated results.

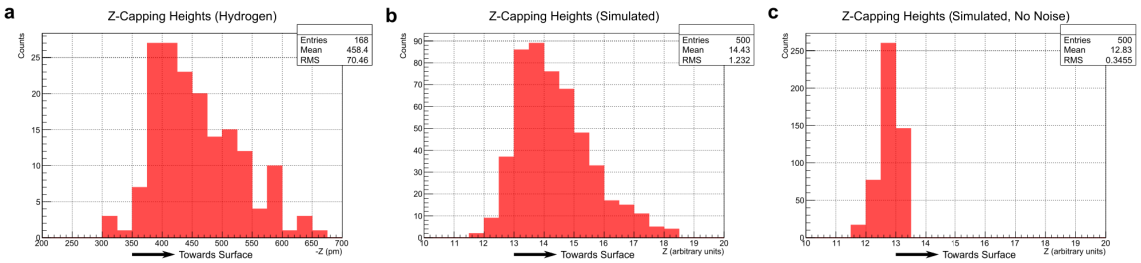

Figure 3.8: Experimental and simulated transfer event histograms. **a**) Distributions of hydrogen transfer events recorded experimentally (same as Figure 3.1). **b**) Simulated hydrogen transfer distribution using Equations 3.1 to 3.9, along with noise in the initial tip-sample separation. **c**) Simulated distribution without the inclusion of noise.

If the simulation is run exactly as described, the results of Figure 3.8c are obtained, which do not fully resemble the shape of the experimental distribution. The only similarity between Figure 3.8a and Figure 3.8c is the sharp onset of transfer events as the tip approaches the sample; the long decaying tail of events toward the sample surface is missing. To generate Figure 3.8b, which appears to reproduce the essential features of the experimental distribution, an amount of uncertainty had to be added to the z position. For each trial, the z position was randomly offset away from the sample by an additional distance (negative distance). The amount was determined by multiplying a noise parameter (set to 4 in the simulation) by the absolute value of a random number drawn from a Gaussian distribution centered about zero with a standard deviation of 0.5.

This form of noise may have some physical meaning that could be represented by

a combination of possible causes. One scenario is that the tip and sample are always at a fixed distance, and the position of the hydrogen atom is randomly distributed along the surface of the tip, with the highest probability of being directly off the apex (for type-I it is always on the apex itself). Alternatively, when the tip changes state/geometry through controlled contact with the surface, the sharpness varies. Sharper tips tend to be farther from the surface to achieve the same magnitude of tunneling current compared to dull tips. Thus, this type of noise could represent the variations in tip sharpness and the associated variations in initial tip-DB separations at 1.4 V and 50 pA. Finally, as the tip is brought in very close to the sample, a repulsive interaction may begin to onset (AFM shows the tip enters the repulsive regime after approaching the surface 500 to 700 pm [25]), causing the hydrogen atom on the tip to move farther from the surface. Such an interaction is not specifically accounted for in this very simple model, as the barrier goes to zero at the surface (Equation 3.11), when in reality, a repulsive interaction would cause the barrier to increase again past a certain distance threshold. Despite events appearing to occur after the barrier has gone to zero in Figure 3.8b, the absolute distance between the tip and sample due to the noise offset never exceeded the limit set by Equation 3.11 for any particular trial.

$$\Delta E = 0, \tag{3.10}$$

$$\Rightarrow z_{\Delta E=0} = s - \sqrt{E}. \tag{3.11}$$

To really disentangle which of these possible explanations has the strongest contributions to the observed tail in the experimental data, sophisticated modeling such as density functional theory would likely be required. With density functional theory, more realistic potentials can be used to model tip-sample interactions, and can also account for flexibility/movement of bonded atoms on the tip [25]. Another aspect of this toy model that would need to be specifically accounted for in more sophisticated treatments is that the barrier height (ΔE) would be calculated between the quantum ground state energies of the system, rather than the classical minima of the potential

curves as has been done here. Further, type-I and type-II signatures were treated together here as part of the same distribution, although there is likely a different barrier height associated with each process. As more experimental data is collected, it will be possible to treat them separately, but at present type-I HR events only make up about 14% of the 168 events in the distribution shown in Figure 3.8a.

3.4 Hydrogen repassivation of a positive DB

Occasionally on the H-Si(100)-2x1 surface, with our degenerate n-type doping, it is still possible to observe what has been classified as a DB in its positive charge state [102]. This is due to local non-uniformity in the electrostatic landscape of the surface [75]. These DBs, commonly observed on the p-type surface, have a characteristic asymmetric geometry in empty states (Figure 3.9a) and appear as dark depressions in filled states (Figure 3.9b) [102]. Using the HR technique, it is possible to repassivate such DBs as well (Figure 3.9c). Unfortunately, due to the rare occurrence of these entities, no conclusions on the relative ease of repassivation compared to a negatively charged DB can currently be made.

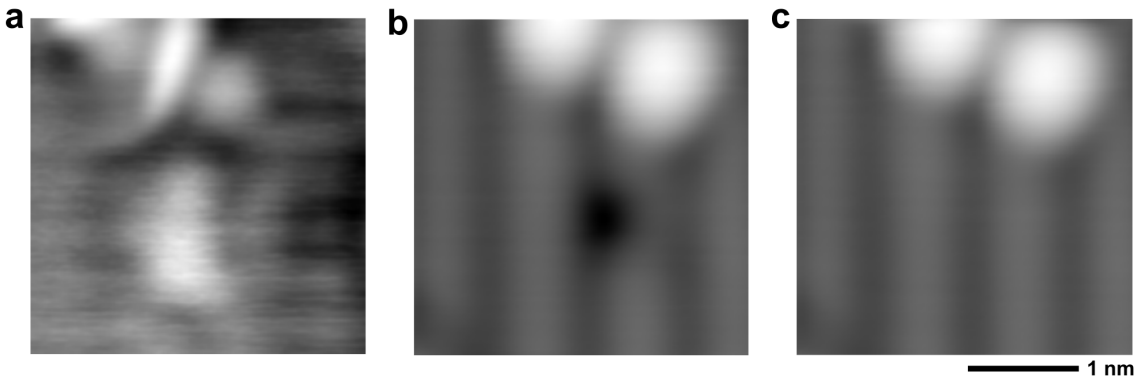

Figure 3.9: Repassivating a positive DB (I = 50 pA, T = 4.5 K, 3 x 3 nm^2).
a) (V = 1.4 V) An empty states image of a positive DB, showing a characteristic crescent shape. **b**) (V = -1.7 V) A filled states image of a positive DB, where it appears as a dark depression, unlike the other two negatively charged DBs in the image. **c**) An image after successfully initiating an HR event at the positive DB.

3.5 Room temperature repassivation trials

Given the observation that hydrogen atoms can still be physisorbed on a tungsten tip and subsequently deposited on a silicon surface at room temperature [83], I explored the possibility of using the HR technique at non-cryogenic conditions.

Despite many attempts, I was unable to perform a controlled repassivation operation. Instead, spontaneous repassivation events were observed on the surface (Figure 3.10). It is possible that controlled HR was not occurring due to an incompatible tip geometry. However, the tip was reconditioned many times through controlled contact with the surface, in an attempt to alter it during these trials, and still no HR was achieved. I believe one of the main issues preventing successful HR was uncertainty in tip position over a DB when working at non-cryogenic temperatures.

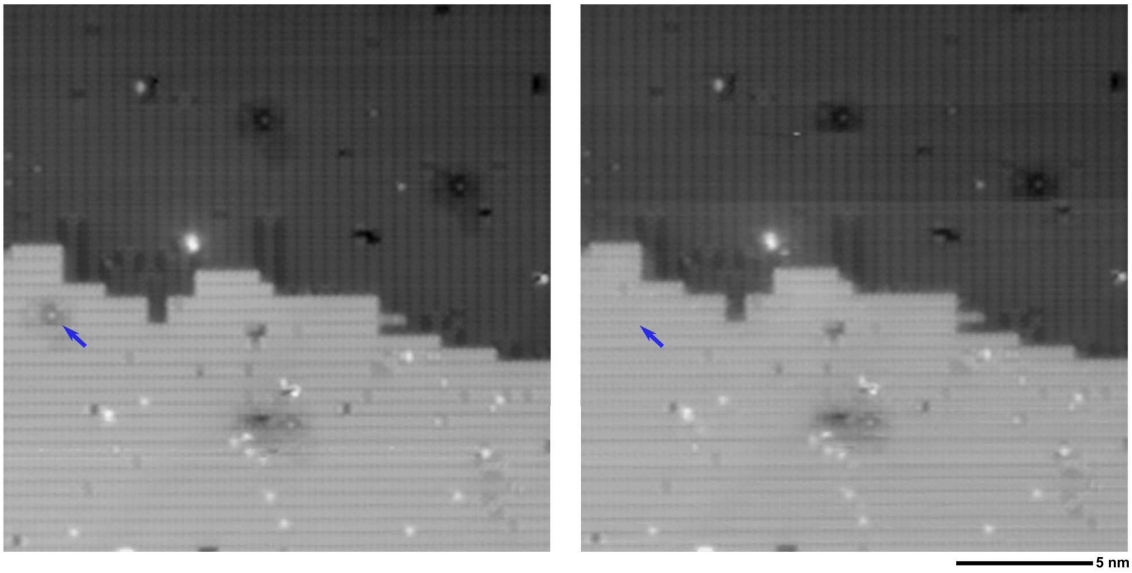

Figure 3.10: Spontaneous repassivation at room temperature ($V = 1.4$ V, $I = 150$ pA, $T = 297$ K, 20 x 20 nm^2).
Sequential scans at room temperature, where a DB was observed to have spontaneously repassivated with hydrogen.

3.6 Possibility of surface damage during hydrogen repassivation

To observe a type-I or type-II repassivation signature in the tunneling current, the HR procedure requires a small bias to be left on the tip (Section 2.5.4). When initially exploring the parameter space during the development of the HR procedure, trials involving larger biases (up to 1.4 V) were undertaken as well. Often, as the tip approached the surface at these elevated bias values, the measured tunneling current would saturate at the 3.5 nA threshold of the current preamplifier. Due to this threshold, the maximum current values reached were unknown.

At tunneling currents approaching 3.5 nA and close tip-sample separations, there is a risk of breaking additional surface Si-H bonds, causing local damage to the surface. At even higher currents, it appears that enough energy can be input into the surface to cause a significant bond rearrangement. Figure 3.11 shows the creation of a dimer dihydride defect on the surface during an HR attempt at a bias of 1.2 V. This type of defect creation has not been further observed since restricting the bias range utilized for HR.

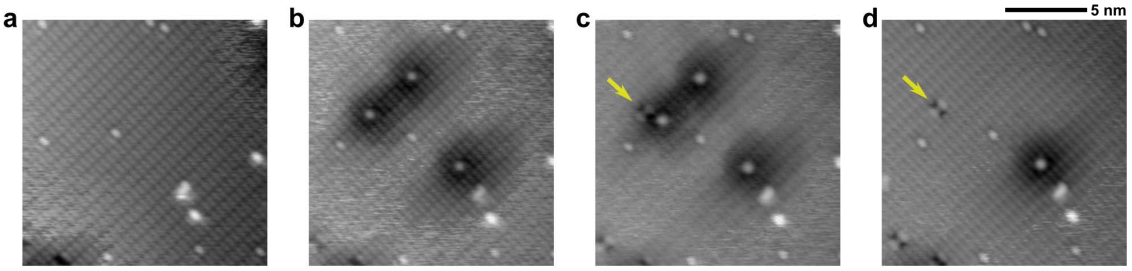

Figure 3.11: Creating a dihydride during HR (V = 1.4 V, I = 50 pA, T = 4.5 K, 15 x 15 nm^2).
a) An empty states image of the H-Si(100)-2x1 surface. **b**) The same area as in **a** after the creation of three DBs. **c**) An HR attempt was made at the leftmost DB at a tip bias of 1.2 V. The DB was not repassivated, and instead a dihydride was created on the surface and the original DB was displaced. **d**) The same area as in **a** after two of the created DBs were successfully repassivated.

3.7 Outlooks

The integration of improved automated HL with controlled and reliable STM-based HR has led to a leap in atomic-scale fabrication capabilities on the H-Si(100)-2x1 surface, as demonstrated by the largest error-free structures ever created from DBs. The previously stringent condition of error-free HL can now be relaxed with the introduction of HR for error correction, making the process more scalable and realistic from a production standpoint. New applications have also emerged from the ability to controllably replace hydrogen in the form of ultra-dense rewritable data storage arrays created from DBs.

Inherent in the HR procedure, however, is the limited amount of hydrogen available on the tip surface. This is a hurdle for the mass production of circuitry and practical implementations of data storage. It was discussed in Section 2.3.3 that other tip materials such as Pt may provide a solution, as others have shown the capability to hold over a thousand atoms of hydrogen at a time [84]. Even with a relatively large supply compared to what is possible right now on a tungsten tip, when circuit structures and data arrays begin to approach the size of tens of thousands of DBs, the speed bottleneck of needing to replenish the tip would still remain. The use of multiple tips during fabrication can ease this bottleneck to some degree, although designing suitable equipment still presents a significant engineering challenge. The next chapter approaches this problem from a different angle, where no new equipment needs to be designed. Rather, the strengths of HL can be harnessed to create a faster, more efficient and scalable repassivation procedure.

The next stage of study for HL and HR is to begin a thorough exploration of these processes and procedures on p-doped silicon. The studies described in this chapter have all so far been performed on n-type silicon. It will be imperative in the future to ensure that the observations and procedures described here function as intended on silicon substrates with both different dopant types and concentrations, as these parameters will change the native charge occupation and properties of the surface DBs [26, 27, 91, 103].

Chapter Four

Detecting and directing single molecule binding events on H-Si(100) with application to ultra-dense data storage

Authors: Roshan Achal[1,2], Mohammad Rashidi[1,2], Jeremiah Croshaw[1,2], Taleana Huff[1,2], Robert A. Wolkow[1,2,3]

[1]Department of Physics, University of Alberta, Edmonton, Alberta, T6G 2E1, Canada
[2]Quantum Silicon, Inc., Edmonton, Alberta, T6G 2M9, Canada
[3]Nanotechnology Research Centre, National Research Council of Canada, Edmonton, Alberta, T6G 2M9, Canada

Author contributions: R.A. conceived of the memory designs, molecular hydrogen repassivation procedure, molecule detection procedure, and performed all STM experiments. M.R., R.A., and R.A.W., conceived of the charge characterization experiment. J.C. and R.A. developed the molecule detection program. T.H. performed the supplementary AFM measurements. R.A.W. supervised the project. R.A. prepared the manuscript. All authors participated in the review and discussion of the manuscript and results.

This chapter has been reproduced from the published article with permission from R. Achal, M. Rashidi, J. Croshaw, T. Huff, R. A. Wolkow, "Detecting and Directing Single Molecule Binding Events on H-Si(100) with Application to Ultradense Data Storage," ACS Nano (Nov, 2019) 10.1021/acsnano.9b07637, Copyright 2019 American Chemical Society. The full manuscript is available at: http://dx.doi.org/10.1021/acsnano.9b07637 [Open Access] [44].

This article was one of the 365 selected in 2019 from the entire ACS family of journals to be featured in ACS Editors' Choice. As such, it was sponsored for Open Access. I was both excited and grateful for this, because while I fully support the open access of scientific work, I am not always in support of the associated fees.

4.1 Abstract

Many diverse material systems are being explored to enable smaller, more capable and energy efficient devices. These bottom-up approaches for atomic and molecular electronics, quantum computation, and data storage all rely on a well-developed understanding of materials at the atomic scale. Here, we report a versatile scanning tunneling microscope (STM) charge characterization technique, which reduces the influence of the typically perturbative STM tip field, to develop this understanding even further. Using this technique, we can now observe single molecule binding events to atomically defined reactive sites (fabricated on a hydrogen-terminated silicon surface) through electronic detection. We then developed a simplified error correction tool for automated hydrogen lithography, quickly directing molecular hydrogen binding events using these sites to precisely repassivate surface dangling bonds (without the use of a scanned probe). We additionally incorporated this molecular repassivation technique as the primary rewriting mechanism in ultra-dense atomic data storage designs (0.88 petabits per in^2).

4.2 Introduction

As the end of the current silicon technological roadmap draws closer, ever more capable tools for atomic-scale fabrication are enabling the use of hydrogen-terminated silicon as a platform for a number of alternative avenues [5,7,10,69,79,104,105]. The technique known as hydrogen lithography [10,34,37] (HL) has been used on this surface in the creation of atomic-scale logic elements [5], quantum structures [40], ultra-dense rewritable memory arrays [10], and controlled chemical reactions [105–107] including the precise placement of dopant atoms [7,79,105]. Using the tip of a scanning probe microscope, single atoms of hydrogen are removed from the surface to create atomically defined dangling bond (DB) patterns. With HL, tailored reactive sites can even be created for specific molecules [91,105–109] (Supplementary Figure 4.5). The precise and reproducible spatial integration of molecules into electronic devices is an important consideration towards scalable production, although it remains a considerable challenge. There is a particular focus on the integration of molecules on silicon surfaces to complement and enhance existing technologies [86, 90, 110–112]. This is because molecules can exhibit an array of properties, adding specific functionalities to a given device [110, 112–116]. The reactivity of a variety of molecules with the silicon surface has been studied, including simple molecules like hydrogen [91, 108], and more complex molecules such as alkenes [90, 109, 110] and phosphine [117, 118].

To propel the spatially controlled integration of molecules with the silicon surface forward, new tools that are capable of uncovering atomic-scale details of single molecule reactions are required. Typical scanning tunneling microscope (STM)-based dynamics studies rely on the observations of the motion and state of molecules, or DB sites, to gain insight into their reactivity. This approach is somewhat limited as the smallest intervals between scans are often many seconds to minutes apart [119, 120], making real-time observations difficult. There is also the impact of the STM tip as it scans over the area of interest, which can inadvertently deposit material, or strongly influence local dynamics through electric field effects and the injection of charge [35, 119, 121–123]. The latter aspects can additionally complicate the characterization of the amount of charge in DB structures when using only STM mea-

surements, although it is possible to determine the exact charge of defects in some systems through careful analysis and comparison to theory [124, 125].

Here, we report an all-STM method, which incorporates HL and hydrogen repassivation (HR) techniques [10, 25, 33] to readily characterize the total charge of DB structures at the single electron level, with reduced influence from the STM tip. With this STM method we were able to reproduce results [5, 75] taken at zero bias with an atomic force microscope (AFM). Once we characterized the number of charges in a given DB structure, such as in an atomically defined reactive site, we then extended this technique to the detection of externally induced charge changes in the DB site and surrounding area. We showed that a single molecule binding event occurring at the DB site can be electronically detected by monitoring for changes in charge. The event can be detected with temporal resolution up to real time, with the possibility of observing multiple bonding events at different DB sites. Combining the ability to precisely create tailored reactive DB sites using HL and the ability to detect a subsequent binding event at those sites provides a framework to study single molecule reactions, and to test the reliability of theoretically predicted pathways [126–130].

In this work, we also further the prospect of the scalable fabrication of atomic electronics and ultra-dense room-temperature stable memory on hydrogen-terminated silicon. The recent discovery of HR [10, 25, 33] to complement automated HL [10] has already resulted in significant fabrication advances [5, 10, 75], although there is still room to improve repassivation speeds. Currently, the only method to controllably add hydrogen to the surface is to sequentially repassivate DBs with atomic hydrogen attached to a scanned probe [10, 25, 33]. When the probe is depleted of hydrogen, it must travel to gather more. By using HL to create specific DB sites we have demonstrated that we can precisely direct where hydrogen molecules react on the surface of both hydrogen-terminated and deuterium-terminated silicon (Supplementary Figure 4.6) to repassivate DBs without a probe, while leaving other DB structures unreacted. This technique is not only simpler, but also faster than HR because it is unencumbered by the finite number of hydrogen atoms that can be adsorbed to a probe [10, 25, 33], resulting in a more convenient tool to repair fabrication errors in HL. We then integrated this improved repassivation method as

the primary rewriting process in a proof-of-concept atomic memory array, with a maximum storage density of 1.36 bits per nm^2.

4.3 Results and discussion

4.3.1 STM charge characterization of atomically defined structures

Single DBs on an otherwise hydrogen-passivated silicon surface introduce an isolated electronic state within the silicon band gap [35, 40, 64]. The current through a DB, as measured by an STM tip, can be influenced by the DB's local electrostatic environment [39, 64], including by the charge state of subsurface dopants [64]. Due to the sample preparation method there is a dopant-depleted region extending over 60 nm from the surface, which largely isolates surface DBs and dopants in this layer from the bulk [63]. At 4.5 K, dopant atoms laterally separated from the tip by up to 15 nm and at a depth of approximately 5 nm to 15 nm remain un-ionized (neutral) until a critical tip voltage is reached [64]. When one such dopant is field ionized by the tip, the now positive ion core causes downward bending of the local energy bands, thereby creating a conduction channel between the bulk silicon conduction band and the DB level, resulting in a measurable increase of current to the STM tip [64]. The DB acts as a window into the dopant ionization state, with this sudden onset of current manifesting as a sharp step in its current-voltage, $I(V)$, spectrum taken over the DB [64] (Figure 4.1). The step is commonly observed in the $I(V)$ spectra of most DBs (enabling their use as sensors), however, the exact strength and critical value of this signature depends on several factors. The sharpness of the tip can alter the value of the critical voltage, as when the tip changes, the strength of its field at the dopant atom changes as well, causing it to ionize at a different critical voltage. The critical voltage also depends on the random proximity of the dopant to the surface and a given DB [64]. By controllably adding local negative charges on the surface, so as to introduce upward band bending, it is possible to increase the magnitude of the critical voltage where this onset occurs, therefore requiring a larger

tip field to achieve dopant ionization. We take advantage of this effect to develop an STM procedure to characterize the amount of net charge in fabricated DB structures (Figure 4.1a-e). This was previously achieved with sensitive AFM frequency shift measurements of the charge state transitions of a sensor DB itself [75], or by using an AFM to map the spatial localization of charge in DB structures [5].

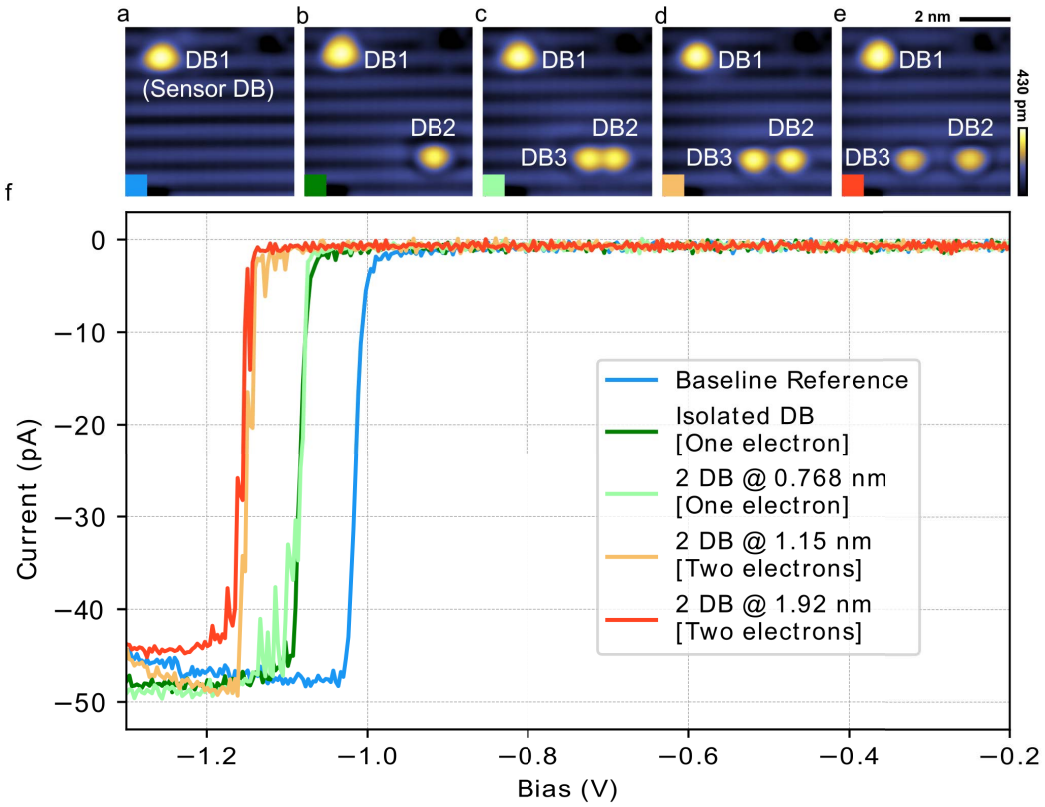

Figure 4.1: Characterizing charge occupations (V = -1.6 V, I = 50 pA, T = 4.5 K, 6.4 x 6.4 nm^2).
a) A scanning tunneling microscope (STM) image of a dangling bond (DB) on the hydrogen-passivated Si(100)-2x1 surface. The DB (DB1) exhibits a sharp current onset in its $I(V)$ spectrum (**f-blue**) due to the ionization of a subsurface arsenic dopant atom caused by the STM tip field. **b**) A second DB (DB2), containing a net charge of one electron is added to the surface 5.4 nm away from DB1, causing the step in the $I(V)$ spectrum of DB1 to shift to the left (**f-dark green**). **c**) A third DB (DB3) is added near DB2, no shift in the $I(V)$ spectrum of DB1 is observed (**f-light green**). **d**, **e**) The distance between DB2 and DB3 is varied to determine the net charge in the structure for each case. **f**) The $I(V)$ spectra taken over DB1, associated with **a-e**, showing the sharp onset of current.

It has been predicted that two closely spaced DBs (<1 nm) on the surface of highly arsenic-doped hydrogen-terminated silicon will share a net charge of one electron, whereas two isolated DBs will have a charge of one electron each [20]. While

recent AFM experiments have verified the single net electron occupation of two closely spaced DBs [5, 75], the analogous capability has been lacking in STM. This is principally because the STM applies a large perturbative field while imaging and is capable of injecting or removing charge on the surface. By working with sharp tips (approximately 5 nm radius) at voltages between -1.2 V to -1.6 V and characterizing structures in excess of 5 nm laterally removed from the STM tip, the possible effects of both charge injection and field perturbations can be greatly reduced (see Methods).

To determine the net charge of a DB structure with an STM, we first recorded a baseline reference $I(V)$ spectrum over a sensor DB (DB1) (Figure 4.1a,f-blue), which was selected because it exhibited the sharp current onset due to the ionization of a nearby isolated arsenic dopant. We then added a second isolated DB (DB2) 5.4 nm away (Figure 4.1b), and a new spectrum was taken over DB1. At this distance, AFM experiments performed with zero applied voltage have shown that DB2 will have a net charge of one electron [5, 75]. In this STM measurement, we observed that the presence of DB2 has increased the critical voltage required to ionize the subsurface dopant, shifting the onset of current observed in the $I(V)$ spectrum of DB1 to a larger negative voltage by -0.06 V (Figure 4.1f-dark green). The direction of the shift indicates that DB2 is negatively charged. The magnitude of the shift is essentially independent of the distance between the two DBs, as they are not interacting when separated by more than 5 nm [75], but rather depends on the distance between DB2 and the dopant atom [64]. Another DB (DB3) was then added 0.768 nm from DB2 (Figure 4.1c), and the spectrum of DB1 was measured once more (Figure 4.1f-light green). The presence of DB3 did not shift the spectrum this time, as would be expected if another negative charge was added into the area, further increasing the critical voltage required to ionize the subsurface dopant. We then erased DB3 using HR and created a new DB 1.15 nm from DB2 (Figure 4.1d). With this new placement, the spectrum taken over DB1 (Figure 4.1f-orange) showed an additional shift of -0.065 V, indicating the presence of another charge of one electron in the local area. Repeating this process, DB3 was positioned 1.92 nm from DB2 (Figure 4.1e), and no additional shift of the $I(V)$ spectrum of DB1 was observed (Figure 4.1f-red).

Since the induced shifts from one and two electrons were very close in magnitude in the $I(V)$ spectrum, we surmise that the un-ionized dopant was sufficiently deep, such that the change in lateral separation of the two DBs in the structure (DB2 and DB3) did not alter their distance to the dopant significantly. Through these STM measurements, we can conclude that 0.768 nm separating DB2 and DB3 gives a net charge of one electron within the pair (due to inter-electron repulsion [20]), while when the spacing is increased to 1.15 nm or more there is a net charge of two electrons within the structure/local area. These results are in agreement with recent AFM studies [5,75] (also see Supplementary Figure 4.7 for additional AFM results).

Using HL and HR to create and erase a number of isolated DBs (with a charge of one electron) in a particular area, we have demonstrated the capability to calibrate the shifts in the $I(V)$ spectrum of a sensor DB in order to characterize the amount of net charge in larger DB structures, with reduced tip field effects. This technique enables minimally perturbative studies of charge occupation using only an STM (Supplementary Figures 4.8, 4.9). In variable-temperature scanned probe systems, we expect it will be possible to observe the $I(V)$ step over a range of temperatures up to approximately 40 K, above which the dopants in the depleted region begin to thermally ionize [131]. Using this technique, we have determined that two immediately adjacent DBs (as shown in Figure 4.2), forming an inter-dimer site, have a net charge of one electron among them (Supplementary Figure 4.8).

4.3.2 Detection of single-molecule binding events

Once the amount of charge in a particular reactive site (like the inter-dimer site) is known, it is possible to use the techniques described above to electronically detect a molecular binding event by periodically recording the $I(V)$ spectrum of a laterally-removed sensor DB (or, to achieve greater time resolution, rapidly sampling the current through it at a fixed bias voltage). If there is a change of at least one electron locally when a molecule binds, then there will be an associated change in the $I(V)$ spectrum (or current). While hydrogen molecules are generally found to be unreactive toward the clean silicon surface [90, 91], they are extremely reactive

with inter-dimer sites on an otherwise hydrogen covered surface [91]. The sites have zero net charge after hydrogen molecules dissociatively adsorb, repassivating their constituent DBs with hydrogen atoms. This is because the two DB states are eliminated upon each DB reforming a bond with a hydrogen atom.

Previous studies were in disagreement over the preferred pathway (inter-dimer [132] *vs.* intra-dimer [133]) for the dissociative adsorption of hydrogen molecules on the silicon surface. It was eventually shown that the inter-dimer pathway was the dominant one [108], corroborated by theoretical calculations, which predicted it to be barrierless [126–129]. These results relied on sequential STM observations of random adsorption events on the surface [108]. With HL, instead of observing random events, we created both the inter- and intra-dimer sites in the same area on the hydrogen-terminated surface. We observed that only the inter-dimer sites reacted with hydrogen molecules, providing additional, very direct support for the dominance of the inter-dimer pathway (Supplementary Figure 4.10).

Figure 4.2 shows the electronic observation/detection of a single hydrogen molecule binding event to a fabricated inter-dimer site. To detect the event, we created an inter-dimer site 10.2 nm (thereby reducing any STM field effects) from a sensor DB exhibiting a sharp onset in its $I(V)$ spectrum (Figure 4.2a,b,e). We then controllably introduced hydrogen gas (H_2) into the vacuum chamber to establish a pressure of $4{\cdot}10^{-7}$ Torr, external to the cryo-shielding, and recorded a spectrum over the sensor DB at 35 s intervals (see Methods). After 875 s elapsed, the step in the $I(V)$ spectrum was detected to have shifted back to its original position (Figure 4.2e), indicating that a binding event occurred, and a hydrogen molecule had dissociatively reacted with the inter-dimer site. Subsequent imaging of the reaction site confirmed the DBs of the inter-dimer site had been repassivated with hydrogen (Figure 4.2c). This technique has the potential to be extended to observe multiple reactive sites, with each site shifting the step of a sensor DB an additional amount (Supplementary Figure 4.11).

The time for a hydrogen molecule to bind to an inter-dimer site depends on the pressure of hydrogen gas at the sample surface. Due to the design of the STM chamber, the pressure measurement outside of the cryo-shielding is not an entirely

accurate representation of the pressure in the vicinity of the tip and sample, where there is no pressure sensor. There is low flux of gas through the shielding and the cold shield surfaces lower the pressure further through cryo-pumping effects. We believe that the hydrogen molecules are arriving at the inter-dimer sites from gas phase, as the pressure and temperature of the system are such that H_2 cannot exist in a liquid phase [134, 135]. By measuring the reaction time of inter-dimer sites with hydrogen molecules, the pressure in the vicinity of the sample surface can be estimated (see Methods).

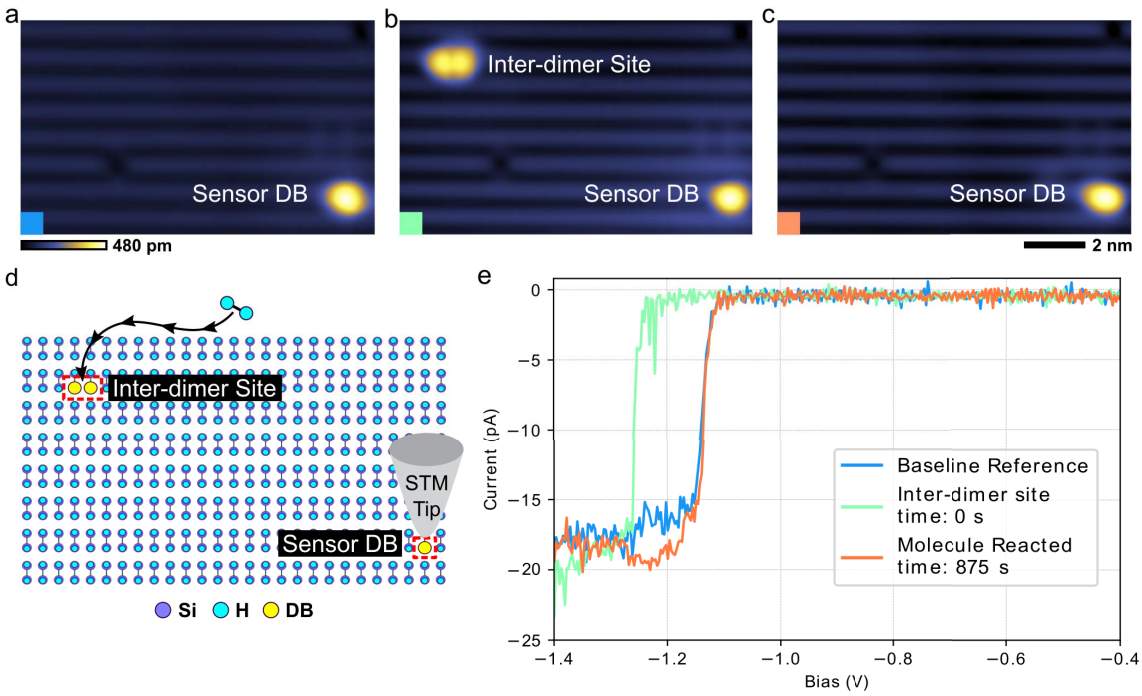

Figure 4.2: Electronically detecting a binding event (V = -1.6 V, I = 50 pA, T = 4.5 K, 11.3 x 7 nm^2).
a) Scanning tunneling microscope (STM) image taken of the area around a sensor dangling bond (DB) exhibiting a sharp current onset in its $I(V)$ spectrum. **b**) STM image after the creation of an inter-dimer site 10.2 nm from the sensor DB. **c**) STM image after hydrogen gas was added into the vacuum chamber, and the reaction of a hydrogen molecule with the inter-dimer site was electronically detected by a shift in the $I(V)$ spectrum taken over the sensor DB. **d**) The geometry of the surface, showing the sensor DB (dashed red square), and the location where an inter-dimer site has been created from DBs (dashed red rectangle) to react with an ambient hydrogen molecule (light blue). **e**) The $I(V)$ spectra taken periodically over the sensor DB associated with **a**, **b**, **c**.

4.3.3 Directing single-molecule binding events (molecular hydrogen repassivation)

We explored the relative reactivity of hydrogen molecules with a variety of DB structures on both a hydrogen-terminated and deuterium-terminated surface, in-

cluding with inter-dimer sites positioned in situations relevant to HL (with different proximities to other DBs and defects) (Supplementary Figures 4.6a,b, 4.11a-e). We observed a lack of reactivity of non-inter-dimer structures with hydrogen molecules (Supplementary Figures 4.5, 4.6a,b, 4.10). We also did not observe any prohibitive effects on the reactivity of the inter-dimer sites during our chosen timescales, instead finding them to be highly reactive, even when close to or part of other multi-DB structures. The reactions occurred even while the tip was fully withdrawn from the surface (Supplementary Figure 4.11). This robust nature and the speed of reaction of hydrogen molecules with inter-dimer sites, at an estimated pressure of $1{\cdot}10^{-9}$ Torr (see Methods for estimation), allowed us to use spatially controlled chemistry to realize a faster and simplified method for both error correction in automated HL and rewritable binary data storage.

Recent advances in HL have enabled the erasure/repassivation of isolated DBs by bringing in individual hydrogen atoms bonded to a probe tip [10, 25, 33]. These HR techniques have led to the demonstration of rewritable ultra-dense information storage [10] and atomic circuitry [5]. One limitation of these techniques, however, is that they require the tip to gather hydrogen atoms from locations outside of the fabrication area whenever the tip becomes depleted of available hydrogen. This can slow the fabrication process when many sequential corrections are required and is one of the rate-limiting factors in the rewriting speed of the atomic memory arrays [10]. Instead of bringing in external hydrogen atoms on a probe for HR we can now direct the reaction of ambient molecular hydrogen to erase DBs. This technique is also more generally accessible as it relies on the well-established process of removing hydrogen atoms from the surface, which is less restricted by specific tip geometries or materials, to achieve repassivation [10, 54].

To initiate spontaneous molecular hydrogen repassivation (M-HR), we first created an additional DB adjacent to a target DB so as to form a reactive inter-dimer site (Figure 4.3). Then, by working at sufficiently high hydrogen gas pressures (in vicinity of the sample surface, approximately $1{\cdot}10^{-9}$ Torr), both the targeted DB and the one created adjacent to it were spontaneously repassivated with hydrogen when a hydrogen molecule dissociatively reacted with the site, leaving all other DBs

unaltered. The inter-dimer site in Figure 4.3c reacted between the acquisition of Figure 4.3c and 4.3d, taking less than 52 s (working at even higher pressures can reduce the time further), while the tip was available to perform other tasks. Working at higher hydrogen pressures has not appeared to impact the long-term stability of the structures fabricated from single DBs (Supplementary Figures 4.5, 4.10). Figure 4.3f shows the same structure in Figure 4.3e unchanged six days later in an environment of an estimated pressure of $1{\cdot}10^{-9}$ Torr.

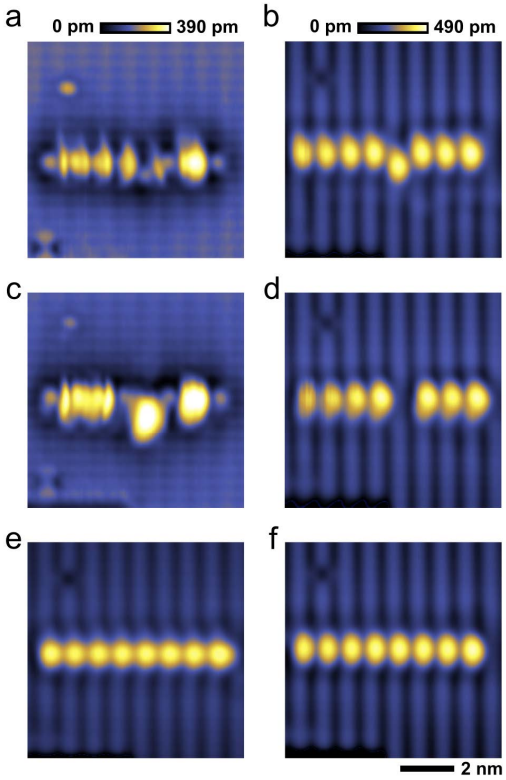

Figure 4.3: Molecular hydrogen repassivation (I = 50 pA, T = 4.5 K, 8 x 8 nm^2).
a) (V = 1.4 V) A Scanning tunneling microscope (STM) image of an 8-bit dangling bond (DB) memory array, with a fabrication error, taken to visualize the location of the surface hydrogen atoms. When imaging DB structures in empty states, there is a dynamic interplay between charge injection from the tip, discharging rates into the bulk, and tip-induced band bending, which causes a dark region to appear surrounding the structure [35, 74, 136]. It has also been proposed that the additional corrugation between neighboring DBs in the structure is due to contributions from excited states [40]. **b**) (V = 1.6 V) The same structure in **a**, taken at a negative sample bias to better visualize the location of the DBs in the array. **c**) (V = 1.4 V) An STM image taken after the erroneous DB in a was converted into an inter-dimer site, by removing an additional hydrogen atom from the surface. **d**) (V = -1.6 V) The STM image taken immediately after **c** (52 s later), during which time the inter-dimer site reacted with an ambient hydrogen molecule to erase the erroneous DB. **e**) (V = -1.6 V) The error-free 8-bit memory array structure, after the removal of the correct hydrogen atom from the surface. **f**) (V = -1.6 V) The same structure shown in **e** unchanged after 6 days in an environment of an estimated pressure of $1{\cdot}10^{-9}$ Torr of hydrogen gas.

This "create-to-erase" style of error correction eliminates the need to bring in external hydrogen atoms on a probe for the majority of situations where erroneous DBs need to be corrected during fabrication of atomic circuitry. Desired circuit patterns need not employ any reactive pairings of DBs [5], making all other parts of the circuit immune to the corrective H_2 exposure. The reduction in tip movements to gather atomic hydrogen realized by implementing M-HR compared to HR will additionally result in a time savings per correction/rewriting operation. M-HR has the potential to reduce the complexity of the machine learning algorithms [73, 137] required for the scalable automation of atomic-scale fabrication and of rewriting atomic memory arrays as well. This is because with M-HR, a single step (the removal of a surface hydrogen atom) can now be used for both fabricating and erasing, as opposed to additionally training neural networks to gather and recognize when a tip is loaded with hydrogen.

With M-HR there is also no physical limitation on the amount of hydrogen available for corrections, as more H_2 can always be added into the chamber. In situations where it is not possible to convert an erroneous DB into an inter-dimer site, previously established HR techniques can still be used to compliment M-HR, providing a more complete and efficient fabrication toolset. Furthermore, the selective reaction of hydrogen with inter-dimer sites has been observed at room temperature [108] and above [132], making it a viable tool for hydrogen lithography in non-cryogenic conditions [34].

4.3.4 Improved ultra-dense atomic data storage

The use of DBs as bits in ultra-dense rewritable atomic memory arrays was recently demonstrated on the hydrogen-terminated silicon surface [10]. Such arrays are a promising candidate for future data storage applications because in addition to the ultra-high densities that are possible, there are high barriers to diffusion for DBs along the surface, providing stability well above ambient room temperature [28, 29]. The primary rewriting mechanism of these arrays is currently HR; however, they can now be redesigned to incorporate M-HR as the main means of altering the stored

information (Supplementary Figure 4.12). In these arrays, each bit/DB is placed along a dimer row, with one lattice site acting as a buffer on each side to separate unit memory cells (Supplementary Figure 4.12a). The primary rewriting mechanism of bits/DBs in this configuration is currently HR. M-HR cannot be incorporated into this design, as removing a buffer atom to change a particular bit into an inter-dimer site would also affect the neighboring bit. However, the arrays can be redesigned to incorporate M-HR as the main means of altering the stored information by shifting the geometry by 90° and redefining the area of a unit memory cell (Supplementary Figure 4.12b,c). In these alternative designs, each bit/DB can now be converted into an inter-dimer site to be rewritten as needed, unlike in the original implementation [10] (Supplementary Figure 4.12a). By incorporating M-HR, the maximum storage density of the arrays is reduced from 1.70 bits per nm^2 to 1.36 bits per nm^2 (Supplementary Figure 4.12b). The slight reduction in maximum storage density is compensated for by the simplicity and increased maximum speed of rewriting multiple bits, compared to HR (where the tip needs to travel away from the array to be loaded with multiple hydrogen atoms). Additionally, the unlimited local supply of hydrogen molecules removes any restriction on the number of possible write/rewrite cycles of the memory arrays.

We have demonstrated the use of M-HR to rewrite a small 24-bit memory array created using automated HL [10] (Figure 4.4a,b). With M-HR, once the bits/DBs to be overwritten were converted into inter-dimer sites (see Methods), the tip was available to perform other tasks, while the repassivation could proceed in the background in a quasi-parallel fashion. We were able to use the tip to record images in between the acquisition of Figure 4.4e and Figure 4.4h (Supplementary Figure 4.13), as well as condition it further. This is unlike the HR procedure, which is inherently serial, where the tip is actively involved during the entire repassivation process.

Since the process to replace surface atoms now only requires the technique for atom removal, techniques like M-HR provide a possible path forward from purely scanned probe-based atomic-scale fabrication. In the future, as ion and electron beam-based fabrication techniques become increasingly capable of imaging and manipulating single atoms [12,138], it is conceivable that the STM probe used to remove

hydrogen atoms from the silicon surface could eventually be replaced. Should such a transition occur for the removal of atoms, M-HR presents the ability to add material back in a controlled manner, with the prospect of completely scanned probe-free writing/rewriting for data storage applications.

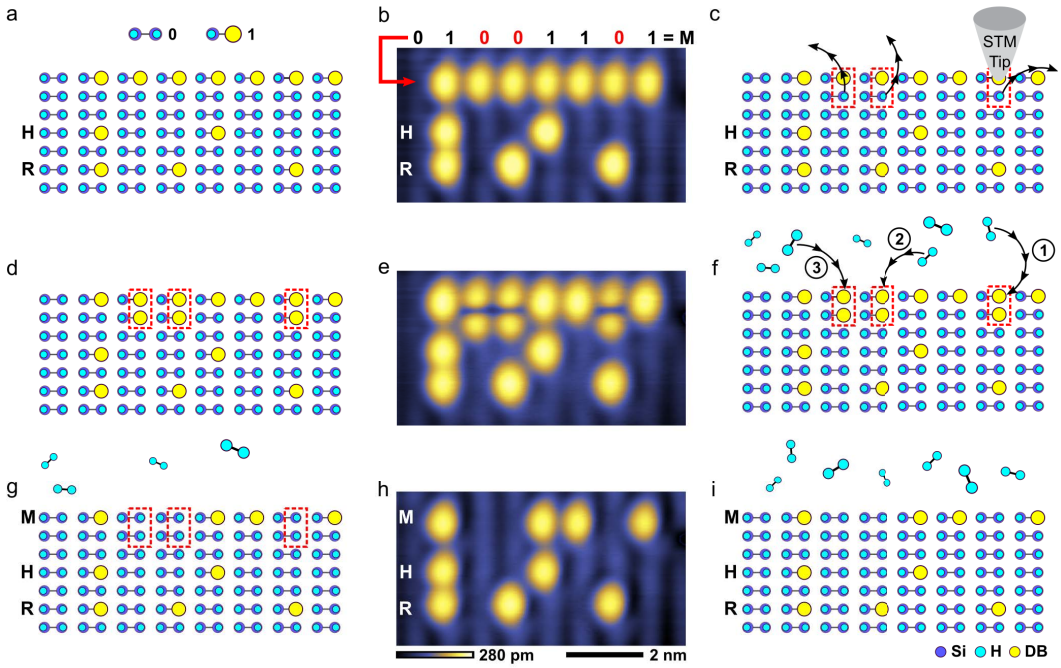

Figure 4.4: Rewriting a 24-bit memory array (V = -1.65 V, I = 50 pA, T = 4.5 K, 4 x 7.5 nm^2).
a) A schematic of a 24-bit memory array created from dangling bonds (DBs). The first line of the array is blank (01111111), the next two lines are the ASCII binary forms of the letters H (01001000) and R (01010010). **b**) An STM image of the 24-bit array created from DBs (using automated hydrogen lithography [10]) with a storage density of 1.36 bits per nm^2. The data in the first line will be rewritten to store the letter M (01001101). **c**) Using the automated scanning tunneling microscope (STM) tip, the surface hydrogen atoms highlighted in red will be removed to create reactive inter-dimer sites in order to rewrite the array. **d**) A schematic of the surface after the three hydrogen atoms shown in **c** have been removed. **e**) An STM image of the 24-bit DB array after three surface hydrogen atoms have been removed with the STM tip to create inter-dimer sites. **f**) Hydrogen gas is introduced into the vacuum chamber to bind with the inter-dimer sites (highlighted in red). The three reactions proceeded in the order indicated. The full sequence of images is available in Supplementary Figure 4.13. **g**) The first line of the array shown in **a** has been rewritten to the letter M, now that hydrogen molecules have dissociatively reacted with the inter-dimer sites shown in **d**. **h**) An STM image of the 24-bit memory array after the inter-dimer sites have reacted with hydrogen molecules, rewriting the stored information. **i**) The remaining hydrogen gas in the chamber does not react with the isolated DBs in the array and can be used in further rewriting operations.

4.4 Conclusions

We have demonstrated a process that can be used to conveniently characterize the charge occupation, or changes, of fabricated DB structures down to a single electron level, with only an STM. Using HL and HR techniques to create and erase single isolated DBs with a charge of one electron, the shifts of a feature in the $I(V)$ spectrum of a sensor DB can be calibrated to compare against those induced by a structure of interest. With this technique we verified prior AFM results with an STM.

We electronically detected the binding event of a hydrogen molecule at a prepared inter-dimer site on the surface, with the tip laterally removed by greater than 10 nm. We expect that the same techniques employed here can also be applied to study the adsorption dynamics of additional molecules of technological interest, including diverse alkenes and aromatic molecules by using other tailored DB reactive sites (such as in Supplementary Figure 4.5). The inter-dimer and intra-dimer sites presented here can directly be used to study cycloaddition reactions on silicon [110], including with ethylene [109, 139]. Due to their charged nature, reactive DB sites can also be directly integrated into field-controlled atomic electronic circuitry designs [5], providing yet another route for sensing applications. The ability to exactly position reactive sites in a particular area will also further the study of the effects of atomic-scale surface variations on the reactivity of otherwise identical DB sites.

We applied the ability to create selective DB sites tailored to react with hydrogen molecules as a more efficient means to correct fabrication errors in automated HL. The unified technique of atom removal and replacement offers several improvements over HR, including no longer requiring external hydrogen atoms to be brought in on a probe. M-HR was then incorporated into alternative designs of atomic memory arrays to improve the future rewriting speeds and overall usability of atom-based data storage, illustrated with a small-scale demonstration. Although this demonstration only contained 24 bits, there are no physical limitations preventing the technique from scaling to larger arrays.

4.5 Methods

4.5.1 Equipment

All measurements were performed with a commercial low-temperature Omicron LT-STM (or LT-AFM) operating at 4.5 K. Polycrystalline tungsten wire (0.25 mm diameter) was used for the STM tips. The tips were electrochemically etched in a solution of 2 M NaOH, then were processed under ultra-high vacuum (UHV) conditions in a field ion microscope to further sharpen them *via* a nitrogen gas etching process [52].

4.5.2 Sample preparation

The highly arsenic-doped Si(100) (0.003-0.004 ohm-cm) samples were degassed at 600 °C under UHV conditions for 24 h. Using resistive heating, the samples were brought to a temperature of 1250 °C three to five times *via* rapid flashes in order to remove all native oxide. We then exposed the samples to $1{\cdot}10^{-6}$ Torr of 99.999% pure hydrogen gas (or 99.7% pure deuterium gas), flowed through a liquid nitrogen trap. A nearby tungsten filament held at 1900 °C was used to crack the gas into its atomic constituents. The samples were exposed to the gas for 120 s without heating, then were rapidly flashed to 1250 °C. The temperature was then quickly brought down to 330 °C for 150 s, giving the hydrogen(or deuterium)-terminated 2x1 surface reconstruction.

4.5.3 Reducing tip field effects

For sharp tips/probes, with radii of less than 20 nm, there is a significant reduction in the strength of the local tip field and charge injection/extraction along the surface with increasing lateral separation from the tip [35, 40, 74, 136, 140–142]. Experimentally, on this substrate, the effects of charge injection from an STM tip into a DB have been observed with lateral separations of approximately 2-4 nm depending on the tip radius [35,40,136], with sharper tips requiring closer tip-DB separations for

charge injection to occur [35, 136]. The effects of the tip field, without the injection of charge, have been observed at up to 7 nm of lateral tip-DB separation, depending on the tip geometry and applied voltage [35, 40, 75, 136]. By working with single atom tips and restricting voltages to between -1.2 V to -1.6 V, and additionally characterizing structures five or more nanometers laterally removed from the STM tip, we greatly reduce the possible effects of both charge injection and field perturbations.

4.5.4 Electronic molecular detection

Once a sensor DB was identified, a baseline $I(V)$ spectrum was recorded, and the desired number of inter-dimer sites were created. The STM tip was then positioned over the sensor DB and the measurement program was initiated to periodically record the $I(V)$ spectrum. We then introduced 99.999% pure hydrogen gas into the system until a pressure of $4{\cdot}10^{-7}$ Torr was achieved, *via* a manual leak valve (the initial base pressure inside of the STM was $5{\cdot}10^{-11}$ Torr). The time interval was selected such that the entire $I(V)$ spectrum of the sensor DB could be recorded (both forward and backward sweeps), and the hydrogen gas pressure could be manually corrected in between measurements. The time window also provided sufficient delay for the majority of the mechanical vibrations of the STM tip (due to the manual actuation of the leak valve) to dissipate before each spectrum was acquired. To undertake real-time measurements, where the acquisition of the full $I(V)$ spectrum is not required, the tip can be held at a fixed voltage and the tunneling current (or z-height) can be monitored for sudden changes in the DB conductivity (Supplementary Figure 4.14). The jump in the tunneling current can be detected in an identical way to the detection of current changes used in HL, with a maximum sampling rate of 10 kHz [10].

4.5.5 Estimating pressure

Using the observations of the reaction time of inter-dimer sites with hydrogen molecules, we can estimate a bound on the pressure of hydrogen inside the shielding, where there is no pressure sensor available. To estimate the hydrogen pressure in the vicinity of the tip and sample (P_{est}) we assume a perfect sticking coefficient

due to the barrierless nature of the reaction of molecular hydrogen with inter-dimer sites [126–129] (along with our observation of the reaction at 4.5 K). Using the ideal gas law, and the thermal distribution of the velocities and number of hydrogen molecules incident on the silicon surface, the pressure is given by [143]:

$$P_{est} = \frac{d \cdot \sqrt{2\pi \cdot m_{H_2} \cdot k_b \cdot T}}{t_{r_x}} \tag{4.1}$$

where d is the number of surface sites per unit area (for Si(100)-2x1: $d \approx 10^{19}$ sites per m^2), m_{H_2} is the mass of a molecule of hydrogen, k_b is the Boltzmann constant, T is the temperature (4.5 K), and t_{r_x} is the observed time for all sites to react. Using conventional sequential STM image acquisition for slower dynamics, we observed three inter-dimer sites react over 45 h (Supplementary Figure 4.10), giving an estimated pressure of approximately $1{\cdot}10^{-12}$ Torr. With observations taken using the electronic detection technique after the introduction of H_2 into the chamber, including Figure 4.2, we estimated a local pressure of approximately $1{\cdot}10^{-10}$ Torr. In Supplementary Figure 4.11, all three inter-dimer sites reacted within 120 s after creating the third inter-dimer site. Including this observation, along with Figure 4.3 (52 s), we estimated a pressure at that time of at least $1{\cdot}10^{-9}$ Torr near the sample surface, recognizing that the reactions may have occurred in less than 120 s in Supplementary Figure 4.11. Given an H_2 pressure of $1{\cdot}10^{-9}$ Torr at a temperature of 4.5 K, Equation 4.1 predicts that $t_{r_x} \approx 60$ s. The average measured t_{r_x} of the inter-dimer sites at an estimated H_2 pressure of approximately $1{\cdot}10^{-9}$ Torr at 4.5 K agrees well with this prediction. The agreement between the predicted and the measured reaction time further supports our notion that the hydrogen molecules arrive at the inter-dimer sites from the gas phase.

4.5.6 Rewriting atomic memory array

Once the bits/DBs identified to be rewritten were converted into inter-dimer sites (Figure 4.4), hydrogen gas was introduced into the vacuum chamber to achieve the same conditions as in Figure 4.3. Because the initial hydrogen background pressure

in the chamber external to the cryo-shielding was low ($<1{\cdot}10^{-11}$ Torr), it took approximately 30 minutes before the pressure in proximity to the tip and sample was sufficiently high for the first M-HR event to occur. The remaining events occurred within one minute of each other after an approximate pressure of $1{\cdot}10^{-9}$ Torr was achieved near the sample surface.

4.6 Supplementary information

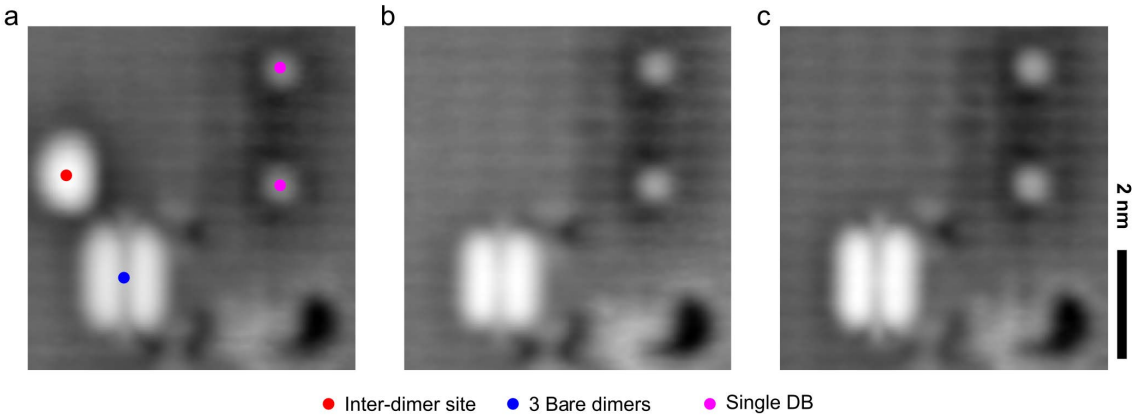

Figure 4.5: Reactive sites (V = 1.4 V, I = 50 pA, T = 4.5 K, 6.34 x 6 nm^2).
a) A scanning tunneling microscope (STM) image of an area where an inter-dimer site (red) has been created along with a site containing three adjacent bare dimers (blue), and two single dangling bonds (DBs) (pink). The inter-dimer site is highly reactive with hydrogen molecules, while the site with three bare dimers is reactive with phosphine molecules [105]. **b**) An STM image of the same area in **a** after sitting in a vacuum chamber with a base pressure of $5{\cdot}10^{-11}$ Torr for 44 hours. In this time, only the inter-dimer site has reacted with a hydrogen molecule, despite the 3 bare dimer site containing areas with equivalent geometry to an inter-dimer site. **c**) An STM image of the same area in **b** after sitting for an additional 97 hours in the vacuum chamber. The cryogens in the STM had to be replenished twice during this time, so the sample was subjected to temperature spikes up to 15 K and pressure spikes of up to $1{\cdot}10^{-8}$ Torr during this process. Again, no reactions were observed in this time.

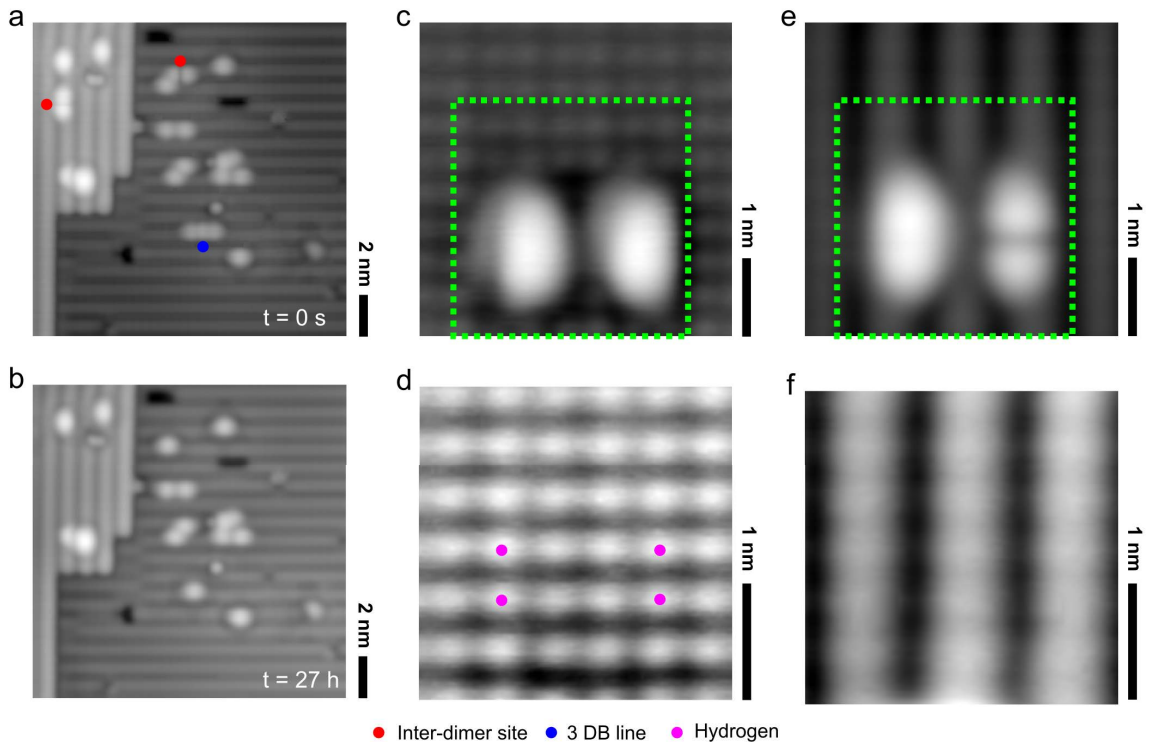

Figure 4.6: Reactions with deuterium-terminated Si(100)-2x1 (I = 50 pA, T = 4.5 K).
a) (V = -1.8 V, 15 x 15 nm^2) A scanning tunneling microscope (STM) image of a deuterium-terminated Si(100)-2x1 surface, with various dangling bond (DB) structures. **b**) (V = -1.8 V, 15 x 15 nm^2) The same area as in the previous figure after 27 hours in an environment of $9{\cdot}10^{-11}$ Torr of hydrogen gas (negligible deuterium background). At each inter-dimer site, a hydrogen molecule has reacted. In the structure with three directly adjacent DBs (containing an inter-dimer site), a hydrogen molecule reacted with two of the DBs, leaving an isolated DB remaining. **c**) (V = 1.4 V, 4 x 4 nm^2) An STM image of two inter-dimer sites created on the deuterated surface, ready to react with an ambient hydrogen molecule. **d**) (V = 1.4 V, 2.7 x 2.7 nm^2) An STM image of the area highlighted in **c** after the reaction of two hydrogen molecules. With the present imaging techniques, the hydrogen and deuterium atoms could not be differentiated. Inelastic tunneling spectroscopy [144] was also unable to resolve a discernible signal to identify the atoms. **e**) (V = -1.8 V, 4 x 4 nm^2) Filled states image of **c**. **f**) (V = -1.8 V, 2.7 x 2.7 nm^2) Filled states image of **d**.

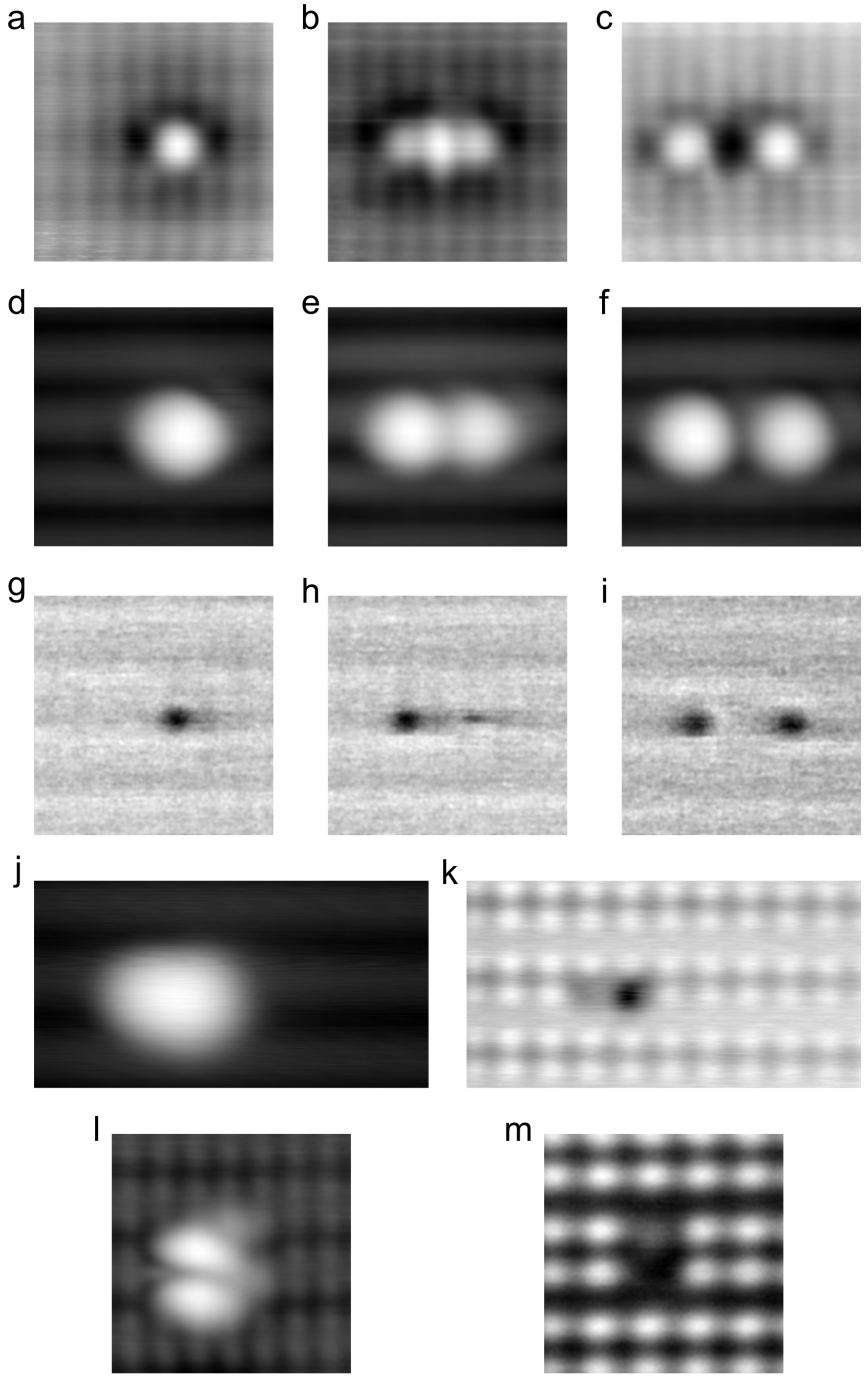

Figure 4.7: AFM measurements of net charge in DB structures.

Figure 4.7: *cont.* AFM measurements of net charge in DB structures. **a-c**) (V = 1.3 V, I = 50 pA, T = 4.5 K, 3 x 3 nm^2) Scanning tunneling microscope (STM) images of two dangling bonds (DBs) with various separations. **d-f**) (V = -1.8 V, I = 50 pA, T = 4.5 K, 3 x 3 nm^2) Filled state STM images of the same DBs in **a-c**. **g-i**) (V = 0 V, Z_{rel} = -300 pm, T = 4.5 K, 3 x 3 nm^2) Constant height AFM frequency shift images of the structures in **a-c**. The dark depressions represent the location of an electron within each structure [5]. In **g** and **h** there is only a net charge of one electron within the structures. In **i** there are two net electrons present. **j**) (V = -1.8 V, I = 50 pA, T = 4.5 K, 2 x 4 nm^2) An STM image of an inter-dimer site. **k**) (V = 0 V, Z_{rel} = -300 pm, T = 4.5 K, 2 x 4 nm^2) Constant height AFM frequency shift image of the inter-dimer site in **j**, showing the presence of only one net electron. **l**) (V = 1.3 V, I = 50 pA, T = 4.5 K, 3 x 3 nm^2) An STM image of an intra-dimer site. **m**) (V = 0 V, Z_{rel} = -300 pm, T = 4.5 K, 2 x 4 nm^2) Constant height AFM frequency shift image of the intra-dimer site (bare dimer) in **l**, showing the presence of only one net electron.

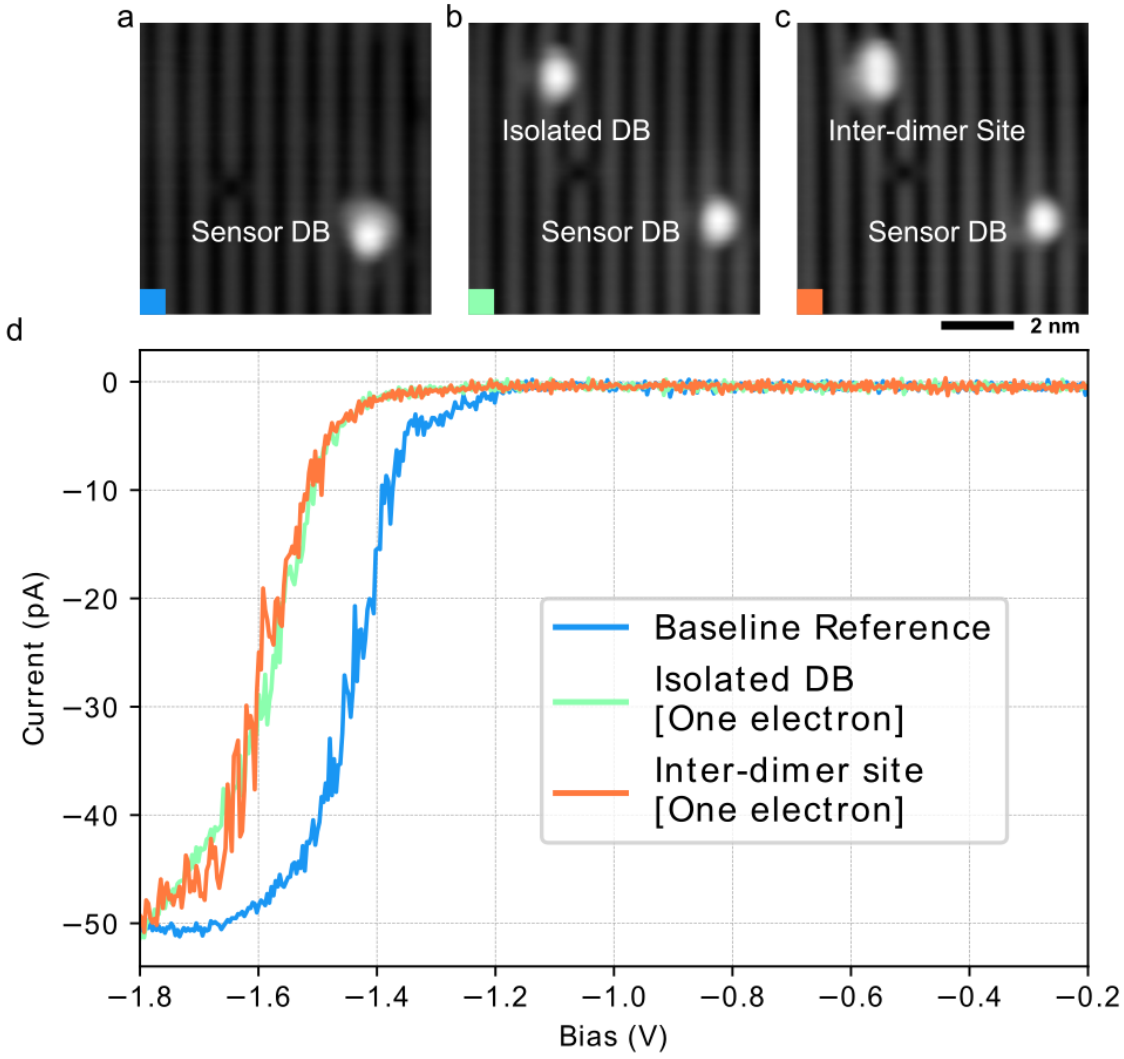

Figure 4.8: Net charge in an inter-dimer site (V = -1.8 V, I = 50 pA, T = 4.5 K, 8 x 8 nm^2).
a) A scanning tunneling microscope (STM) image of a dangling bond (DB) on the hydrogen-passivated Si(100)-2x1 surface. This DB exhibits a sharp current onset in its $I(V)$ spectrum due to the ionization of a subsurface arsenic dopant atom caused by the STM tip field, making it suitable to act as a charge sensor. **b**) A second DB, containing a net charge of one electron, is added to the surface to calibrate the sensor. **c**) The DB in **b** is converted into an inter-dimer site. **d**) The $I(V)$ spectra taken over the first DB, associated with **a-c**, showing the shift in the sharp onset of current.

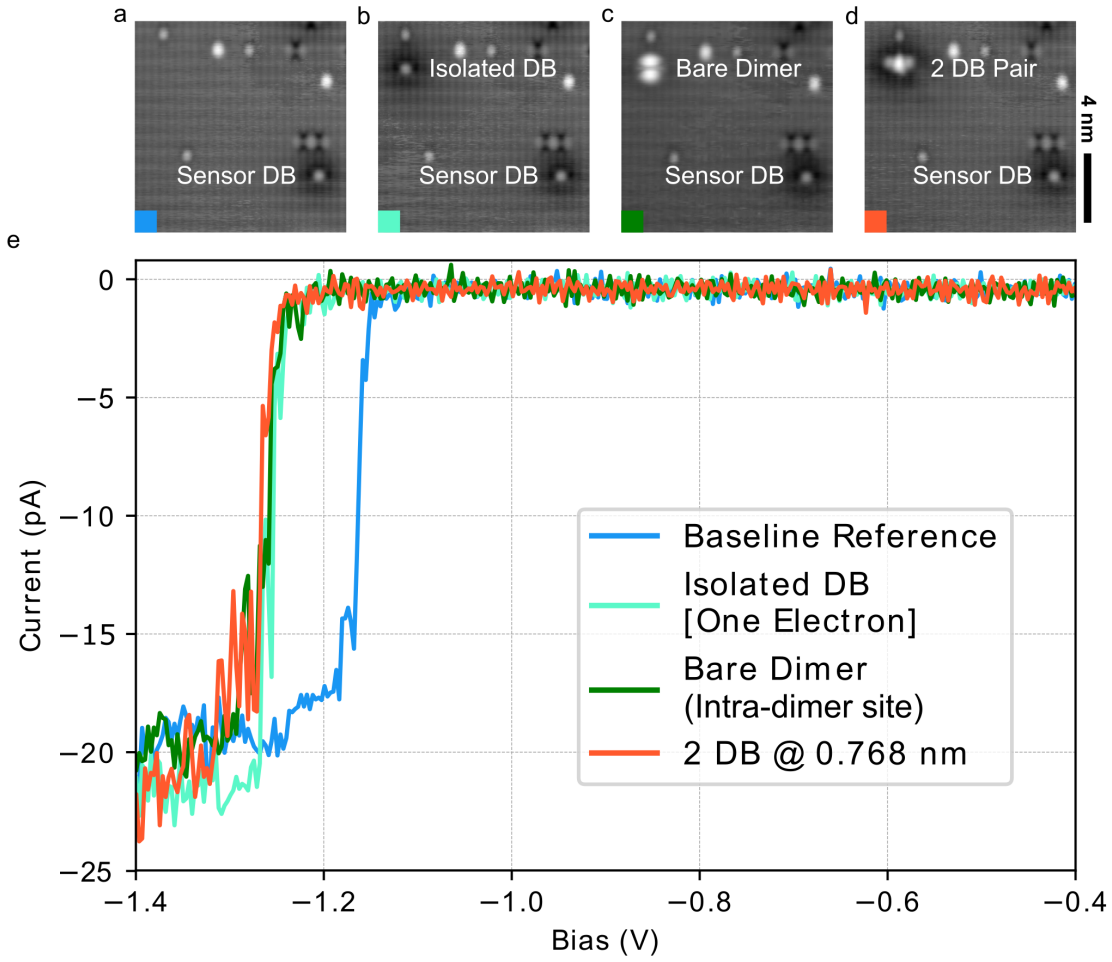

Figure 4.9: Net charge in other structures ($V = 1.4$ V, $I = 50$ pA, $T = 4.5$ K, 12 x 12 nm^2).
a-d) Scanning tunneling microscope (STM) images of the dangling bond (DB) structures associated with the spectra in **e**. **e**) The $I(V)$ spectra taken over the sensor DB in **a-d**. After the shift in the $I(V)$ spectrum of the sensor DB was calibrated in **b**, the structures in **c** and **d** were determined to have a net charge of one electron. These results correspond with the AFM measurements shown in Supplementary Figure 4.7.

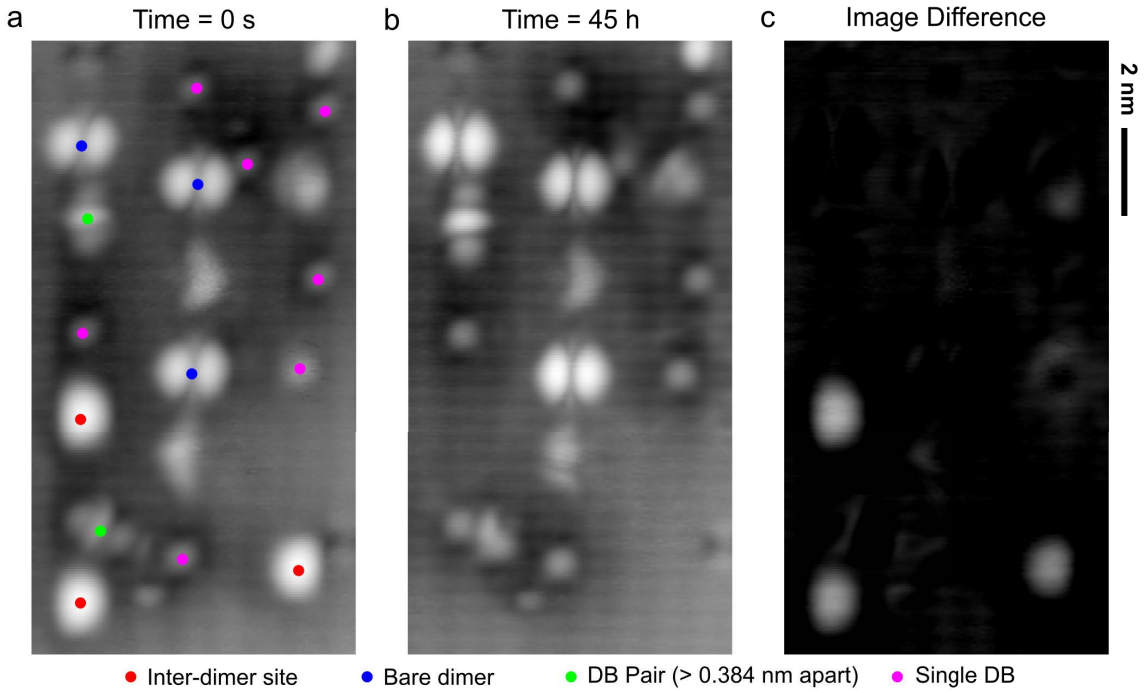

Figure 4.10: Various dangling bond structures (V = 1.4 V, I = 50 pA, T = 4.5 K, 14 x 8 nm^2).
a) A scanning tunneling microscope (STM) image of an area where a number of various DB structures have been created. Inter-dimer sites are denoted in red, while the intra-dimer sites (bare dimers) are denoted in blue. **b**) An STM image of the same area after sitting in a vacuum chamber with a base pressure of $5{\cdot}10^{-11}$ Torr for 45 hours. **c**) A difference image between **a** and **b**. Only the inter-dimer sites have reacted after 45 hours, with no other significant changes occurring in this time with any of the isolated DBs or other DB structures.

4.6.1 Multiple inter-dimer sites

We created three inter-dimer sites 6.6 nm to 8.9 nm from a sensor DB, with the intention of detecting three sequential binding events. The observation of multiple sites is possible because the presence of each subsequent inter-dimer site shifted the $I(V)$ step used for electronic detection to increasingly negative voltages, as seen in Supplementary Figure 4.11f. While the tip was withdrawn from the surface (in preparation of adding additional H_2 into the chamber before initiating monitoring),

however, all three sites reacted within 120 s. The sites reacted so quickly because the base-pressure near the sample surface remained elevated after earlier trials (estimated to be at least $1{\cdot}10^{-9}$ Torr). With an improved experimental procedure and lower hydrogen background pressure such multi-reaction sequences can be monitored.

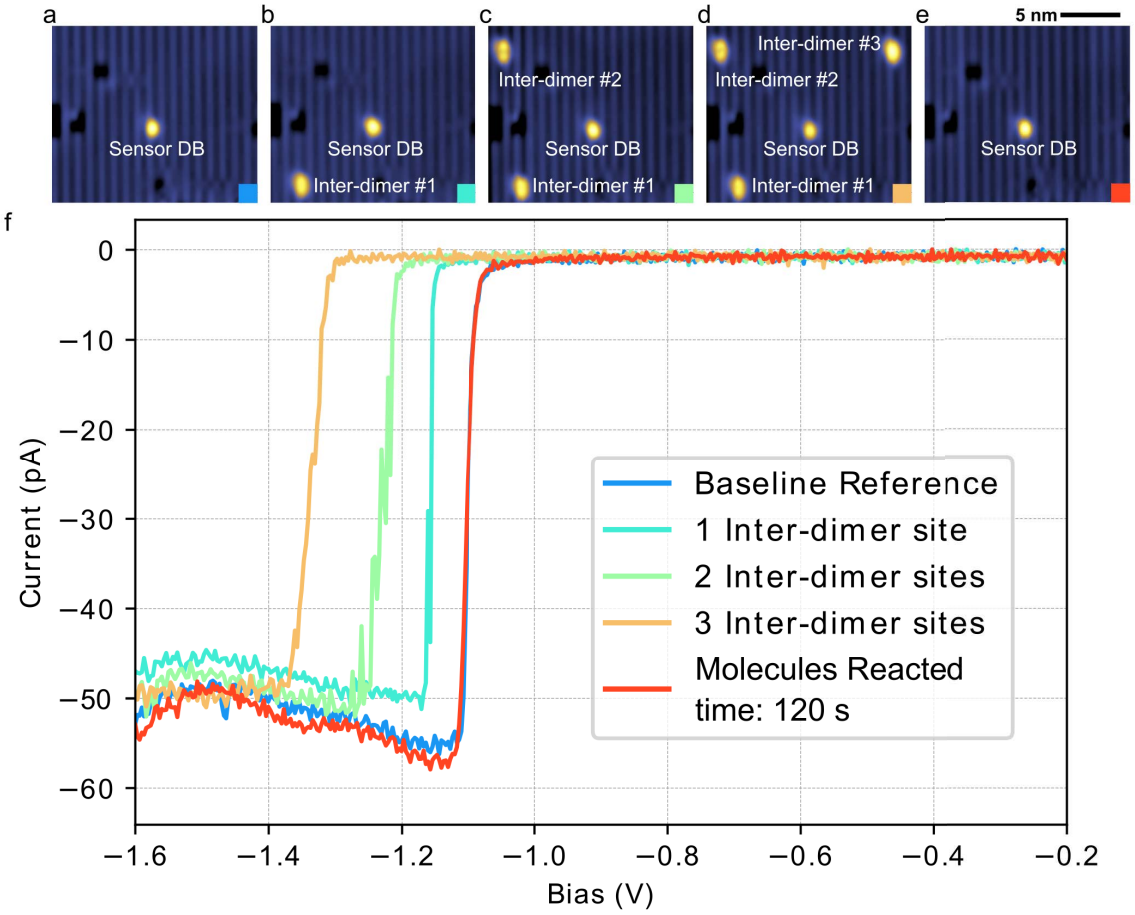

Figure 4.11: Multiple inter-dimer sites (V = -1.7 V, I = 50 pA, T = 4.5 K, 15 x 13 nm^2).
a) A scanning tunneling microscope (STM) image of an isolated dangling bond (DB) on the hydrogen-passivated Si(100)-2x1 surface, which exhibits a sharp current onset in its $I(V)$ spectrum (**f-blue**). **b-d**) STM images of a sequence of inter-dimer sites being added at various distances and locations relative to the sensor DB (6.6 nm, 8.9 nm, 8.4 nm). **e**) An STM image taken 120 s after the creation of the inter-dimer site in **d**, before any additional hydrogen gas was added into the vacuum chamber. **f**) The $I(V)$ spectra taken over the sensor DB, associated with **a-e**.

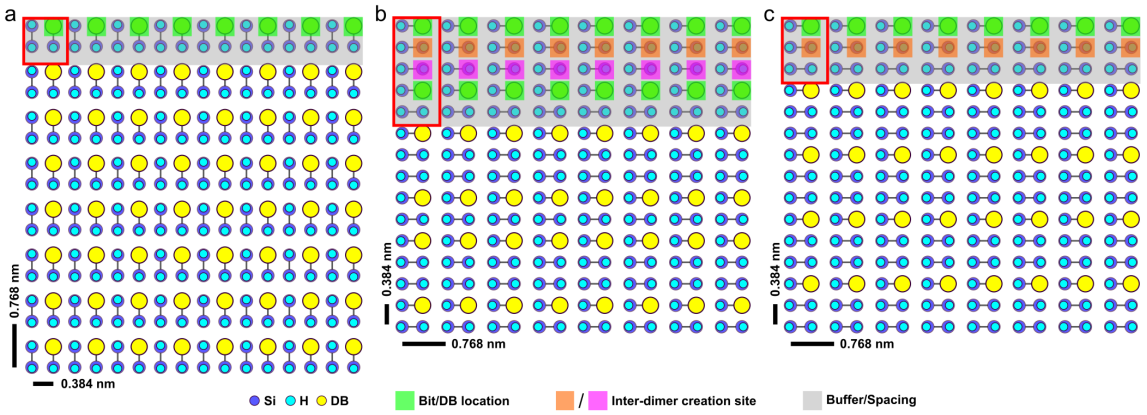

Figure 4.12: Ultra-dense atomic memory designs (8 bits per line). **a**) The original design of the ultra-dense memory array using dangling bonds (DBs) to represent one bit of information [10], with a maximum bit density of 1.7 bits per nm^2. The unit memory cell is denoted in red, containing one bit, the sites where hydrogen atoms are removed or replaced to store information are highlighted in green, the area in grey represents sites used to space each bit from the next. This memory was designed to be rewritten by bringing in external hydrogen atoms on a probe tip, which presented a potential bottleneck for the speed of rewriting operations. **b**) An altered array design for DB-based atomic storage, with a maximum storage density of 1.36 bits per nm^2. In this scheme the surface geometry has been rotated by 90° relative to **a**. The memory cell denoted in red now contains two bits highlighted in green (one upper bit and one lower bit). Each bit within the cell can now be rewritten by converting the DB into an inter-dimer site, which subsequently reacts with an ambient molecule of hydrogen. This removes the need to bring in hydrogen atoms externally. The sites that are used to convert the upper and lower bits in the cell to inter-dimer sites are highlighted in orange and pink respectively. In this design, the upper and lower bits within the same unit cell cannot both be converted into inter-dimer sites during the same rewriting operation because a hydrogen molecule could then instead react in between the upper and lower bits, leaving them unaltered. The array would have to be rewritten line by line in this case or employ an optimization algorithm to ensure no pair of upper and lower bits are converted into inter-dimer sites during the same rewriting cycle. **c**) This issue can be overcome at the expense of storage density. Here, the unit memory cell denoted in red contains one bit, which can also be rewritten through molecular hydrogen repassivation. The array has a maximum bit density of 1.13 bits per nm^2 and a more analogous geometry to **a**, where a given bit can be rewritten without consideration of any other bit. The choice in design between **b** and **c** depends on the particular application, where factors such as density and computational overhead for optimizing rewriting cycles need to be considered.

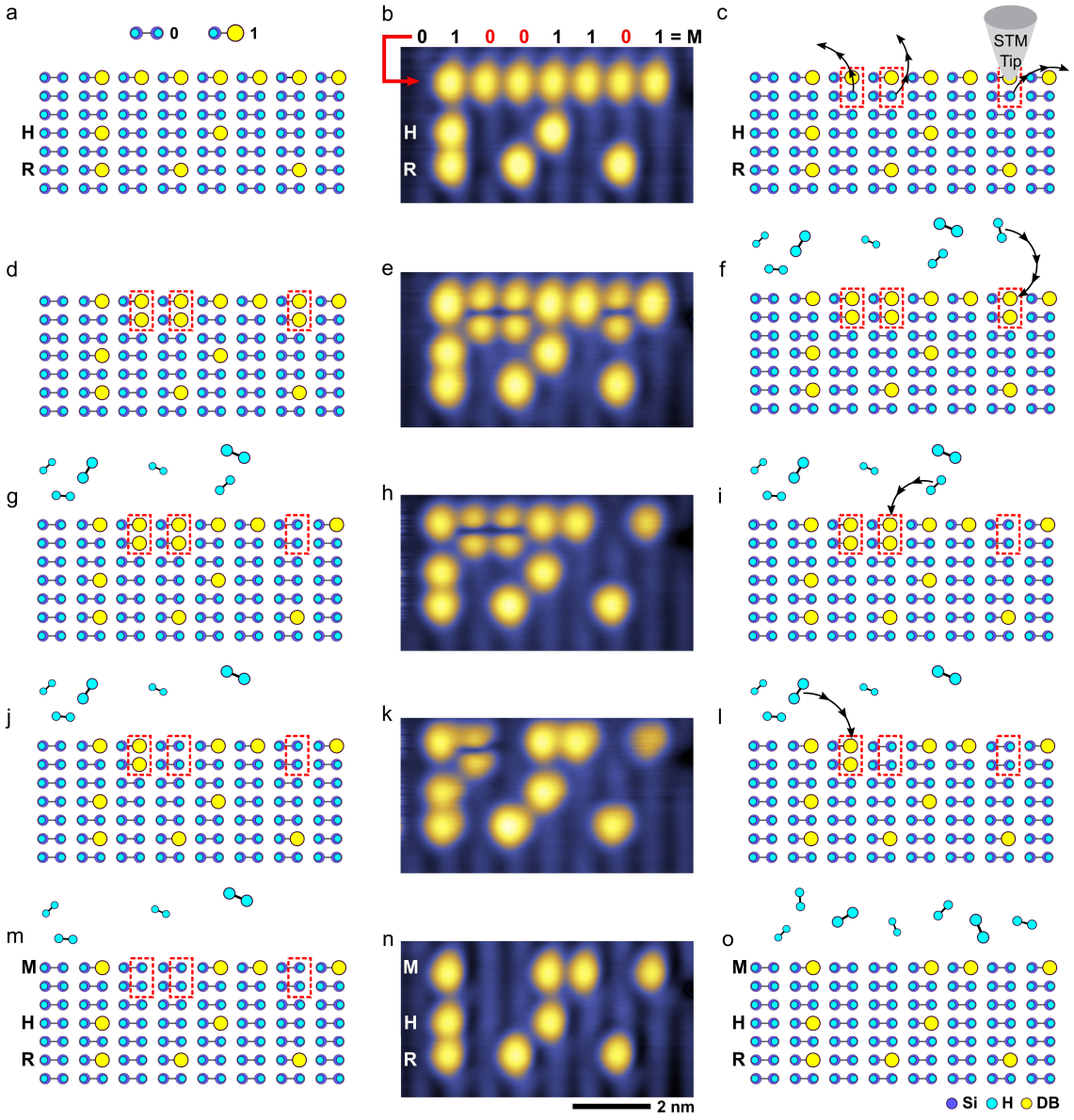

Figure 4.13: Full - rewriting a 24-bit memory array (V = -1.65 V, I = 50 pA, T = 4.5 K, 4 x 7.5 nm^2).

Figure 4.13: *cont.* Full - rewriting a 24-bit memory array (V = -1.65 V, I = 50 pA, T = 4.5 K, 4 x 7.5 nm^2).
a) A schematic of a 24-bit memory array created from dangling bonds (DBs). The first line of the array is blank (01111111), the next two lines are the ASCII binary forms of the letters H (01001000) and R (01010010). **b**) An STM image of the 24-bit array created from DBs (using automated hydrogen lithography [10]) with a storage density of 1.36 bits per nm^2. The data in the first line will be rewritten to store the letter M (01001101). **c**) Using the automated scanning tunneling microscope (STM) tip, the surface hydrogen atoms highlighted in red will be removed to create reactive inter-dimer sites in order to rewrite the array. **d**) A schematic of the surface after the three hydrogen atoms shown in **c** have been removed. **e**) An STM image of the 24-bit DB array after three surface hydrogen atoms have been removed with the STM tip to create inter-dimer sites. **f**) Hydrogen gas is introduced into the vacuum chamber to bind with the inter-dimer sites (highlighted in red). **g**-**l**) Schematics and associated STM images with each molecular hydrogen repassivation event. The first event took 30 minutes to occur while the system reached a working pressure of $1{\cdot}10^{-9}$ Torr of hydrogen gas. The following events occurred within a minute of each other. **m**) The first line of the array shown in **a** has been rewritten to the letter M, now that hydrogen molecules have dissociatively reacted with the inter-dimer sites shown in **d**. **n**) An STM image of the 24-bit memory array after the inter-dimer sites have reacted with hydrogen molecules, rewriting the stored information. **o**) The remaining hydrogen gas in the chamber does not react with the isolated DBs in the array and can be used in further rewriting operations.

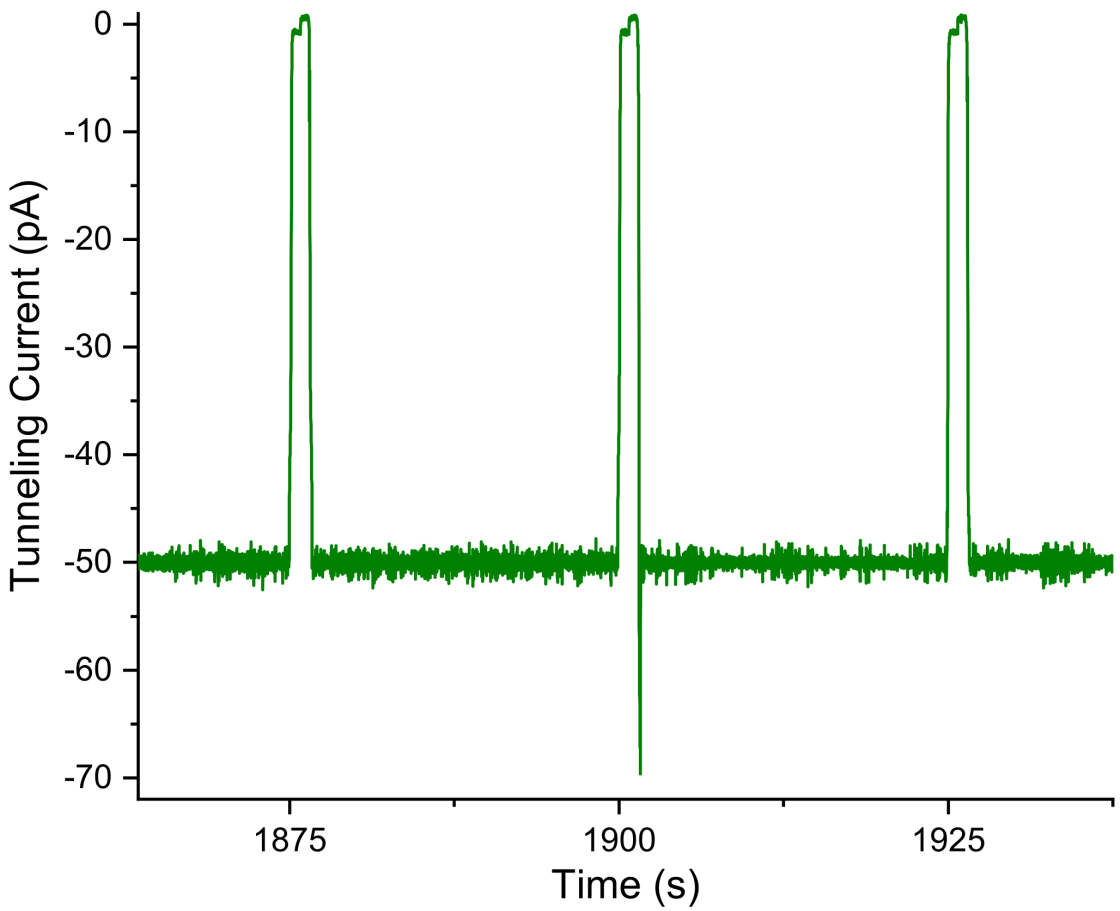

Figure 4.14: Tunneling current spike during molecular monitoring. Live sampling of the tunneling current while periodically monitoring a sensor dangling bond (DB). The periodic $I(V)$ measurements were taken every 25 s beginning at a bias of -1.6 V. When a hydrogen molecule binds to the monitored inter-dimer site, the conductivity of the sensor DB changes, causing a spike in the tunneling current, before the feedback control adjusts the tip height to return to the set current. The spike in current just after 1900 s indicates that the monitored inter-dimer site reacted with a hydrogen molecule. For fast time resolution of binding events, the tunneling current can be monitored for spikes, rather than recording $I(V)$ traces periodically.

4.7 Acknowledgments

The authors thank M. Salomons and M. Cloutier for their technical assistance, J. Pitters for helpful discussions, and J. Phillips for proofreading the manuscript. We would like to also thank NSERC, AITF, NRC, and QSi for their financial support.

4.8 Competing interest

A patent application is in process related to molecular hydrogen repassivation and memory designs as described in the manuscript. All of the authors are affiliated with Quantum Silicon Inc (QSi). QSi is seeking to commercialize atomic silicon quantum dot-based technologies.

Chapter Five

Extended details - Detecting and directing single molecule binding events on H-Si(100) with application to ultra-dense data storage

5.1 Selecting a sensor DB

Most DBs on the surface display the characteristic step in their $I(V)$ spectra due to the ionization of a subsurface dopant [64], making them suitable to act as a sensor DB. The exact strength and critical value of this signature depends largely on the random depth and lateral separation between an un-ionized dopant atom and the sensor DB [64]. The deeper the dopant, the larger the tip field required to cause ionization. In practice, despite the random nature of the dopant placement, it is always possible to find a suitable DB to act as a sensor or to position a DB on the surface (using HL and HR/M-HR) until a step is observed in its spectroscopy. Once a sensor DB has been selected (or positioned) that is at sufficient lateral separation along the surface (to reduce tip effects, as described in 4.5.3) from a target area, isolated DBs can be created and removed from there to calibrate the shifts of the sensor DB for charge characterization. The induced shifts of the sensor DB are generally independent of the absolute distance along the surface between the DBs in

the target area and the sensor DB itself. This is valid so long as the distance between each respective DB in the target area and the subsurface dopant is approximately the same (DB-target area distance $\gg$ individual lateral DB-DB separations within the target area). It also requires that the target area is further than 5 nm away from the sensor DB along the surface to ensure that the sensor DB will not interact with the DBs in the target area [75].

Instead, the induced shifts of the sensor DB are dependent on the distance between the subsurface dopant and the DBs in the target site, which alters the Coulombic gating effect on the dopant [64]. Changing this distance significantly (by moving the target area) will alter the field caused by the charges in the target area at the dopant, causing it to ionize at a different critical voltage. Supplementary Figure 4.11 illustrates this effect, where the first two inter-dimer sites are made 6.6 nm and 8.9 nm from a sensor DB respectively, yet induce approximately the same shift in the $I(V)$ spectrum, indicating that they are approximately the same distance from the randomly positioned subsurface dopant, while being different distances from the sensor DB. The third inter-dimer site created 8.4 nm from the sensor DB actually induces a larger shift, indicating that it is closer to the dopant atom.

If the sensor DB is to be used for charge characterization, then care must be taken to build the structure of interest in just one target area, to reduce any substantial distance changes between its constituent DBs and the dopant atom. If the sensor DB is being used to detect molecular binding events, quantifying the induced shifts from different target areas (as in Supplementary Figure 4.11) is less necessary. Instead, the main focus in this scenario is to detect when the position of the step changes over time, signaling a binding event.

5.2 Decreasing variability of sensor signatures

As discussed in Section 4.3.1 and 5.1, the exact strength and voltage of the dopant ionization signature in the $I(V)$ spectrum of a sensor DB depends on the random proximity of the dopant atom and sensor DB. With the current STM imaging techniques, it is not possible to determine the position and depth of the subsurface

dopant atom. As such, there is no reliable way to control the variability in the strength and voltage of the signature of a particular sensor DB. While this does not limit their practical use for charge characterization and sensing, standardizing their signature will allow for better and more reliable devices to be made.

A recent AFM result showed that it was possible to estimate the depth of a dopant atom using a movable DB as a quantum dot probe [75]. Such a technique will make it possible to eventually correlate dopant position with the corresponding ionization signature in the $I(V)$ spectrum of a sensor DB. Once such measurements have taken place, an ideal dopant depth/position can be identified. Pioneering work in using precisely placed dopant atoms has established techniques to position dopant atoms on a hydrogen-terminated silicon surface [46, 79], and subsequently cover it with additional layers of silicon [46, 79, 145]. These techniques can enable the control over both dopant placement and depth, which are necessary for fabricating identical devices.

5.3 Long-term sensing stability

Depending on the experimental parameters and the properties of the entity of interest (such as its sticking coefficient), long-term measurements over a sensor DB spanning many hours may be required before a binding event occurs. This can pose a potential problem as thermal drift and creep of the piezoelectric scanner will eventually cause the tip to move away from the sensor DB, making it impossible to sense a binding event. One solution to this problem is to utilize active "atom tracking" to ensure that the tip remains centred on the sensor DB during the entire experiment. The Nanonis control software for the STM includes such an atom tracking module. By moving the tip in small circles and mapping height, the software determines the height gradient of whatever feature it is positioned over. By moving the tip position along the gradient until the highest point of the feature is reached, it is able to maintain position there by correcting for any negative changes in gradient (caused by the tip drifting away from the highest point).

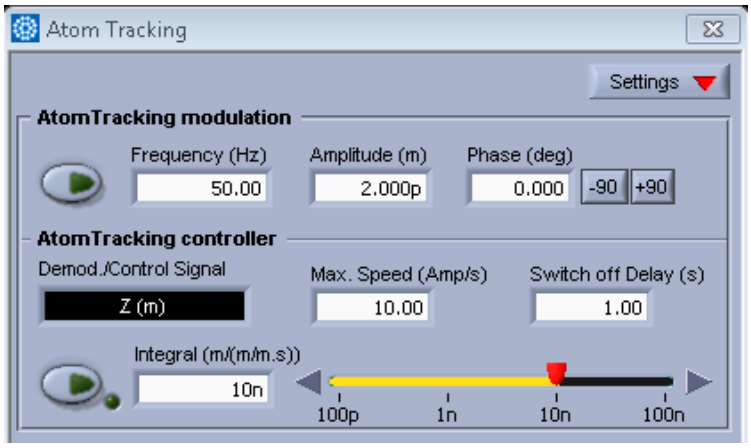

Figure 5.1: Atom tracking settings in Nanonis SPM control software. The settings used for long-term molecular sensing experiments to ensure that the tip stays centred over the sensor DB. These settings are suitable for tracking the position of a DB with a negative sample bias below -1.3 V. These settings have been found to not alter any features measured in an $I(V)$ spectrum of a DB once the tracking loop has stabilized.

When using the atom tracking module, with the parameters in Figure 5.1, the radius of the tip movements to map the gradient was sufficiently small such that the $I(V)$ spectrum recorded of a sensor DB did not differ significantly from a spectrum taken with a static tip. This is an important consideration, as the tip position over the sensor DB can affect the strength of the current onset signature observed, so the smallest radius possible to achieve stable tracking is optimal. During several hydrogen molecule sensing trials at low base pressures (less than 10^{-12} Torr), where it takes over 45 h for some events to occur, the atom tracking module kept the tip centred over the sensor DB. Figure 5.2 shows the spectrum of a sensor DB after positioning the tip over it and measuring in 10 minute intervals for 19 h with the atom tracking module active. No event was observed in this window due to the low hydrogen gas pressure in the vicinity of the tip and sample. However, the spectrum at the beginning and end of that time interval were identical as atom tracking kept the tip in the same location over the sensor DB.

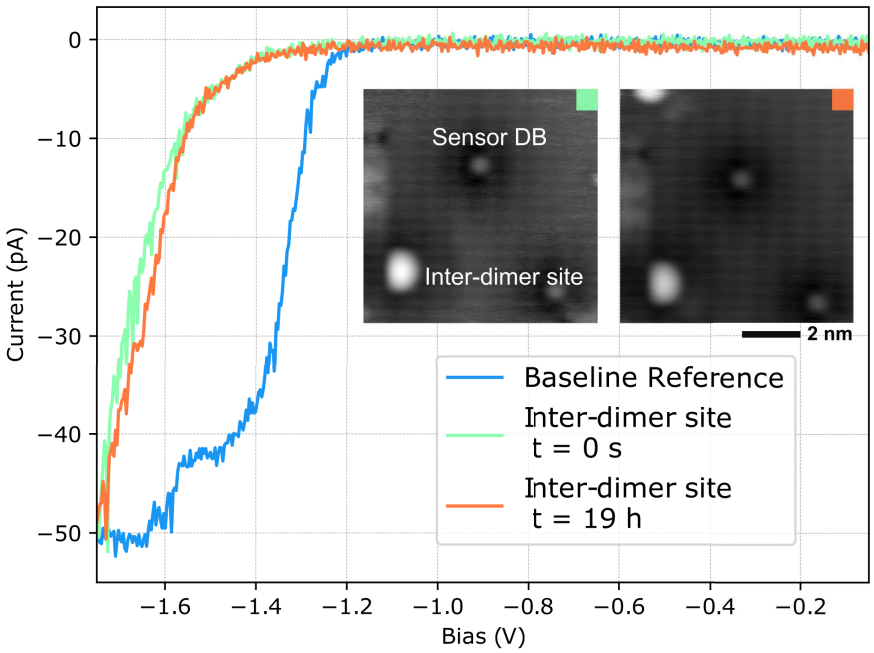

Figure 5.2: Active atom tracking for sensing (V = 1.4 V, I = 50 pA, T = 4.5 K, 8 x 8 nm^2).
After the creation of an inter-dimer site, the tip was positioned over the sensor DB and the atom tracking module was initiated (inset image, green). After 19 h, the position of the sensor DB in the scan frame has shifted (inset image, orange) due to thermal drift and creep of the piezoelectric scanner. However, thanks to the atom tracking module, the tip remained centred over the sensor DB during the entire measurement, ensuring that a binding event could be detected. No event was detected in this time interval due to the low hydrogen gas background pressure.

5.4 Current limitations of sensing multiple events

Using the sensing techniques of Section 4.3.2, it is possible to monitor multiple reactive DB sites using one sensor DB. Supplementary Figure 4.11 shows three inter-dimer sites inducing shifts of the current step of a sensor DB. While the same temporal resolution is maintained when monitoring multiple reactive sites compared to a single site, there is no way at present to exactly determine the order in which each site reacts using electronic detection. This lack of spatial specificity is due to

the fact that if the dopant is sufficiently deep, there are only small variations in distance between each site and itself. Since the shifts in the ionization threshold are due to the total field at the dopant location, then removing any particular site would remove a roughly equal fraction of the total induced field, making it difficult to determine which site reacted. The lack of spatial resolution does not limit the general utility of sensing multiple events with a single sensor DB. In uses such as pressure sensing, the order in which the sites disappear is not an important quantity, but rather detecting when all the sites have reacted.

5.5 Characterizing charge in larger DB structures

It was mentioned in Section 4.3.1 that the critical voltage shift of a sensor DB is essentially independent of the distance between the sensor and target DBs when it exceeds approximately 5 nm. The charge characterization application relies on the relative insensitivity of the critical voltage step of a sensor DB to the separation between itself and the target DBs of a structure. This is important when characterizing larger structures because the electrons within them will be at different distances from the sensor DB. If the critical voltage was very sensitive to such differences, then it would be difficult to properly characterize multi-DB structures relative to the calibrated one-electron shifts of the critical voltage induced by isolated DBs. This is because the isolated DBs may not have been at equivalent distances to the sensor DB as the DBs in the current structure. In Figure 4.1 for example, the two DBs in the structure induce nearly identical shifts of the critical voltage, despite being at different distances from the sensor DB. This is because the spectral feature is due to the tip-field ionization of a subsurface dopant atom, rather than the field at the sensor DB itself. This is valid if the subsurface dopant is sufficiently deep that the distance between any of the target DBs and dopant is nearly identical throughout the entire target site (so that their respective fields are only a small fraction different at the dopant).

Figure 5.3 shows a large fabricated DB structure before and after the addition of one DB, and the corresponding $I(V)$ spectra of the sensor DB. It was possible

to detect a charge change in Figure 5.3 because the already present DB box only altered the background field at the dopant atom. The additional field contribution of the newly created DB in the centre (one electron) still introduced a shift in the $I(V)$ spectrum of the sensor DB. This is an example of just how sensitive the charge characterization technique described in Section 4.3.1 is, even when characterizing charge changes of larger structures. It is important to note that the DBs at the target site (including the box) are distant enough as to not interact with the sensor DB, so it cannot be concluded if the box would provide any shielding of DB-DB interactions in this situation.

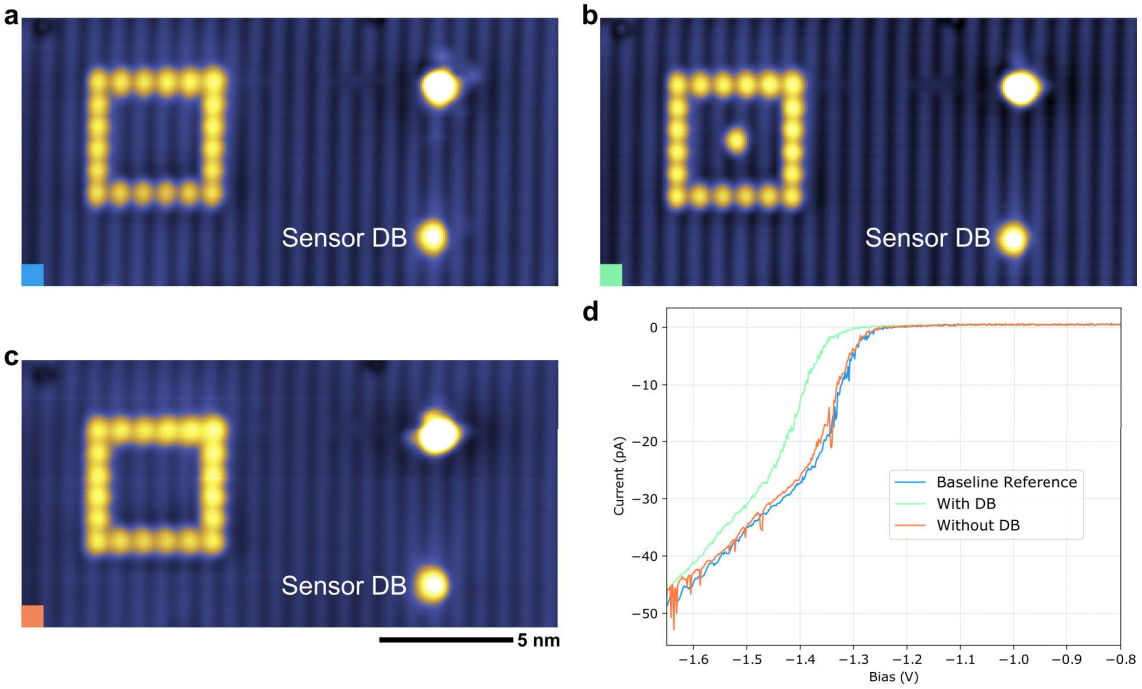

Figure 5.3: Detecting charge in larger DB structures (V = -1.65 V, I = 50 pA, T = 4.5 K, 10 x 20 nm^2).
a) A filled states STM image of a large 2D DB box structure consisting of 20 DBs. **b**) STM image of the structure after a single DB has been made inside of the box using HL. **c**) STM image of the same area after the DB inside the box has been removed using HR. **d**) The corresponding $I(V)$ spectra of the sensor DB to the images in **a** to **c**.

One of the initial thoughts when it was observed that the introduction of a target DB caused the $I(V)$ step of a sensor DB to shift was that it was due in part to a DB-DB interaction. The investigation in Figure 5.3 was carried out to see if a fabricated DB box surrounding a newly introduced target DB could "shield" it from the sensor DB and prevent its $I(V)$ spectrum from shifting. In Figure 5.3, the target DB created inside the DB box still shifted the step in the $I(V)$ spectrum of the sensor DB. This result agrees with the improved understanding that the primary mechanism of the charge-induced shifts of the sensor DB is the effect of the target DB (Coulombic gating) on a nearby dopant atom's ionization state [64, 146], and that the sensor DB and the target DB are not interacting with each other at this separation (no DB-DB interactions) [5].

It would be interesting to calibrate the sensor DB shifts with 5 or more isolated DBs and then repeat this measurement to characterize the net charge of the box structure itself. Based on the experiments in Section 4.3.1, since each DB is spaced about 0.768 nm apart, there should be less than one electron per DB within the structure. The charge characterization technique described in the previous chapter would enable the measurement of the number of charges in the box. However, their spatial location within the structure could still only be visualized at present using an AFM.

5.6 Inter-dimer site reactivity in high DB density

In order for M-HR to be a reliable tool for rewriting atomic memories, and atomic-scale fabrication, binding to inter-dimer sites must occur unencumbered by the presence of other DB structures and defects. This notion was already introduced in Section 4.3.3, where inter-dimer site reactions were found to be robust, reacting with hydrogen molecules in a number of different configurations with varying proximity to other DBs and defects.

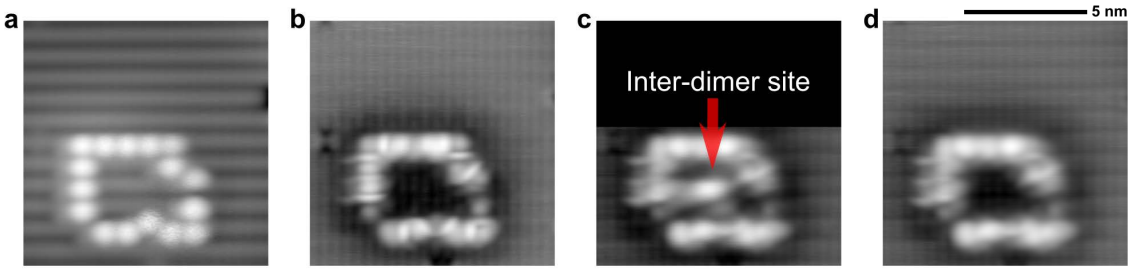

Figure 5.4: Inter-dimer site in a DB box (I = 50 pA, T = 4.5 K, 10 x 10 nm^2).
a) (V = -1.6 V) A filled states image of a 2D DB box enclosure. **b**) (V = 1.4 V) An empty states image of the same 2D DB box. **c**) An inter-dimer site was created in the centre of the box. **d**) An image acquired 38 s after the creation of the inter-dimer site. It has reacted with an ambient hydrogen molecule during this time.

One scenario that remained was to test whether or not an inter-dimer site that was fully surrounded by other DBs would also bind with an ambient hydrogen molecule. Figure 5.4 shows a crude 2D box made of DBs, inside of which an inter-dimer site was made. After sufficient time had passed, the site did indeed react with a molecule of hydrogen. The ability of an inter-dimer site to react even while enclosed from all sides by other DBs is important for both fabrication and memories, as in both situations there will be dense arrangements of DBs surrounding any site that needs to be erased. The ability itself is not surprising, as it is expected that the molecules are arriving at the sites in gas phase (Section 4.3.2), and as such should not be greatly influenced by structures on the surface.

5.7 Surface reactivity

While inter-dimer sites on an otherwise hydrogen-passivated surface are highly reactive to ambient hydrogen molecules [91], sites which contain areas with seemingly equivalent geometries have not been observed to react at 4.5 K (Supplementary Figures 4.5 and 4.10). In order for dissociative adsorption to occur, the anti-bonding orbital of the hydrogen molecule must be able to hybridize with the two surface DBs in order for the molecule to be destabilized. If the DBs are at different energies

from each other, then this process does not proceed as easily [91]. Intra-dimer sites (bare dimer) undergo a Jahn-Teller relaxation in order to reduce the surface energy, leading to a tilt in the dimer that causes an energy difference between the now upper and lower DBs (in the z direction) [55, 91]. This also occurs to a lesser extent for the inter-dimer sites [91, 103, 147, 148], although it does not appear to hamper reactivity of longer lines of inter-dimer sites along a dimer row (Supplementary Figure 4.6a,b, also observed in [148]). On the bare silicon surface, each subsequent adjacent dimer is tilted in the opposite direction to its neighbour to form an alternating pattern [55, 149]. Such an asymmetry also reduces the reactivity of adjacent DBs in an inter-dimer configuration within a line of multiple intra-dimer sites. This can be seen in Supplementary Figure 4.5, where no binding was observed to a line of three intra-dimer sites.

There is an additional consideration for the dissociative adsorption of hydrogen onto the surface for both the inter- and intra- dimer pathways: the ability of the substrate to distort into a more symmetric transition geometry. This type of rearrangement as a hydrogen molecule approaches the site can symmetrize the two DBs to reduce their energy difference in order to promote effective hybridization, and ultimately a reaction (so long as the rearrangement energy cost is not too high) [91]. The distortion of an intra-dimer site towards a symmetric transition geometry, while bringing the energy of the two constituent DBs closer together, causes the strengthening of a π-bond between them [55, 91], negating the otherwise beneficial energetic/geometric rearrangement for reactivity [91].

5.7.1 Surface condition after 18 days

One of the most important considerations for the viability of DBs as building blocks for atomic-scale memories and devices is their thermal stability (the ability to remain in place at specified temperatures) and their reactive stability (the ability to not bond with another entity). These aspects were discussed at the end of Section 2.3.3 in relation to a memory array observed for 72 h. Slightly longer observations of a surface/structure were undertaken spanning 6 days in an environment of higher

background pressure ($1{\cdot}10^{-9}$ Torr) than is typical inside the cryo-shielding. The surface/structure showed no migration or chemical reactions of isolated DBs in this time period (Figure 4.3). In this same baseline environment, observations were taken 18 days apart of an area with several different types of features in order to observe if any changes occurred. In an 18 day span the cryogens used to keep the STM at 4.5 K needed to be replaced 9 times. During this time, the sample typically experienced temperature spikes up to 12 K (the cryogens were sufficiently depleted once that the sample temperature reached 19 K) and pressure spikes near 10^{-8} Torr. Figure 5.5a shows an area at the beginning of the 18 day period with many isolated DBs, and a patch of bare silicon where the STM tip was used in the coarse lithography mode (field emission regime) to desorb hydrogen atoms in a square shape. After the 18 day period, the Figure 5.5b shows that none of the isolated DBs have diffused or reacted with any ambient molecules. One of the DBs does not appear in this image due to a change in the tip state over the 18 days. However, imaging at a different bias voltage reveals it is still present (Figure 5.5c). Additionally, no hydrogen molecules have reacted within the bare silicon patch as well, despite the availability of inter-dimer sites. This is expected because of the surface relaxation considerations discussed above, reducing their reactivity due to electronic and geometric distortions along each row of dimers (Section 5.7).

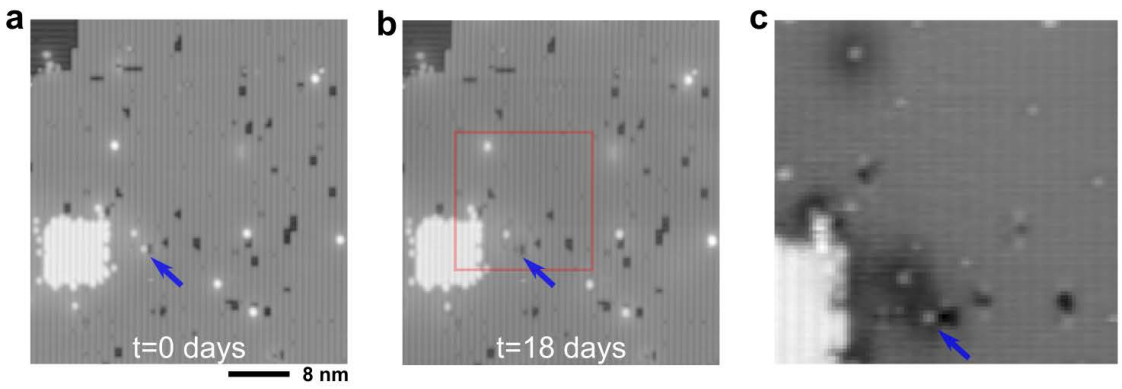

Figure 5.5: Surface condition after 18 days (I = 50 pA, T = 4.5 K). **a**) (V = -1.6 V, 50 x 50 nm^2) A filled states image of a large area with many isolated DBs and a square area of bare silicon. **b**) (V = -1.6 V, 50 x 50 nm^2) The same area as in **a**, 18 days later. **c**) (V = 1.4 V) An empty states image of the area highlighted in **b**, showing the remaining presence of a DB that does not image under the filled states conditions in **b**.

5.8 Supplementary movie

A video showing the sequential reaction of three molecules of hydrogen to rewrite the 24-bit memory array shown in Figure 4.4 can be viewed on YouTube at: https://youtu.be/-HPX2fMS1Uk.

5.9 Outlooks

The results of Chapter 4 presented the culmination of a number of STM observations and techniques, which now form the basis for a more accessible and versatile fabrication toolkit for atomic-scale sensing, fabrication, and data storage. Some future experiments and ideas are detailed in the following sections.

5.9.1 Atomic-scale fabrication and data storage

The demonstration of M-HR to further enhance the capabilities of HL and HR has led to a new implementation of ultra-dense data storage at the atomic scale. Although there is a very long road ahead, I believe it has the potential to eventually be realized without the need for probes or an STM. This is because the ability to manipulate single atoms with electron/ion beams [12, 138] is continually improving, and may eventually reach the required resolution to remove single atoms of hydrogen from a hydrogen-passivated surface.

Until now, there has not been a method to add material back to a surface with true atomic precision without a probe. The future combination of precision beams and precision controlled surface reactions could lead to a massive change in both atomic-scale fabrication and data storage. In the case of data storage, the production of gas filled hard drives already exists. High capacity conventional mechanical hard drives, which have been filled with helium gas (in order to reduce drag on the spinning disk) are currently in production and available, so memory in a hydrogen gas environment is not unreasonable. The storage density of such atomic-scale schemes has the potential to be increased even further as well. By using hydrogen-passivated carbon(100)-2x1, the maximum theoretical storage density of the memories described here can be increased by approximately 30% due to the stronger C-C bonds creating a tighter surface geometry [150, 151].

The removal of the need to pick up and deposit atoms on the surface with a probe to correct fabrication errors or rewrite arrays will also lead to significant speedups as the size and complexity of storage arrays and circuitry increase. The speedup in the context of atomic-scale fabrication is important for the economical and scalable production of devices. M-HR has the potential to increase fabrication yields by reducing the total "downtime" of the tip, as it moves to gather hydrogen atoms and then participate in the repassivation process. Under this new implementation, the tip never has to travel to gather materials (ambient hydrogen molecules are always available locally), and once a site to be repassivated has been created, the tip is able to move onto the next task instead of needing to be actively involved.

Moving forward, another aspect that needs to be addressed for atomic-scale data storage is the operating temperature, as it is impractical to require a constant supply of cryogens. The removal of hydrogen atoms and thermal stability of the resulting structures has already been established at room temperature (discussed in Section 2.3.3, 2.4). However, M-HR needs to be thoroughly tested at these conditions as well to ensure it is a viable tool for rewriting data at real-world temperatures. The prospects look promising, as inter-dimer sites have already been observed reacting with ambient molecules of hydrogen at room temperature [108].

5.9.2 Fabrication considerations for DB wires and circuitry

There are a number of proposals for the fabrication of DB wires to act as electrical interconnects between device elements. Some experimental and theoretical work has been completed in search of ideal geometries and properties of DB wires [152–156]. One of the main candidates is a 1D DB wire (no hydrogen atoms between DBs), however, there is still a lack of consensus in the community of whether they are metallic [152] or semiconducting [153, 154] in nature.

Another consideration that now needs to be made in light of the results of the previous chapter and the discussion in Section 5.7 is the reactivity of these wires with ambient gas molecules. The geometry of the 1D wire for instance is highly susceptible to reactions with hydrogen gas molecules, as it is essentially a long string of ideal inter-dimer sites (Supplementary Figure 4.6a,b). This may pose a problem for the longevity of atomic circuit elements that require such interconnects. With this in mind, it seems that the optimal design for DB wires must balance their conductive properties with their reactive properties to ensure functional circuitry.

A possible candidate that meets these two criteria is the use of lines of intra-dimer sites as wires. Calculations have predicted that long wires in such a configuration are sufficiently conductive for application in circuits [153,154]. Since each intra-dimer site within the lines tilts in the opposite direction to its neighbours, the overall reactivity of the wires is reduced (Section 5.7). Other larger and wider DB wire designs, more closely resembling a patch of bare silicon have been proposed as well [154], which

will also benefit from a reduced reactivity for the same reason.

The present logic gate designs for binary atomic silicon logic field-controlled computing do not require the inclusion of 1D DB wires or single inter-dimer sites [5, 43]. As such, by having at least one surface site in between each DB, this type of circuitry is robust against random reactions with ambient molecules. Reactivity constraints such as this will help guide the design of future elements as well.

5.9.3 Studying and sensing chemistry

The ability to exactly direct and detect the reaction of hydrogen molecules with atomic precision is hopefully just the tip of the iceberg of what is now possible. These tools for the creation of, and subsequent detecting at, tailored reactive sites has the potential to enable very detailed investigations of chemical reactions and their dependence on atomic-scale properties. As mentioned in Section 4.4, it is expected that they can be applied to create tailored reactive sites to study the adsorption dynamics of alkenes and aromatic molecules. Cycloaddition reactions can possibly be studied as well using the reliably reproducible inter-dimer and intra-dimer sites presented here [109, 110, 139]. By creating candidate-tailored sites with different geometries (as was done for H_2 in Supplementary Figure 4.10), theoretical predictions of the most reactive sites may be investigated for other specific molecules. At cryogenic temperatures, laser light might be able to introduce sufficient energy to overcome energy barriers for different reaction pathways as well. The precise inclusion of light with the tip may allow for studies of photo-induced chemistry at reactive DB sites, where a site with the tip present (coupling light) can be directly compared to an identical site in absence of the tip [157, 158].

There are a number of studies still related to the simple case of hydrogen molecule adsorption that would be interesting to undertake, with additional implications for atomic-scale devices. One such study would be to investigate the reactivity of inter-dimer sites on silicon substrates with varying doping concentrations and types. The charge of DBs on the surface depends on the substrate doping concentration and type. When the anti-bonding level of a hydrogen molecule begins interacting with

the DBs of an inter-dimer site, the availability of negative charges at the DBs (DB level is close to the Fermi-level) helps destabilize the molecule to promote disassociation [91]. With lower doping levels, the DBs could be neutral and the reaction may not proceed as easily. This might also be the case for p-type doped silicon samples, where the DBs can be made positive. Another interesting study would be to investigate the reactivity of inter-dimer sites on hydrogen-terminated germanium [31, 159] or diamond [150, 151] to see just how universal the adsorption mechanism is. Chlorine-terminated silicon surfaces have also been created and studied, where similar lithographic capabilities to what is now possible on silicon may eventually be realized [72, 94]. Much like what was done with H_2 on the deuterated silicon surface in Supplementary Figure 4.6, it should even be possible to fabricate inter-dimer sites on the chlorinated surface to pattern hydrogen-passivated areas (lines, wires) otherwise surrounded by chlorine.

The ability to sense the reaction of a molecule at a given DB site with minimal perturbations from the STM tip also opens up the door for new investigations of molecular dynamics and applications of DBs. While the dopant-ionization-based sensing described in the previous chapter is currently restricted to studying dynamics and reactions below 40 K, the charged nature of the reactive sites makes them ideal for integration within the proposed DB-based field-controlled electronics [5]. For example, the inter-dimer site has a charge of one electron, so it can be used as an input of each terminal of the logical-OR gate shown in [5] (Figure 1.2) in lieu of the single DBs. Now, when both sites/inputs react, the output state of the gate will transition from "1" to "0". At present, this change can be detected by the AFM tip, which is useful for small-scale demonstrations. Eventually, as the technology matures, I believe using the exact same mechanism, it should be possible to integrate tailor-made single molecule detectors within other logic gates and real electronic devices.

Chapter Six

Conclusions

Chapter 2 introduced the main methodology for the automation of HL, along with the development of the HR technique. HL and HR were then used to demonstrate the fabrication of perfect DB structures and rewritable atomic memory. Chapter 3 further explored the versatility of the HR technique, including the use of deuterium, and the underlying transfer mechanism of atoms from the tip. Chapter 4 detailed the use of particular sensor DBs to characterize the charge of, and electronically detect single molecule binding events to, reactive DB sites created using HL. These reactive sites were shown to be able to direct chemical reactions of hydrogen molecules with atomic precision, leading to their use in an improved error correction/rewriting technique, M-HR, that was incorporated into new data storage designs. Chapter 5 further explored the reactivity of DB sites with hydrogen, along with the reliability of the charge characterization and molecule detection technique. Considerations and experiments related to future chemical and technological applications were also discussed.

Now that many of the limitations of atomic-scale fabrication on the hydrogen-terminated Si(100)-2x1 surface have been addressed and overcome, the path towards scalable low-power circuit elements [5] is less winding. The lithographic capabilities have reached a point where larger numbers of interconnected gates can now be created without errors for tests and demonstrations. Even in the short term, making and testing the individual functionality of new gate designs [43] would be a significant advance. One of the most important gates to successfully demonstrate is an inverter (NOT-gate), which can subsequently be connected to the already demonstrated OR-gate. The resulting NOR-gate is important because it is functionally complete. That is, with multiple NOR-gates, all other logic gates can be constructed, enabling the

creation of fully capable circuits.

As the need to scale further towards mass production arises, continued improvements to the accuracy and ease of HL, HR, and M-HR will eventually be realized through future automation. For example, the work of Jeremiah Croshaw to continue the integration of machine learning into the fabrication process has already resulted in the ability to automatically identify and avoid surface defects during lithography [137]. The development of better piezoelectric scanners that respond linearly to an applied voltage will also improve lithographic accuracy by entirely eliminating scanner creep. Work led by Mark Salomons, Dr. Robert Wolkow, and Jason Pitters has already made significant progress towards this end.

The fact that all of these techniques translate to other material systems such as hydrogen-terminated germanium or diamond substrates offers many interesting avenues for fundamental studies of chemical reactivity. Such surfaces may even prove to be the next candidates for device applications. If hydrogen-terminated diamond, in particular, could be used for the data storage applications presented here, then the maximum storage densities of the memory designs (Figure 4.12) could be increased by approximately 30%. This is due to the approximately 30% decrease in bond lengths in diamond compared to silicon. The increase in density would essentially close the storage density gap between the current demonstrations of atomic-scale storage and the best implementation of DNA data storage (Section 1.1.4).

Just 150 years after the elements were organized into the periodic table [160], real spatial control over the placement of single entities of the first element on the table, hydrogen, has now been reproducibly demonstrated for its atomic and molecular forms. Despite its age, the STM has also proven that it is not too old to learn new tricks. Together, the improvements in writing atomic-scale patterns [10], the discovery of atomic white-out [25], and the realization of molecular erasers [44] form a veritable nano-stationery set that is available to craft the next generation of devices and memories. It is my hope that these tools help move candidate technologies towards the realization of their potential, as well as to lay the foundation for future innovations and explorations.

Bibliography

[1] P. M. Solomon, "Device Proposals Beyond Silicon CMOS," in *Future Trends in Microelectronics*, pp. 127–140. John Wiley & Sons, Inc., Hoboken, NJ, USA, Aug, 2010.

[2] D. Etiemble, "45-year CPU evolution: one law and two equations," arXiv:1803.00254.

[3] K. Rupp, "42 Years of Microprocessor Trend Data (Accessed Dec 03, 2019)." https://www.karlrupp.net/2018/02/42-years-of-microprocessor-trend-data/.

[4] M. Hazas, J. Morley, O. Bates, and A. Friday, "Are there limits to growth in data traffic?," in *Proceedings of the Second Workshop on Computing within Limits - LIMITS '16*, pp. 1–5. ACM Press, New York, New York, USA, 2016.

[5] T. Huff, H. Labidi, M. Rashidi, L. Livadaru, T. Dienel, R. Achal, W. Vine, J. Pitters, and R. A. Wolkow, "Binary atomic silicon logic," *Nature Electronics* **1** no. 12, (2018) 636–643.

[6] L. Livadaru, P. Xue, Z. Shaterzadeh-yazdi, G. A. DiLabio, J. Mutus, J. L. Pitters, C. Barry, B. C. Sanders, and R. A. Wolkow, "Dangling-bond charge qubit on a silicon surface," *New Journal of Physics* **12** no. 8, (Aug, 2010) 083018, arXiv:0910.1797.

[7] M. Fuechsle, J. A. Miwa, S. Mahapatra, H. Ryu, S. Lee, O. Warschkow, L. C. L. Hollenberg, G. Klimeck, and M. Y. Simmons, "A single-atom

transistor," *Nature Nanotechnology* **7** no. April, (2012) 242–246, arXiv:1505.03565.

[8] M. Y. Simmons, S. R. Schofield, J. L. O'Brien, N. J. Curson, L. Oberbeck, T. Hallam, and R. G. Clark, "Towards the atomic-scale fabrication of a silicon-based solid state quantum computer," *Surface Science* **532-535** (Jun, 2003) 1209–1218.

[9] F. E. Kalff, M. P. Rebergen, E. Fahrenfort, J. Girovsky, R. Toskovic, J. L. Lado, J. Fernández-Rossier, and a. F. Otte, "A kilobyte rewritable atomic memory," *Nature Nanotechnology* **11** no. 11, (2016) 926–929, arXiv:1604.02265.

[10] R. Achal, M. Rashidi, J. Croshaw, D. Churchill, M. Taucer, T. Huff, M. Cloutier, J. Pitters, and R. A. Wolkow, "Lithography for robust and editable atomic-scale silicon devices and memories," *Nature Communications* **9** (Dec, 2018) 2778.

[11] S. Loth, S. Baumann, C. P. Lutz, D. M. Eigler, and A. J. Heinrich, "Bistability in Atomic-Scale Antiferromagnets," *Science (New York, N.Y.)* **335** no. 6065, (Jan, 2012) 196–199.

[12] O. Dyck, S. Kim, E. Jimenez-Izal, A. N. Alexandrova, S. V. Kalinin, and S. Jesse, "Building Structures Atom by Atom via Electron Beam Manipulation," *Small* **14** no. 38, (Sep, 2018) 1801771.

[13] G. Binnig and H. Rohrer, "Scanning tunneling microscope," *US Patent US4343993A* (1982) .

[14] G. Binnig, H. Rohrer, C. Gerber, and E. Weibel, "Surface Studies by Scanning Tunneling Microscopy," *Physical Review Letters* **49** no. 1, (Jul, 1982) 57–61.

[15] G. Binnig, H. Rohrer, C. Gerber, and E. Weibel, "7 x 7 Reconstruction on Si(111) Resolved in Real Space," *Physical Review Letters* **50** no. 2, (Jan, 1983) 120–123.

[16] D. M. Eigler and E. K. Schweizer, "Positioning single atoms with a scanning tunnelling microscope," *Nature* **344** (1990) 524–526.

[17] W. Ko, C. Ma, G. D. Nguyen, M. Kolmer, and A. Li, "Atomic-scale manipulation and in situ characterization with scanning tunneling microscopy," *Advanced Functional Materials* **1903770** (May, 2019) 1903770, arXiv:1905.09807.

[18] M. F. Crommie, C. P. Lutz, and D. M. Eigler, "Confinement of electrons to quantum corrals on a metal surface.," *Science (New York, N.Y.)* **262** no. 5131, (1993) 218–220.

[19] R. A. Wolkow, L. Livadaru, J. Pitters, M. Taucer, P. Piva, M. Salomons, M. Cloutier, and B. V. Martins, "Silicon atomic quantum dots enable beyond-CMOS electronics," in *Lecture Notes in Computer Science (including subseries Lecture Notes in Artificial Intelligence and Lecture Notes in Bioinformatics)*, S. B. Neal G. Anderson, ed., vol. 8280 LNCS, pp. 33–58. Springer, 2014. arXiv:1310.4148.

[20] M. B. Haider, J. L. Pitters, G. a. Dilabio, L. Livadaru, J. Y. Mutus, and R. A. Wolkow, "Controlled coupling and occupation of silicon atomic quantum dots at room temperature," *Physical Review Letters* **102** no. 4, (2009) 046805, arXiv:0807.0609.

[21] R. J. Celotta, S. B. Balakirsky, A. P. Fein, F. M. Hess, G. M. Rutter, and J. A. Stroscio, "Invited Article: Autonomous assembly of atomically perfect nanostructures using a scanning tunneling microscope," *Review of Scientific Instruments* **85** no. 12, (Dec, 2014) 121301.

[22] G. Meyer, J. Repp, S. Zöphel, K.-f. Braun, S. W. Hla, S. Fölsch, L. Bartels, F. Moresco, and K. H. Rieder, "Controlled Manipulation of Atoms and Small

Molecules with a Low Temperature Scanning Tunneling Microscope," *Single Molecules* **1** no. 1, (Apr, 2000) 79–86.

[23] A. J. Heinrich, C. P. Lutz, J. A. Gupta, and D. M. Eigler, "Molecule cascades," *Science (New York, N.Y.)* **298** no. 5597, (2002) 1381–1387.

[24] L. Gross, N. Moll, F. Mohn, A. Curioni, G. Meyer, F. Hanke, and M. Persson, "High-resolution molecular orbital imaging using a p-wave STM tip," *Physical Review Letters* **107** no. 8, (2011) 086101.

[25] T. Huff, H. Labidi, M. Rashidi, M. Koleini, R. Achal, M. H. Salomons, and R. A. Wolkow, "Atomic White-Out: Enabling Atomic Circuitry Through Mechanically Induced Bonding of Single Hydrogen Atoms to a Silicon Surface," *ACS Nano* **11** no. 9, (Sep, 2017) 8636–8642, arXiv:1706.05287.

[26] E. Foley, A. Kam, J. Lyding, and P. Avouris, "Cryogenic UHV-STM Study of Hydrogen and Deuterium Desorption from Si(100)," *Physical Review Letters* **80** no. 100, (1998) 1336–1339.

[27] T.-C. Shen and P. Avouris, "Electron stimulated desorption induced by the scanning tunneling microscope," *Surface Science* **390** (1997) 35–44.

[28] M. McEllistrem, M. Allgeier, and J. J. Boland, "Dangling Bond Dynamics on the Silicon (100)-2x1 Surface: Dissociation, Diffusion, and Recombination," *Science (New York, N.Y.)* **279** no. 5350, (Jan, 1998) 545 – 548.

[29] C. H. Schwalb, M. Dürr, and U. Höfer, "High-temperature investigation of intradimer diffusion of hydrogen on Si(001)," *Physical Review B* **82** no. 19, (2010) 193412.

[30] R. Drost, T. Ojanen, A. Harju, and P. Liljeroth, "Topological states in engineered atomic lattices," *Nature Physics* **13** no. 7, (2017) 668–671, arXiv:1611.01049.

[31] M. Kolmer, S. Godlewski, H. Kawai, B. Such, F. Krok, M. Saeys, C. Joachim, and M. Szymonski, "Electronic properties of STM-constructed dangling-bond dimer lines on a Ge(001)-(2 x 1):H surface," *Physical Review B* **86** no. 12, (Sep, 2012) 125307.

[32] S. Chen, H. Xu, K. E. J. Goh, L. Liu, and J. N. Randall, "Patterning of sub-1 nm dangling-bond lines with atomic precision alignment on H:Si(100) surface at room temperature," *Nanotechnology* **23** no. 100, (2012) 275301.

[33] N. Pavliček, Z. Majzik, G. Meyer, and L. Gross, "Tip-induced passivation of dangling bonds on hydrogenated Si(100)-2 x 1," *Applied Physics Letters* **111** no. 5, (Jul, 2017) 53104, arXiv:1706.02560.

[34] J. B. Ballard, J. H. G. Owen, J. D. Alexander, W. R. Owen, E. Fuchs, J. N. Randall, R. C. Longo, and K. Cho, "Spurious dangling bond formation during atomically precise hydrogen depassivation lithography on Si(100): The role of liberated hydrogen," *Journal of Vacuum Science & Technology B, Nanotechnology and Microelectronics: Materials, Processing, Measurement, and Phenomena* **32** no. 100, (2014) 021805.

[35] M. Taucer, L. Livadaru, P. G. Piva, R. Achal, H. Labidi, J. L. Pitters, and R. A. Wolkow, "Single-Electron Dynamics of an Atomic Silicon Quantum Dot on the H-Si(100)-(2x1) Surface," *Physical Review Letters* **112** no. June, (2014) 256801.

[36] M. Kolmer, S. Godlewski, R. Zuzak, M. Wojtaszek, C. Rauer, A. Thuaire, J. M. Hartmann, H. Moriceau, C. Joachim, and M. Szymonski, "Atomic scale fabrication of dangling bond structures on hydrogen passivated Si(0 0 1) wafers processed and nanopackaged in a clean room environment," *Applied Surface Science* **288** (2014) 83–89.

[37] M. Møller, S. P. Jarvis, L. Guérinet, P. Sharp, R. Woolley, P. Rahe, and P. Moriarty, "Automated extraction of single H atoms with STM: tip state dependency," *Nanotechnology* **28** no. 111, (2017) 075302.

[38] A. Bellec, L. Chaput, G. Dujardin, D. Riedel, L. Stauffer, and P. Sonnet, "Reversible charge storage in a single silicon atom," *Physical Review B* **88** no. 24, (Dec, 2013) 241406.

[39] M. Rashidi, E. Lloyd, T. R. Huff, R. Achal, M. Taucer, J. J. Croshaw, and R. A. Wolkow, "Resolving and Tuning Carrier Capture Rates at a Single Silicon Atom Gap State," *ACS Nano* **11** no. 11, (2017) 11732–11738, arXiv:1711.00566v1.

[40] S. R. Schofield, P. Studer, C. F. Hirjibehedin, N. J. Curson, G. Aeppli, and D. R. Bowler, "Quantum engineering at the silicon surface using dangling bonds.," *Nature communications* **4** (Jan, 2013) 1649.

[41] U. J. Quaade, K. Stokbro, R. Lin, and F. Grey, "Single-atom reversible recording at room temperature," *Nanotechnology* **12** no. 100, (2001) 265–272.

[42] J. W. Lyding, T. C. Shen, J. S. Hubacek, J. R. Tucker, and G. C. Abeln, "Nanoscale patterning and oxidation of H-passivated Si(100)-2x1 surfaces with an ultrahigh vacuum scanning tunneling microscope," *Applied Physics Letters* **64** no. 100, (1994) 2010–2012.

[43] S. Ng, J. Retallick, H. N. Chiu, R. Lupoiu, M. Rashidi, W. Vine, T. Dienel, L. Livadaru, R. A. Wolkow, and K. Walus, "SiQAD: A Design and Simulation Tool for Atomic Silicon Quantum Dot Circuits," arXiv:1808.04916.

[44] R. Achal, M. Rashidi, J. Croshaw, T. R. Huff, and R. A. Wolkow, "Detecting and Directing Single Molecule Binding Events on H-Si(100) with Application to Ultradense Data Storage," *ACS Nano* (Nov, 2019) acsnano.9b07637, arXiv:1907.03218.

[45] M. R. Slot, T. S. Gardenier, P. H. Jacobse, G. C. P. van Miert, S. N. Kempkes, S. J. M. Zevenhuizen, C. M. Smith, D. Vanmaekelbergh, and I. Swart, "Experimental realization and characterization of an electronic Lieb lattice," *Nature Physics* **13** no. 7, (Jul, 2017) 672–676.

[46] S. Fölsch, J. Martínez-Blanco, J. Yang, K. Kanisawa, and S. C. Erwin, "Quantum dots with single-atom precision," *Nature Nanotechnology* **9** no. 7, (2014) 505–508.

[47] J. Wyrick, X. Wang, P. Namboodiri, S. W. Schmucker, R. V. Kashid, and R. M. Silver, "Atom-by-Atom Construction of a Cyclic Artificial Molecule in Silicon," *Nano Letters* **18** no. 12, (Dec, 2018) 7502–7508.

[48] M. Mandelkern, J. G. Elias, D. Eden, and D. M. Crothers, "The dimensions of DNA in solution," *Journal of Molecular Biology* **152** no. 1, (Oct, 1981) 153–161.

[49] Y. Erlich and D. Zielinski, "DNA Fountain enables a robust and efficient storage architecture," *Science* **355** no. 6328, (2017) 950–954.

[50] G. M. Church, Y. Gao, and S. Kosuri, "Next-Generation Digital Information Storage in DNA," *Science* **337** no. 6102, (Sep, 2012) 1628–1628.

[51] L. Organick, S. D. Ang, Y.-J. Chen, R. Lopez, S. Yekhanin, K. Makarychev, M. Z. Racz, G. Kamath, P. Gopalan, B. Nguyen, C. N. Takahashi, S. Newman, H.-Y. Parker, C. Rashtchian, K. Stewart, G. Gupta, R. Carlson, J. Mulligan, D. Carmean, G. Seelig, L. Ceze, and K. Strauss, "Random access in large-scale DNA data storage," *Nature Biotechnology* **36** no. 3, (Mar, 2018) 242–248.

[52] M. Rezeq, J. Pitters, and R. Wolkow, "Tungsten nanotip fabrication by spatially controlled field-assisted reaction with nitrogen," *Journal of Chemical Physics* **124** (2006) 204716.

[53] H. Labidi, M. Koleini, T. Huff, M. Salomons, M. Cloutier, J. Pitters, and R. A. Wolkow, "Indications of chemical bond contrast in AFM images of a hydrogen-terminated silicon surface," *Nature Communications* **8** (2017) .

[54] S. Jarvis, A. Sweetman, J. Bamidele, L. Kantorovich, and P. Moriarty, "Role of orbital overlap in atomic manipulation," *Physical Review B* **85** no. 23, (Jun, 2012) 235305.

[55] J. Kubby and J. Boland, "Scanning tunneling microscopy of semiconductor surfaces," *Surface Science Reports* **26** no. 3-6, (Dec, 1996) 61–204.

[56] J. Bardeen, "Tunnelling from a Many-Particle Point of View," *Physical Review Letters* **6** no. 2, (Jan, 1961) 57–59.

[57] A. D. Gottlieb and L. Wesoloski, "Bardeen's tunnelling theory as applied to scanning tunnelling microscopy: a technical guide to the traditional interpretation," *Nanotechnology* **17** no. 8, (Apr, 2006) R57–R65.

[58] J. Tersoff and D. R. Hamann, "Theory of the scanning tunneling microscope," *Physical Review B* **31** no. 2, (Jan, 1985) 805–813.

[59] J. J. Boland, "Scanning tunnelling microscopy of the interaction of hydrogen with silicon surfaces," *Advances in Physics* **42** no. July 2015, (1993) 129–171.

[60] H. Bender, S. Verhaverbeke, M. Caymax, O. Vatel, and M. M. Heyns, "Surface reconstruction of hydrogen annealed (100) silicon," *Journal of Applied Physics* **75** no. 100, (1994) 1207–1209.

[61] G. F. Cerofolini, C. Galati, S. Reina, L. Renna, N. Spinella, D. Jones, and V. Palermo, "Formation of terraced, nearly flat, hydrogen-terminated, (100) Si surfaces after high-temperature treatment in H2 of single-crystalline silicon," *Physical Review B - Condensed Matter and Materials Physics* **72** no. 100, (2005) 1–10.

[62] N. Ashcroft and N. Mermin, *Solid State Physics*. Brooks Cole, 1976.

[63] J. L. Pitters, P. G. Piva, and R. A. Wolkow, "Dopant depletion in the near surface region of thermally prepared silicon (100) in UHV," *Journal of Vacuum Science & Technology B: Microelectronics and Nanometer Structures* **30** no. 100, (2012) 021806.

[64] M. Rashidi, J. A. J. Burgess, M. Taucer, R. Achal, J. L. Pitters, S. Loth, and R. A. Wolkow, "Time-resolved single dopant charge dynamics in silicon," *Nature Communications* **7** (2016) 13258, arXiv:1512.01101.

[65] L. Soukiassian, A. J. Mayne, M. Carbone, and G. Dujardin, "Atomic-scale desorption of H atoms from the Si(100)-2x1:H surface: Inelastic electron interactions," *Physical Review B* **68** no. 3, (Jul, 2003) 035303.

[66] J. N. Randall, J. W. Lyding, S. Schmucker, J. R. Von Ehr, J. Ballard, R. Saini, H. Xu, and Y. Ding, "Atomic precision lithography on Si," *Journal of Vacuum Science & Technology B: Microelectronics and Nanometer Structures* **27** no. 2009, (2009) 2764.

[67] J. B. Ballard, J. H. G. Owen, W. Owen, J. R. Alexander, E. Fuchs, J. N. Randall, J. R. Von Ehr, S. McDonnell, D. D. Dick, R. M. Wallace, Y. J. Chabal, M. R. Bischof, D. L. Jaeger, R. F. Reidy, J. Fu, P. Namboodiri, K. Li, and R. M. Silver, "Pattern transfer of hydrogen depassivation lithography patterns into silicon with atomically traceable placement and size control," *Journal of Vacuum Science & Technology B, Nanotechnology and Microelectronics: Materials, Processing, Measurement, and Phenomena* **32** no. 4, (Jul, 2014) 041804.

[68] T. C. C. Shen, C. Wang, G. C. Abeln, J. R. Tucker, J. W. Lyding, P. Avouris, and R. E. Walkup, "Atomic-scale desorption through electronic and vibrational excitation mechanisms.," *Science (New York, N.Y.)* **268** (1995) 1590–1592.

[69] A. N. Ramanayaka, H.-S. Kim, K. Tang, X. Wang, R. M. Silver, M. D. Stewart, and J. M. Pomeroy, "STM patterned nanowire measurements using photolithographically defined implants in Si(100)," *Scientific Reports* **8** no. 1, (Dec, 2018) 1790.

[70] X. Tong and R. A. Wolkow, "Electron-induced H atom desorption patterns created with a scanning tunneling microscope: Implications for controlled atomic-scale patterning on H-Si(1 0 0)," *Surface Science* **600** (2006) .

[71] P. Guyot-Sionnest, P. Dumas, and Y. Chabal, "Lifetime of an adsorbate-substrate vibration measured by sum frequency generation : H on Si(111)," *Journal of Electron Spectroscopy and Related Phenomena* **54-55** no. 18, (Jan, 1990) 27–38.

[72] K. J. Dwyer, M. Dreyer, and R. E. Butera, "STM-induced desorption and lithographic patterning of Cl-Si(100)-(2x1)," arXiv:1808.05690.

[73] M. Rashidi and R. A. Wolkow, "Autonomous Scanning Probe Microscopy in Situ Tip Conditioning through Machine Learning," *ACS Nano* **12** no. 6, (Jun, 2018) 5185–5189.

[74] L. Livadaru, J. Pitters, M. Taucer, and R. A. Wolkow, "Theory of nonequilibrium single-electron dynamics in STM imaging of dangling bonds on a hydrogenated silicon surface," *Physical Review B* **84** no. 20, (Nov, 2011) 205416, arXiv:1105.2332.

[75] T. R. Huff, T. Dienel, M. Rashidi, R. Achal, L. Livadaru, J. Croshaw, and R. A. Wolkow, "Electrostatic Landscape of a Hydrogen-Terminated Silicon Surface Probed by a Moveable Quantum Dot," *ACS Nano* (Aug, 2019) 10.1021/acsnano.9b04653, arXiv:1902.11296.

[76] H. Raza, "Theoretical study of isolated dangling bonds, dangling bond wires, and dangling bond clusters on a H:Si(100)-2x1 surface," *Physical Review B* **76** no. 4, (Jul, 2007) 045308, arXiv:0611417 [cond-mat].

[77] T. Blomquist and G. Kirczenow, "Controlling the Charge of a Specific Surface Atom by the Addition of a Non-Site-Specific Single Impurity in a Si Nanocrystal," *Nano Letters* **6** no. 1, (Jan, 2006) 61–65.

[78] J. Repp and G. Meyer, "Scanning tunneling microscopy of adsorbates on insulating films. from the imaging of individual molecular orbitals to the manipulation of the charge state," *Applied Physics A: Materials Science and Processing* **85** (2006) 399–406.

[79] M. A. Broome, S. K. Gorman, M. G. House, S. J. Hile, J. G. Keizer, D. Keith, C. D. Hill, T. F. Watson, W. J. Baker, L. C. L. Hollenberg, and M. Y. Simmons, "Two-electron spin correlations in precision placed donors in silicon," *Nature Communications* **9** no. 1, (Dec, 2018) 980.

[80] B. Weber, Y. H. Tan, S. Mahapatra, T. F. Watson, H. Ryu, R. Rahman, L. C. Hollenberg, G. Klimeck, and M. Y. Simmons, "Spin blockade and exchange in Coulomb-confined silicon double quantum dots," *Nature Nanotechnology* **9** no. 6, (2014) 430–435.

[81] L. Soukiassian, A. J. Mayne, M. Carbone, and G. Dujardin, "Atomic wire fabrication by STM induced hydrogen desorption," in *Surface Science*, vol. 528, pp. 121–126. 2003.

[82] I. Dogel, S. Dogel, J. Pitters, G. DiLabio, and R. Wolkow, "Chemical methods for the hydrogen termination of silicon dangling bonds," *Chemical Physics Letters* **448** no. 4-6, (Nov, 2007) 237–242.

[83] D. H. Huang and Y. Yamamoto, "Physical mechanism of hydrogen deposition from a scanning tunneling microscopy tip," *Applied Physics A: Materials Science & Processing* **64** (1997) 419–422.

[84] H. Kuramochi, H. Uchida, and M. Aono, "Local hydride formation of the Si(111)-(7x7) surface by hydrogen atoms deposited from a scanning tunneling microscope tip," *Physical Review Letters* **72** no. 6, (Feb, 1994) 932–935.

[85] M. Taucer, *Silicon Dangling Bonds Non-equilibrium Dynamics and Applications*. PhD thesis, University of Alberta, 2015.

[86] M. C. Hersam, N. P. Guisinger, and J. W. Lyding, "Silicon-based molecular nanotechnology," *Nanotechnology* **11** (2000) 70–76.

[87] R. Gomer, R. Wortman, and R. Lundy, "Mobility and Adsorption of Hydrogen on Tungsten," *The Journal of Chemical Physics* **26** (1957) 1147.

[88] P. G. Piva, G. A. DiLabio, L. Livadaru, and R. A. Wolkow, "Atom-scale surface reactivity mediated by long-ranged equilibrium charge transfer," *Physical Review B* **90** no. 15, (Oct, 2014) 155422.

[89] J. L. Pitters, L. Livadaru, M. B. Haider, and R. A. Wolkow, "Tunnel coupled dangling bond structures on hydrogen terminated silicon surfaces," *The Journal of Chemical Physics* **134** no. 6, (Feb, 2011) 064712.

[90] R. A. Wolkow, "Controlled Molecular Adsorption on Silicon: Laying a Foundation for Molecular Devices," *Annual Review of Physical Chemistry* **50** no. 1, (Oct, 1999) 413–441.

[91] M. Dürr and U. Höfer, "Dissociative adsorption of molecular hydrogen on silicon surfaces," 2006.

[92] A. J. Mayne, D. Riedel, G. Comtet, and G. Dujardin, "Atomic-scale studies of hydrogenated semiconductor surfaces," *Progress in Surface Science* **81** no. 1, (2006) 1–51.

[93] K. Bobrov, A. Mayne, G. Comtet, G. Dujardin, L. Hellner, and A. Hoffman, "Atomic-scale visualization and surface electronic structure of the hydrogenated diamond C(100)-(2 x 1):H surface," *Physical Review B* **68** no. 19, (Nov, 2003) 195416.

[94] R. Butera and M. Dreyer, "STM-based lithography on chlorine-terminated Si(100)," in *APS March Meeting*, p. V17.00010. Los Angeles, California, 2018.

[95] K. Eng, R. N. McFarland, and B. E. Kane, "High mobility two-dimensional electron system on hydrogen-passivated silicon(111) surfaces," *Applied Physics Letters* **87** no. 111, (2005) 052106, `arXiv:0501608 [cond-mat]`.

[96] K. Salaita, Y. Wang, and C. A. Mirkin, "Applications of dip-pen nanolithography," *Nature Nanotechnology* **2** no. 1, (2007) 145–155.

[97] B. Reddy and B. Chatterji, "An FFT-based technique for translation, rotation, and scale-invariant image registration," *IEEE Transactions on Image Processing* **5** no. 8, (1996) 1266–1271.

[98] L. J. Lauhon and W. Ho, "Direct Observation of the Quantum Tunneling of Single Hydrogen Atoms with a Scanning Tunneling Microscope," *Phys. Rev. Lett.* **85** no. 21, (2000) 4566–4569.

[99] H.-H. Limbach, J. Miguel Lopez, and A. Kohen, "Arrhenius curves of hydrogen transfers: tunnel effects, isotope effects and effects of pre-equilibria," *Philosophical Transactions of the Royal Society B: Biological Sciences* **361** no. 1472, (Aug, 2006) 1399–1415.

[100] R. J. McMahon, "Chemical Reactions Involving Quantum Tunneling," *Science* **299** no. 5608, (Feb, 2003) 833–834.

[101] K. Lee, K. Berland, M. Yoon, S. Andersson, E. Schröder, P. Hyldgaard, and B. I. Lundqvist, "Benchmarking van der Waals density functionals with experimental data: potential-energy curves for H2 molecules on Cu(111), (100) and (110) surfaces," *Journal of Physics: Condensed Matter* **24** no. 42, (Oct, 2012) 424213, `arXiv:1206.0775`.

[102] H. Kawai, O. Neucheva, T. L. Yap, C. Joachim, and M. Saeys, "Electronic characterization of a single dangling bond on n- and p-type Si(001)-(2x1):H," *Surface Science* **645** (Mar, 2016) 88–92.

[103] M. Engelund, R. Zuzak, S. Godlewski, M. Kolmer, T. Frederiksen, A. García-Lekue, D. Sánchez-Portal, and M. Szymonski, "Tunneling spectroscopy of close-spaced dangling-bond pairs in Si(001):H," *Scientific Reports* **5** no. 1, (Nov, 2015) 14496.

[104] E. Crane, A. Köolker, T. Z. Stock, N. Stavrias, K. Saeedi, M. A. W. van Loon, B. N. Murdin, and N. J. Curson, "Hydrogen resist lithography and electron beam lithography for fabricating silicon targets for studying donor orbital states," *Journal of Physics: Conference Series* **1079** no. 1, (Aug, 2018) 012010.

[105] S. R. Schofield, N. J. Curson, M. Y. Simmons, F. J. Rueß, T. Hallam, L. Oberbeck, and R. G. Clark, "Atomically Precise Placement of Single Dopants in Si," *Physical Review Letters* **91** no. 13, (Sep, 2003) 136104.

[106] M. C. Hersam, N. P. Guisinger, and J. W. Lyding, "Isolating, imaging, and electrically characterizing individual organic molecules on the Si(100) surface with the scanning tunneling microscope," *Journal of Vacuum Science & Technology A: Vacuum, Surfaces, and Films* **18** no. 4, (Jul, 2000) 1349–1353.

[107] A. J. Mayne, L. Soukiassian, N. Commaux, G. Comtet, and G. Dujardin, "Molecular molds," *Applied Physics Letters* **85** no. 22, (2004) 5379–5381.

[108] M. Dürr, Z. Hu, A. Biedermann, U. Höfer, and T. F. Heinz, "Real-Space Study of the Pathway for Dissociative Adsorption of H2 on Si(001)," *Physical Review Letters* **88** no. 4, (Jan, 2002) 046104.

[109] G. Mette, C. H. Schwalb, M. Dürr, and U. Höfer, "Site-selective reactivity of ethylene on clean and hydrogen precovered Si(0 0 1)," *Chemical Physics Letters* **483** no. 4-6, (2009) 209–213.

[110] S. F. Bent, "Organic functionalization of group IV semiconductor surfaces: Principles, examples, applications, and prospects," *Surface Science* **500** no. 1-3, (2002) 879–903.

[111] P. G. Piva, G. A. DiLabio, J. L. Pitters, J. Zikovsky, M. Rezeq, S. Dogel, W. A. Hofer, and R. A. Wolkow, "Field regulation of single-molecule conductivity by a charged surface atom," *Nature* **435** no. 7042, (Jun, 2005) 658–661.

[112] N. Xin, J. Guan, C. Zhou, X. Chen, C. Gu, Y. Li, M. A. Ratner, A. Nitzan, J. F. Stoddart, and X. Guo, "Concepts in the design and engineering of single-molecule electronic devices," *Nature Reviews Physics* **1** no. 3, (Mar, 2019) 211–230.

[113] A. C. Aragonès, N. Darwish, S. Ciampi, F. Sanz, J. J. Gooding, and I. Díez-Pérez, "Single-molecule electrical contacts on silicon electrodes under ambient conditions," *Nature Communications* **8** no. 1, (Apr, 2017) 15056.

[114] E. Lörtscher, "Wiring molecules into circuits," *Nature Nanotechnology* **8** no. 6, (2013) 381–384.

[115] R. M. Metzger, "Unimolecular Electronics," *Chemical Reviews* **115** no. 11, (Jun, 2015) 5056–5115.

[116] H. Song, M. A. Reed, and T. Lee, "Single Molecule Electronic Devices," *Advanced Materials* **23** no. 14, (Apr, 2011) 1583–1608.

[117] O. Warschkow, N. J. Curson, S. R. Schofield, N. A. Marks, H. F. Wilson, M. W. Radny, P. V. Smith, T. C. G. Reusch, D. R. McKenzie, and M. Y. Simmons, "Reaction paths of phosphine dissociation on silicon (001)," *The Journal of Chemical Physics* **144** no. 1, (Jan, 2016) 014705.

[118] H. F. Wilson, O. Warschkow, N. A. Marks, N. J. Curson, S. R. Schofield, T. C. G. Reusch, M. W. Radny, P. V. Smith, D. R. McKenzie, and M. Y. Simmons, "Thermal dissociation and desorption of PH3 on Si(001): A reinterpretation of spectroscopic data," *Physical Review B* **74** no. 19, (Nov, 2006) 195310.

[119] J. Schaffert, M. C. Cottin, A. Sonntag, H. Karacuban, C. a. Bobisch, N. Lorente, J.-P. Gauyacq, and R. Möller, "Imaging the dynamics of individually adsorbed molecules.," *Nature materials* **12** no. 3, (Mar, 2013) 223–227.

[120] Y. Wakayama, J. P. Hill, and K. Ariga, "Real-time STM observation of molecular dynamics on a metal surface," *Surface Science* **601** no. 18, (2007) 3984–3987.

[121] M. Engelund, S. Godlewski, M. Kolmer, R. Zuzak, B. Such, T. Frederiksen, M. Szymonski, and D. Sánchez-Portal, "The butterfly – a well-defined constant-current topography pattern on Si(001):H and Ge(001):H resulting from current-induced defect fluctuations," *Physical Chemistry Chemical Physics* **18** no. 28, (2016) 19309–19317.

[122] S. Godlewski, H. Kawai, M. Kolmer, R. Zuzak, A. M. Echavarren, C. Joachim, M. Szymonski, and M. Saeys, "Single-Molecule Rotational Switch on a Dangling Bond Dimer Bearing," *ACS Nano* **10** no. 9, (2016) 8499–8507.

[123] J. L. Pitters and R. A. Wolkow, "Detailed Studies of Molecular Conductance Using Atomic Resolution Scanning Tunneling Microscopy," *Nano Letters* **6** no. 3, (Mar, 2006) 390–397.

[124] K.-J. Chao, A. R. Smith, and C.-K. Shih, "Direct determination of exact charge states of surface point defects using scanning tunneling microscopy: As vacancies on GaAs (110)," *Physical Review B* **53** no. 11, (Mar, 1996) 6935–6938.

[125] D. Gohlke, R. Mishra, O. D. Restrepo, D. Lee, W. Windl, and J. Gupta, "Atomic-scale engineering of the electrostatic landscape of semiconductor surfaces," *Nano Letters* **13** no. 6, (2013) 2418–2422.

[126] C. Filippi, S. B. Healy, P. Kratzer, E. Pehlke, and M. Scheffler, "Quantum Monte Carlo Calculations of H2 Dissociation on Si(001)," *Physical Review Letters* **89** no. 16, (Sep, 2002) 166102.

[127] Y. Kanai, A. Tilocca, A. Selloni, and R. Car, "First-principles string molecular dynamics: An efficient approach for finding chemical reaction pathways," *Journal of Chemical Physics* **121** no. 8, (2004) 3359–3367.

[128] Y. Narita, S. Inanaga, and A. Namiki, "Kinetics of hydrogen adsorption and desorption on Si(100) surfaces," *Journal of Applied Physics* **113** no. 23, (Jun, 2013) 234309.

[129] E. Pehlke, "Highly reactive dissociative adsorption of hydrogen molecules on partially H-covered Si(001) surfaces: A density-functional study," *Physical Review B* **62** no. 19, (2000) 12932–12939.

[130] O. Warschkow, H. F. Wilson, N. A. Marks, S. R. Schofield, N. J. Curson, P. V. Smith, M. W. Radny, D. R. McKenzie, and M. Y. Simmons, "Phosphine adsorption and dissociation on the Si(001) surface: An ab initio survey of structures," *Physical Review B* **72** no. 12, (Sep, 2005) 125328.

[131] R. Pires, R. Dickstein, S. Titcomb, and R. Anderson, "Carrier freezeout in silicon," *Cryogenics* **30** no. 12, (Dec, 1990) 1064–1068.

[132] M. Dürr, M. B. Raschke, E. Pehlke, and U. Höfer, "Structure sensitive reaction channels of molecular hydrogen on silicon surfaces," *Physical Review Letters* **86** no. 1, (2001) 123–126.

[133] E. J. Buehler and J. J. Boland, "Dimer Preparation That Mimics the Transition State for the Adsorption of H2 on the Si(100)-2 x 1 Surface," *Science* **290** no. 5491, (Oct, 2000) 506–509.

[134] A. Züttel, "Materials for hydrogen storage," *Materials Today* **6** no. 9, (Sep, 2003) 24–33.

[135] W. Leung, N. March, and H. Motz, "Primitive phase diagram for hydrogen," *Physics Letters A* **56** no. 6, (May, 1976) 425–426.

[136] R. Achal, *Detailed Study of Atomic Silicon Dangling Bond Charge State Dynamics on the Surface of Hydrogen Terminated Silicon (100)-2x1*. Masters' thesis, University of Alberta, 2015.

[137] M. Rashidi, J. Croshaw, K. Mastel, M. Tamura, H. Hosseinzadeh, and R. A. Wolkow, "Autonomous Atomic Scale Manufacturing Through Machine Learning," arXiv:1902.08818.

[138] T. Susi, J. Kotakoski, D. Kepaptsoglou, C. Mangler, T. C. Lovejoy, O. L. Krivanek, R. Zan, U. Bangert, P. Ayala, J. C. Meyer, and Q. Ramasse, "Silicon-carbon bond inversions driven by 60-kev electrons in graphene," *Physical Review Letters* **113** no. 11, (2014) 1–5.

[139] J. Pecher, G. Mette, M. Dürr, and R. Tonner, "Site-Specific Reactivity of Ethylene at Distorted Dangling-Bond Configurations on Si(001)," *ChemPhysChem* **18** no. 4, (2017) 357–365.

[140] R. M. Feenstra, "A prospective: Quantitative scanning tunneling spectroscopy of semiconductor surfaces," *Surface Science* **603** no. 18, (2009) 2841–2844.

[141] R. M. Feenstra, "Electrostatic potential for a hyperbolic probe tip near a semiconductor," *Journal of Vacuum Science & Technology B: Microelectronics and Nanometer Structures* **21** no. 5, (2003) 2080.

[142] D. Lee, D. Gohlke, A. Benjamin, and J. A. Gupta, "Influence of the local environment on Mn acceptors in GaAs," *Journal of Physics: Condensed Matter* **27** no. 15, (Apr, 2015) 154202.

[143] V.-M. Freire, A. Ramirez, E. Pascual, E. Bertran, and J.-L. Andujar, "Investigation of monolayer-formation time for the synthesis of graphene on copper/nickel/silicon using very-low pressure pulses of methane," arXiv:1406.2640.

[144] M. A. Reed, "Inelastic electron tunneling spectroscopy," *Materials Today* **11** no. 11, (Nov, 2008) 46–50.

[145] X. Wang, J. A. Hagmann, P. Namboodiri, J. Wyrick, K. Li, R. E. Murray, A. Myers, F. Misenkosen, M. D. Stewart, C. A. Richter, and R. M. Silver,

"Quantifying atom-scale dopant movement and electrical activation in Si:P monolayers," *Nanoscale* **10** no. 9, (2018) 4488–4499.

[146] H. Labidi, M. Taucer, M. Rashidi, M. Koleini, L. Livadaru, J. Pitters, M. Cloutier, M. Salomons, and R. A. Wolkow, "Scanning tunneling spectroscopy reveals a silicon dangling bond charge state transition," *New Journal of Physics* **17** no. 7, (Jul, 2015) 073023, arXiv:1503.00646.

[147] T. Hitosugi, S. Heike, T. Onogi, T. Hashizume, S. Watanabe, Z.-Q. Li, K. Ohno, Y. Kawazoe, T. Hasegawa, and K. Kitazawa, "Jahn-Teller Distortion in Dangling-Bond Linear Chains Fabricated on a Hydrogen-Terminated Si(100)-2x1 Surface," *Physical Review Letters* **82** no. 20, (May, 1999) 4034–4037.

[148] A. Biedermann, E. Knoesel, Z. Hu, and T. F. Heinz, "Dissociative adsorption of H2 on Si(100) induced by atomic H," *Physical Review Letters* **83** no. 9, (1999) 1810–1813.

[149] R. A. Wolkow, "Direct observation of an increase in buckled dimers on Si(001) at low temperature," *Physical Review Letters* **68** no. 17, (Apr, 1992) 2636–2639.

[150] P. V. Smith and X. M. Zheng, "The Clean and Hydrogen-Terminated (100) and (111) Surfaces of Diamond and Silicon," in *Surface Science. Springer Proceedings in Physics, vol 73.*, pp. 161–174. Springer, Berlin, Heidelberg, 1993.

[151] T. I. Hukka, T. A. Pakkanen, and M. P. D'Evelyn, "Chemisorption of Hydrogen on the Diamond (100)2x1 Surface: An ab Initio Study," *The Journal of Physical Chemistry* **98** no. 47, (Nov, 1994) 12420–12430.

[152] S. Bohloul, Q. Shi, R. A. Wolkow, and H. Guo, "Quantum transport in gated dangling-bond atomic wires," *Nano Letters* **17** no. 1, (2017) 322–327.

[153] M. Engelund, N. Papior, P. Brandimarte, T. Frederiksen, A. Garcia-Lekue, and D. Sánchez-Portal, "Search for a Metallic Dangling-Bond Wire on n -Doped H-Passivated Semiconductor Surfaces," *The Journal of Physical Chemistry C* **120** no. 36, (Sep, 2016) 20303–20309.

[154] B. Naydenov and J. J. Boland, "Engineering the electronic structure of surface dangling bond nanowires of different size and dimensionality.," *Nanotechnology* **24** no. 27, (Jul, 2013) 275202.

[155] J. A. Wood, M. Rashidi, M. Koleini, J. L. Pitters, and R. A. Wolkow, "Multiple Silicon Atom Artificial Molecules," arXiv:1607.06050.

[156] H. Kawai, O. Neucheva, T. L. Yap, C. Joachim, and M. Saeys, "Electronic Properties of a Single Dangling Bond and of Dangling Bond Wires on a Si(001):H Surface," in *On-Surface Atomic Wires and Logic Gates. Advances in Atom and Single Molecule Machines*, pp. 105–120. Springer, 2017.

[157] S. W. Wu, N. Ogawa, and W. Ho, "Atomic-Scale Coupling of Photons to Single-Molecule Junctions," *Science* **312** no. 5778, (Jun, 2006) 1362–1365.

[158] V. Jelic, K. Iwaszczuk, P. H. Nguyen, C. Rathje, G. J. Hornig, H. M. Sharum, J. R. Hoffman, M. R. Freeman, and F. A. Hegmann, "Ultrafast terahertz control of extreme tunnel currents through single atoms on a silicon surface," *Nature Physics* **13** no. 6, (2017) 591–597.

[159] G. Scappucci, G. Capellini, W. C. T. Lee, and M. Y. Simmons, "Atomic-scale patterning of hydrogen terminated Ge(001) by scanning tunneling microscopy," *Nanotechnology* **20** no. 49, (Dec, 2009) 495302.

[160] S. Shaik, E. Cremades, and S. Alvarez, "The Periodic-Table-A Universal Icon: Its Birth 150 Years Ago, and Its Popularization Through Literature Art and Music," *Angewandte Chemie International Edition* **58** no. 38, (Sep, 2019) 13194–13206.

[161] M. Rashidi, W. Vine, J. A. Burgess, M. Taucer, R. Achal, J. L. Pitters, S. Loth, and R. A. Wolkow, "All-electronic Nanosecond-resolved Scanning Tunneling Microscopy: Facilitating the Investigation of Single Dopant Charge Dynamics," *Journal of Visualized Experiments* no. 131, (Jan, 2018) .

[162] J. Adey, R. Jones, D. W. Palmer, P. R. Briddon, and S. Öberg, "Degradation of Boron-Doped Czochralski-Grown Silicon Solar Cells," *Physical Review Letters* **93** no. 5, (Jul, 2004) 055504.

[163] K. Bothe and J. Schmidt, "Electronically activated boron-oxygen-related recombination centers in crystalline silicon," *Journal of Applied Physics* **99** no. 1, (Jan, 2006) 013701.

Appendices

Appendix A

List of peer reviewed publications and patents

- R. Achal, M. Rashidi, J. Croshaw, T. R. Huff, and R. A. Wolkow, "Detecting and Directing Single Molecule Binding Events on H-Si(100) with Application to Ultradense Data Storage," *ACS Nano* (Nov, 2019) acsnano.9b07637, arXiv:1907.03218

- T. R. Huff, T. Dienel, M. Rashidi, R. Achal, L. Livadaru, J. Croshaw, and R. A. Wolkow, "Electrostatic Landscape of a Hydrogen-Terminated Silicon Surface Probed by a Moveable Quantum Dot," *ACS Nano* (Aug, 2019) 10.1021/acsnano.9b04653, arXiv:1902.11296

- T. Huff, H. Labidi, M. Rashidi, L. Livadaru, T. Dienel, R. Achal, W. Vine, J. Pitters, and R. A. Wolkow, "Binary atomic silicon logic," *Nature Electronics* **1** no. 12, (2018) 636–643

- R. Achal, M. Rashidi, J. Croshaw, D. Churchill, M. Taucer, T. Huff, M. Cloutier, J. Pitters, and R. A. Wolkow, "Lithography for robust and editable atomic-scale silicon devices and memories," *Nature Communications* **9** (Dec, 2018) 2778

- M. Rashidi, W. Vine, J. A. Burgess, M. Taucer, R. Achal, J. L. Pitters, S. Loth, and R. A. Wolkow, "All-electronic Nanosecond-resolved Scanning Tunneling Microscopy: Facilitating the Investigation of Single Dopant Charge Dynamics," *Journal of Visualized Experiments* no. 131, (Jan, 2018)

- M. Rashidi, E. Lloyd, T. R. Huff, R. Achal, M. Taucer, J. J. Croshaw, and R. A. Wolkow, "Resolving and Tuning Carrier Capture Rates at a Single Silicon Atom Gap State," *ACS Nano* **11** no. 11, (2017) 11732–11738, arXiv:1711.00566v1

- T. Huff, H. Labidi, M. Rashidi, M. Koleini, R. Achal, M. H. Salomons, and R. A. Wolkow, "Atomic White-Out: Enabling Atomic Circuitry Through Mechanically Induced Bonding of Single Hydrogen Atoms to a Silicon Surface," *ACS Nano* **11** no. 9, (Sep, 2017) 8636–8642, arXiv:1706.05287

- M. Rashidi, J. A. J. Burgess, M. Taucer, R. Achal, J. L. Pitters, S. Loth, and R. A. Wolkow, "Time-resolved single dopant charge dynamics in silicon," *Nature Communications* **7** (2016) 13258, arXiv:1512.01101

- **Patent:** "Lithography for Editable Atomic-Scale Devices and Memories". R. Achal, R. A. Wolkow, J. Pitters, Martin Cloutier, M. Rashidi, M. Taucer, T. Huff, International Publication Number WO 2019/241887A1. International Filing Date 19/06/2019. International Publication Date 26/12/2019.

- **Patent:** "Multiple Silicon Atom Quantum Dot and Devices Inclusive Thereof". R. A. Wolkow, R. Achal, T. Huff, H. Labidi, L. Livadaru, P. Piva, M. Rashidi, International Publication Number WO 2018/015809A3. International Filing Date 19/07/2016. International Publication Date 01/03/2018.

Appendix B

Gallery of additional images

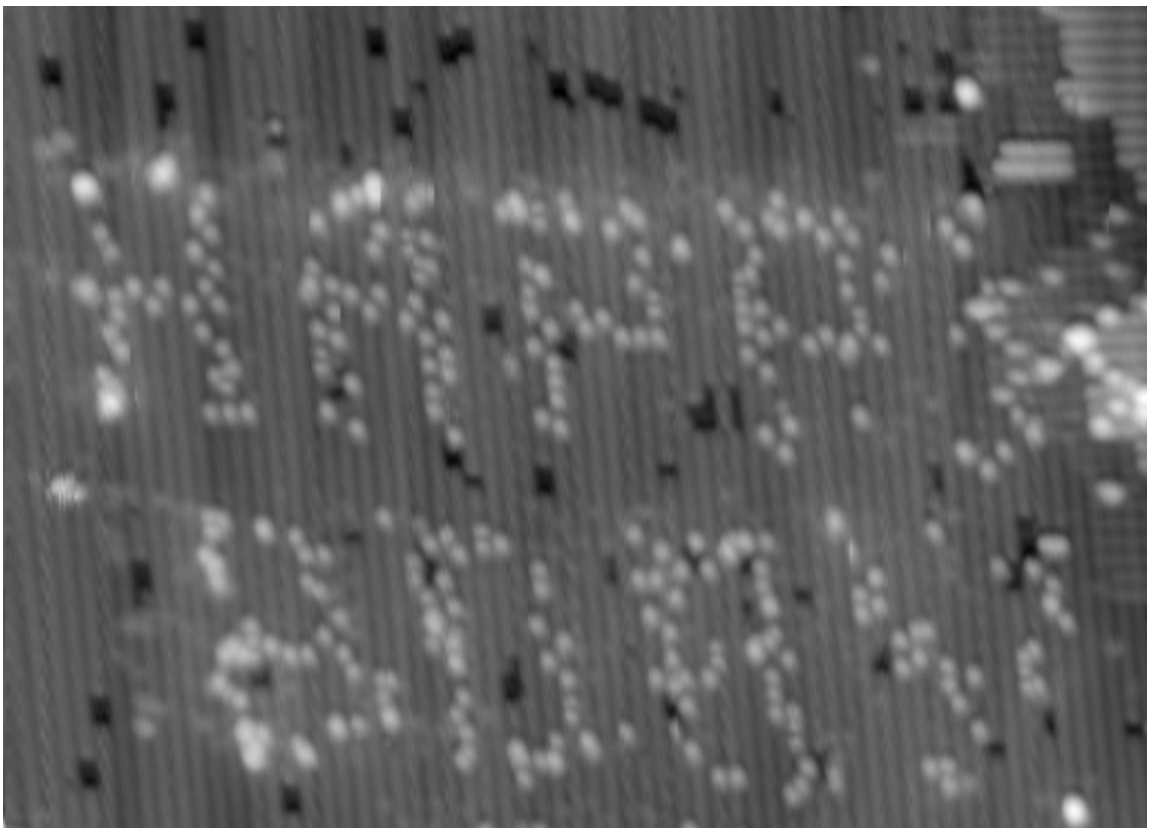

Figure B.1: A nanoscale note (V = -2.0 V, I = 80 pA, T = 4.5 K). This image is representative of the state of HL in 2013. When I was being introduced to the STM and lithography this was one of the first times I had the opportunity to design a pattern and see it *roughly* appear at the atomic scale. If you squint, you might be able to make out the nanoscale note: "HAPPY BDAY".

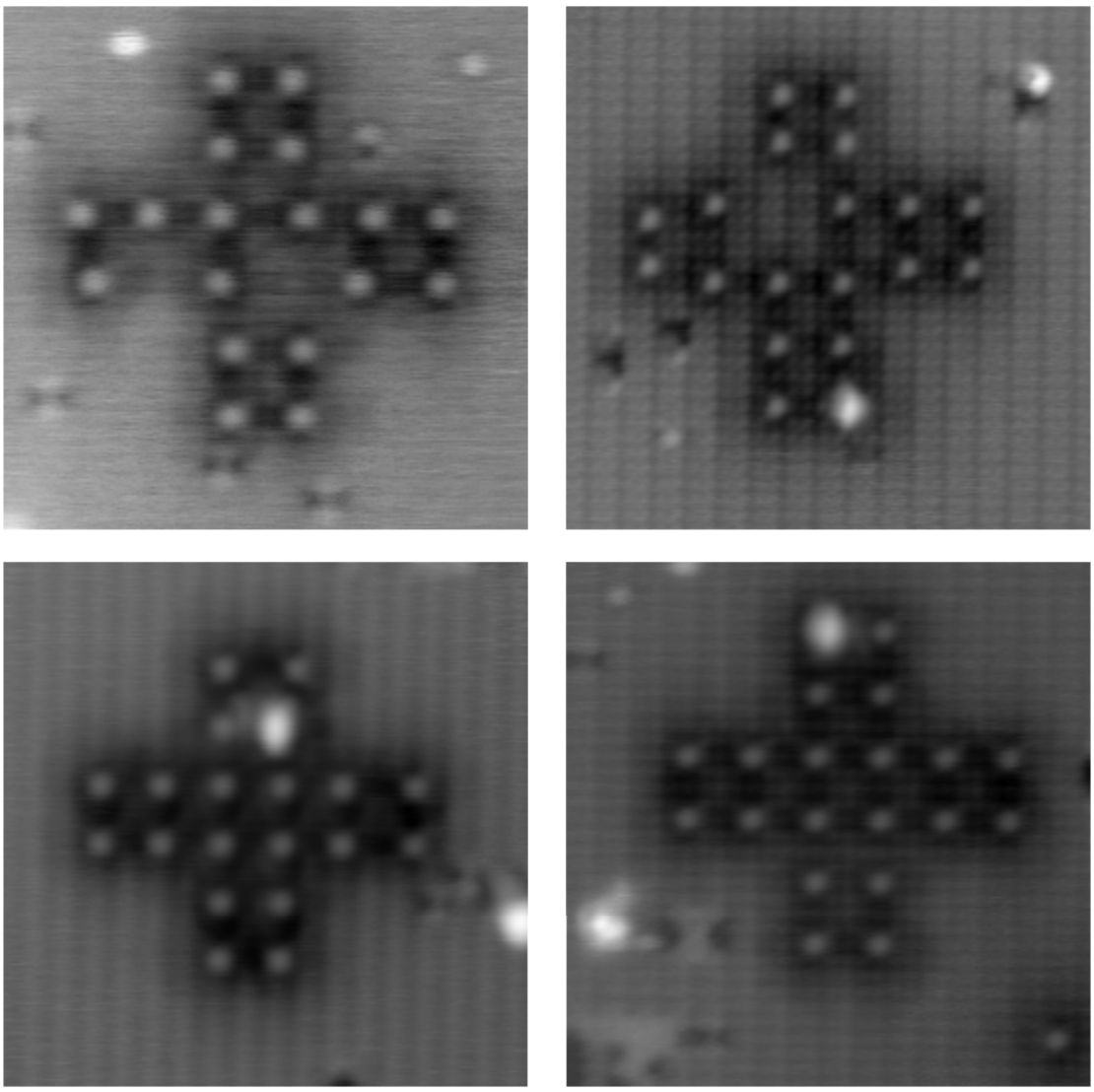

Figure B.2: Pursuit of perfection ($V = 1.4$ V, $I = 50$ pA, $T = 4.5$ K). These images are representative of the state of HL throughout 2016. The fabrication accuracy of larger structures had progressed significantly towards the end of the year. However, in spite of the improved algorithms and techniques for HL, the goal of a perfect 20 atom pattern had yet to be realized. These designs caused many late nights, only to be one atom off. If only there had been a way to repair them instead of starting again from scratch each time...

Figure B.3: Perfection (V = -1.6 V, I = 50 pA, T = 4.5 K, 11 x 22 nm^2). This image is representative of the state of HL in 2017, after the development of HR. Now it was possible to repair the one or two erroneous DBs to achieve perfect large DB structures. The leaf consists of 32 DBs, and it is one of my favorite images.

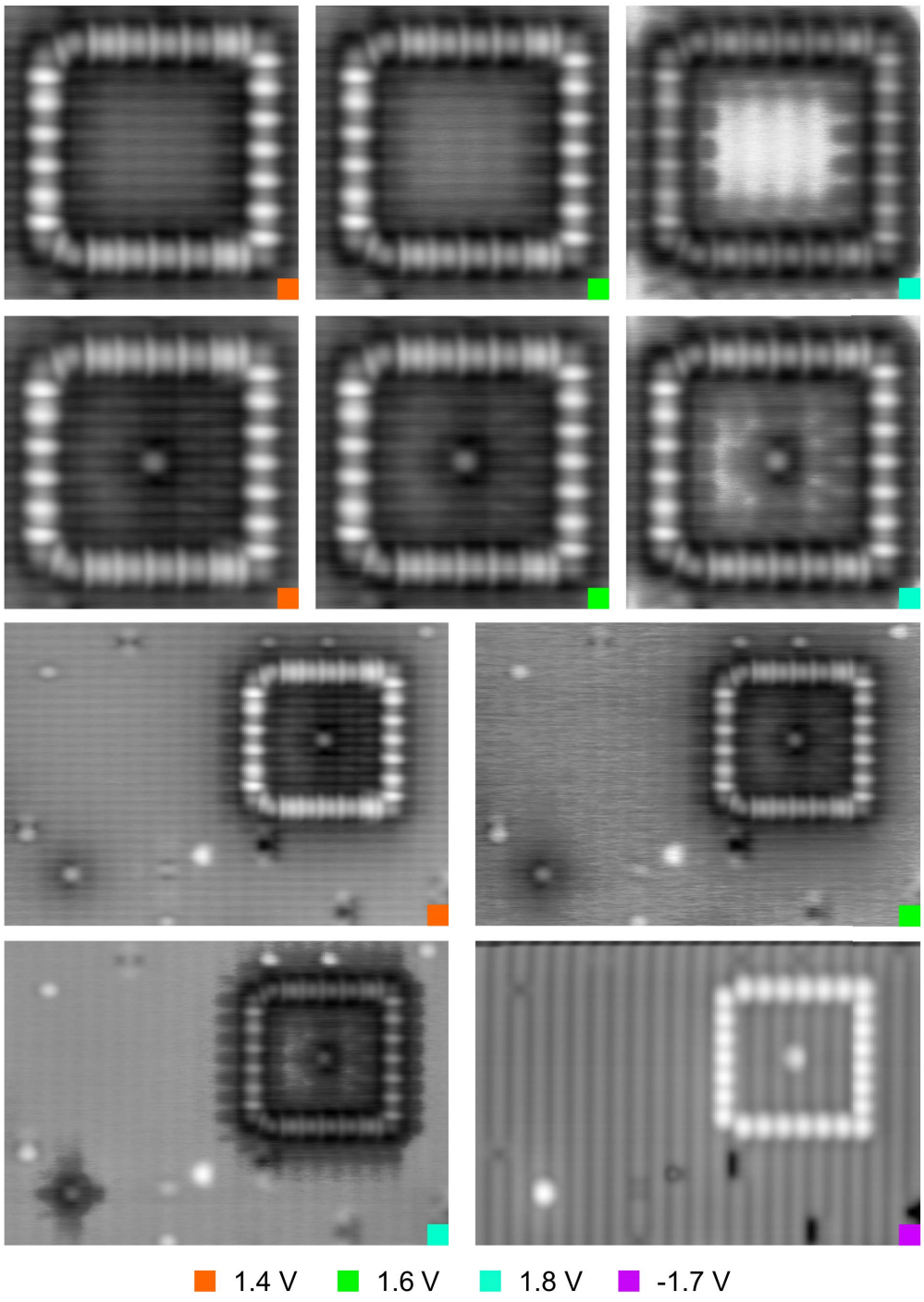

Figure B.4: Asymmetric DB box (I = 50 pA, T = 4.5 K).

Figure B.4: *cont.* Asymmetric DB box (I = 50 pA, T = 4.5 K).
First row) (8 x 8 nm^2) An asymmetric box structure made of DBs, imaged at various empty state conditions. The ability to create perfect DB structures will make it possible to study the rich electronic properties of such structures in the future. **Second row**) The same DB structure as above with a single extra DB in the centre. **Third and fourth row**) (13 x 19 nm^2) The same structure as above, with an isolated DB to the left for comparison with the DB in the centre of the box.

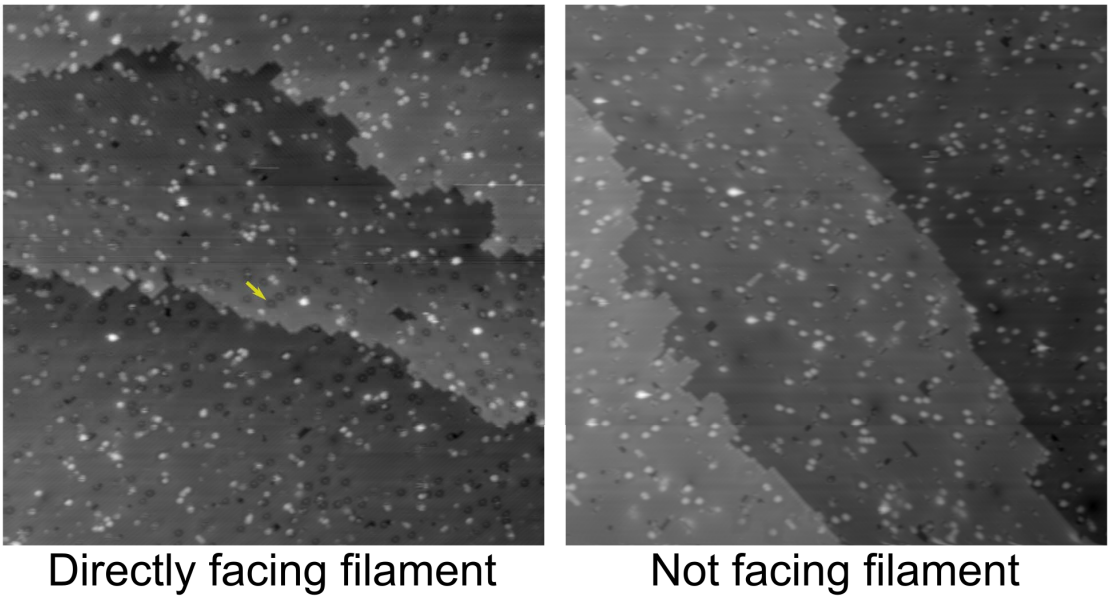

Figure B.5: p-type preparation considerations. (V = 1.6 V, I = 50 pA, T = 77 K, 100 x 100 nm^2).
These images come from some work done on highly boron-doped silicon (0.0018 ohm-cm) that was outside the main scope of this thesis. In the typical preparation method for hydrogen-terminated Si(100)-2x1, the sample surface is facing directly in line with the hydrogen gas cracking filament (approximately 20 cm away). We noticed a high surface concentration of negative "dark DBs" (shown with the yellow arrow) when the surface was prepared this way. By tilting the sample away from the filament during preparation, we noticed that the concentration of dark DBs dropped significantly. Different orientations during sample preparation of n-type silicon has not been observed to result in different DB character such as this.

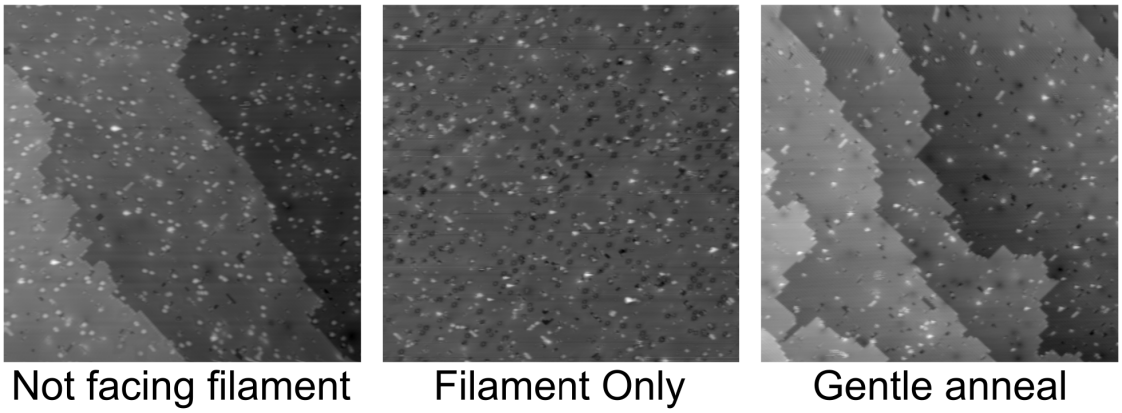

Figure B.6: Solar implications (V = 1.7 V, I = 50 pA, T = 77 K, 100 x 100 nm^2).
We decided to see if exposing an already hydrogen-terminated sample with a low concentration of dark DBs to the filament would induce the same effect as above. The sample was placed in the standard preparation position, without heating or the addition of hydrogen gas into the chamber as in a typical preparation, and the filament was brought to the normal cracking current (1.5 A). The sample was exposed to the illuminated filament for 4 min and 30 s. Upon imaging the sample, there appeared to be a large increase in the number of dark DBs. We then gently annealed the sample at 270 °C for 2 min. Upon re-imaging the sample, the number of dark DBs appeared to have been reduced again. Due to experimental limitations, it was not possible to image the exact same area of the sample after each step. These experiments need to be repeated and future studies will need to explore larger areas of the sample to collect sufficient statistics on the changes. However, these initial results may be evidence of atomic-scale modifications of electronic properties of the surface due to light exposure. Degradation of p-type silicon solar cell efficiency is known to be caused by exposure to light, which leads to the formation of positively charged boron-oxygen complexes [162,163]. The decrease in the number of dark DBs after heating also corresponds well with the known recovery of solar cell efficiency after annealing to similar temperatures [162, 163]. One thought I have to explain these observations is defect-induced modification of the local electrostatic landscape of each DB. The downward band bending caused by the presence of positive defects can reduce the emptying rate of electrons from the DB into the bulk, giving them a net negative charge when imaged by the tip in empty states [136]. We have observed that imaging the dark DBs at sufficiently high positive voltages causes them to appear bright. The required voltage is different for each DB, as its proximity to a defect is random. This observation is consistent with the fact that higher biases increase the emptying rate, preventing the DBs from being net negative.

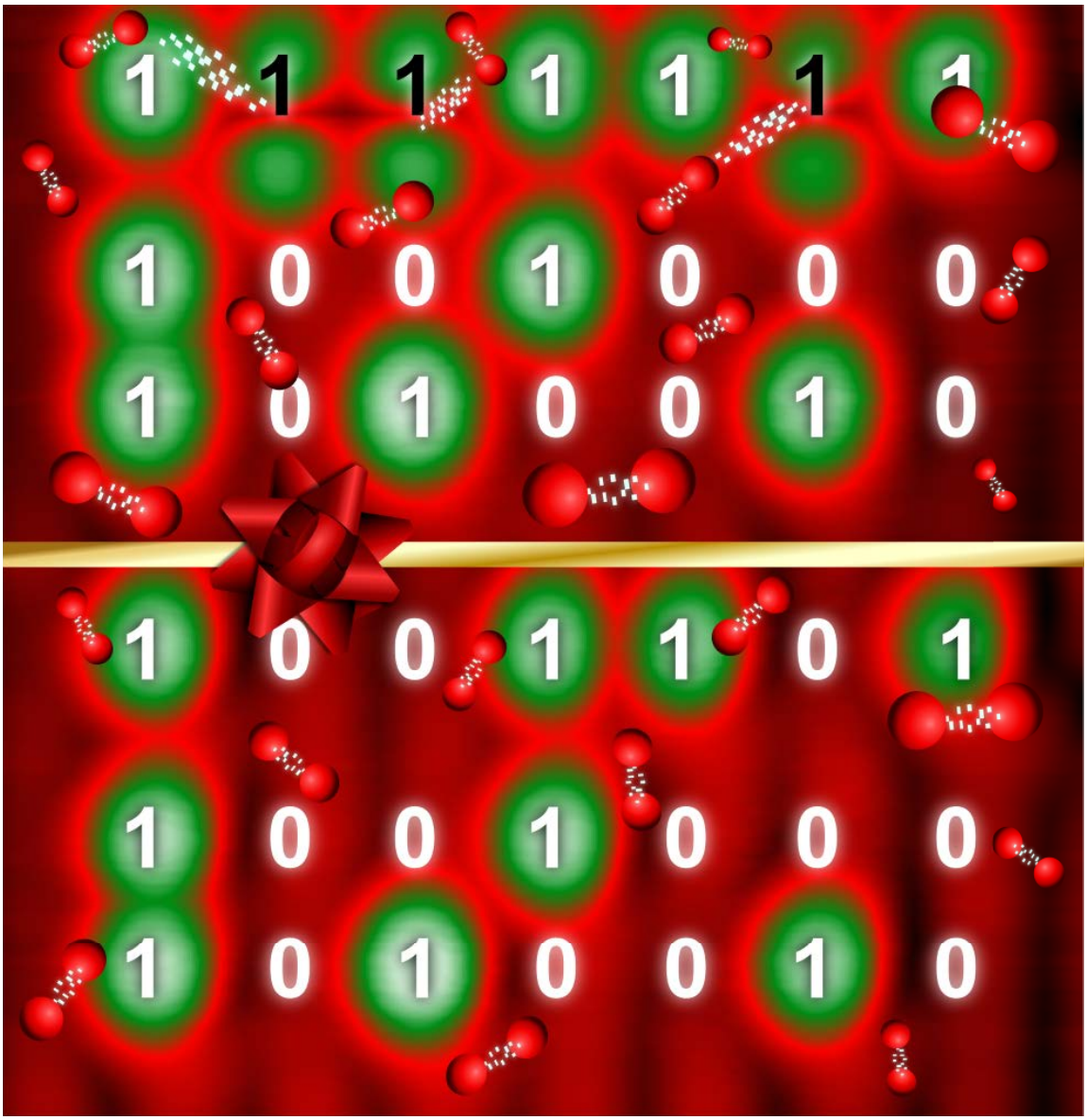

Figure B.7: Merry molecular erasers.
I made this festive image for public outreach to help explain one of the last results of my PhD work. I have made the joke about it quite a few times now (to many eye rolls), but one more time couldn't hurt. With this last image on the last page, my thesis is officially *wrapped* up!